DEVELOPMENT OF LIQUID ARMOR MATERIALS AND RHEOLOGICAL BEHAVIOR OF SHEAR THICKENING FLUIDS (STFs)

A Thesis Submitted to
the Graduate School of Engineering and Sciences of
İzmir Institute of Technology
in Partial Fulfillment of the Requirements for the Degree of

MASTER OF SCIENCE

in Materials Science

by
Taner ERDOĞAN

November 2011
İZMİR

We approve the thesis of **Taner ERDOĞAN**

Prof. Dr. Metin TANOĞLU
Supervisor

Assist. Prof. Dr. H. Seçil ARTEM
Co-Supervisor

Prof. Dr. Bülent YARDIMOĞLU
Committee Member

Assist. Prof. Dr. Sevgi KILIÇ ÖZDEMİR
Committee Member

Assoc. Prof. Dr. Mustafa M. DEMİR
Committee Member

16 November 2011

Assoc. Prof. Dr. Mustafa M. DEMİR
Head of the Department of
Materials Science and Engineering

Prof. Dr. R. Tuğrul SENGER
Dean of the Graduate School of
Engineering and Sciences

ACKNOWLEDGEMENTS

I would like to thank and express my deepest gratitude to my advisor, Prof. Dr. Metin TANOĞLU, for his supervision, guidance, support, understanding and encouragement during my study. I would also like to thank to my co-advisor Assist. Prof. Dr. Seçil ARTEM for her help and support.

I would like to express my special thanks to committee members of my thesis, Prof Dr. Bülent YARDIMOĞLU and Assist. Prof. Dr. Sevgi KILIÇ ÖZDEMİR for their suggestions and evaluations on my study.

I would also like to express my sincere gratitude to Assoc. Prof. Dr. Mustafa M. DEMİR for his help, support and encouragement during my study.

I would like to thank to the Center for Materials Research staff at İzmir Institute of Technology for their help and patience during my study.

I would like to appreciate deeply to all my friends for their help, support, motivation and friendship.

I would like to express my sincere thanks to Filiz KÜNÜROĞLU, Ozan HOŞKEN, Sinem BEZİRCİLİOĞLU and Yasir YAREN for their help and support.

I would also like to thank to Fikret ŞENEL for his help and contribution.

I would like to acknowledge Sarsılmaz Fişek San. A.Ş. for providing ballistic test facilities.

Finally, I would like to express my special thanks to my mother and father, Fehime and idris ERDOĞAN for their help, support, motivation and encouragement during this thesis and all through my life.

ABSTRACT

DEVELOPMENT OF LIQUID ARMOR MATERIALS AND RHEOLOGICAL BEHAVIOR OF SHEAR THICKENING FLUIDS (STFs)

Colloidal dispersions have been extensively used in many industrial applications such as cosmetic, paint, cement, lubricant and ceramic. Shear thickening is non-Newtonian flow behavior often observed in concentrated colloidal dispersions as an increase in viscosity with increasing shear rate or applied stress. Shear thickening fluids (STFs) exhibit fluid and solid-like properties depending on the shear rate and thus can be used in a variety of applications.

In the present study, STFs have been synthesized with various weight fractions of silica nanoparticles in polyethylene glycol (PEG)/ethyl alcohol by mechanical mixing method. The steady and dynamic rheological behavior of shear thickening fluids (STFs) was investigated with rheometer. STFs thermal properties were investigated through thermogravimetric analysis. STFs have been used to improve the performance of Kevlar woven fabrics for protective applications in ballistic and stab. STFs/Kevlar fabric composites have been prepared with different impregnation techniques to evaluate the effects of the STFs. The ballistic performance and stab resistance of STFs impregnated Kevlar fabrics were investigated.

Rheological measurements revealed the shear thickening effect of silica nanoparticles/PEG systems depending on the shear rate. In dynamic experiments, the strain thickening behavior was found at critical combination of strain amplitude and frequency. The viscous G'' modulus values were found to be greater than the elastic G' modulus. The elastic G' and the viscous G'' modulus values were found to increase when the strain amplitude is kept constant and frequency is increased. The same strain thickening behavior was also found when the frequency was kept constant and the strain amplitude was increased. The puncture resistance of STFs/Kevlar fabric composites exhibited significant improvements as compared to the neat Kevlar targets. Based on the SEM results, STFs were uniformly impregnated over the entire surface on the Kevlar fabric and Kevlar fabrics completely coated with STFs. The ballistic test results revealed STF/Kevlar fabric composites have potential to obtain liquid armor materials.

ÖZET

SIVI ZIRH MALZEMELERİNİN GELİŞTİRİLMESİ VE AKMA İLE KALINLAŞAN SIVILARIN REOLOJİK DAVRANIŞI (AKS)

Koloidal dağılımlar kozmetik, boya, çimento, yağ ve seramik gibi birçok endüstriyel uygulamalarda yaygın olarak kullanılmaktadır. Kayma kalınlaşan, genellikle koloidal dağılımlarda gözlenen artan kayma hızı veya uygulanan stres ile viskozitesinde bir artışla sonuçlanan Newtonian olmayan bir akma davranışıdır. Kayma kalınlaşan sıvılar (AKS) kayma hızına bağlı olarak sıvı ve katı-gibi özellikleri gösterirler ve bu nedenle çeşitli uygulamalarda kullanılabilmektedirler.

Bu çalışmada, AKS'ler mekanik karıştırma yöntemi ile PEG/etil alkol içerisinde çeşitli silika nanopartikül ağırlık oranlarında sentezlenmiştir. Kayma kalınlaşan sıvıların (AKS) kararlı ve dinamik reolojik davranışı reometre ile araştırılmıştır. AKSlerin termal özellikleri termogravimetrik analiz yöntemleri ile araştırılmıştır. AKS'ler balistik ve batma koruyucu uygulamalar için Kevlar dokuma kumaşlarının performansını artırmak için kullanılmaktadır. AKS/Kevlar kumaş kompozitler AKS'nin etkisini ortaya çıkarmak için farklı emdirme teknikleri ile hazırlanmıştır. AKS emdirilmiş Kevlar kumaşların balistik performansı ve delinme direnci araştırılmıştır.

Reolojik ölçümler silika nanopartikül/PEG sisteminin kayma hızına da bağlı olarak kayma kalınlaşma etkisinin olduğunu göstermiştir. Dinamik deneylerde, gerilme kalınlaşan davranışı kritik gerilme ve frekansının kombinasyonunda tespit edimiştir. Viskoz G'' modülünün elastik G' modülünden daha yüksek olduğu bulunmuştur. Gerilme genliği sabit tutulduğu ve frekans arttırıldığında, elastik G' ve vizkoz G'' modül değerlerinin arttığı bulunmuştur. Frekans sabit tutulduğu ve gerilme genliği artırıldığında aynı gerilme kalınlaşan davranışının olduğu tespit edilmiştir. AKS/Kevlar kumaş kompozitlerin delinme direnci Kevlar kumaşlarla karşılaştırıldığında önemli gelişmeler göstermiştir. SEM sonuçlarına göre, AKS'ler Kevlar kumaşların tüm yüzeyleri üzerinde homojen olarak emdirilmiştir ve Kevlar kumaşlar AKS ile tamamen kaplanmıştır. Balistik test sonuçları AKS/Kevlar kumaş esaslı kompozitlerin sıvı zırh malzemesi elde edebilmek için potansiyele sahip olduğunu göstermiştir.

TABLE OF CONTENTS

LIST OF FIGURES

LIST OF TABLES

LIST OF SYMBOLS AND ABBREVIATIONS

DDP	Didodecyl Phthalate
DLS	Dynamic Light Scattering
DOP	Dioctyl Phthalate
Flow-SANS	Flow Small Angle Neutron Scattering
FTIR	Fourier Transform Infrared Spectroscopy
G	Shear Modulus (Pa)
G'	Shear storage Modulus (Pa)
G''	Shear loss Modulus (Pa)
$G*$	Complex Shear Modulus (Pa)
η	Viscosity (Pa·s)
$\eta*$	Complex Viscosity (Pa·s)
$\eta_{\circ}$	Limiting Viscosity at Zero Shear Rate (Pa·s)
η_{∞}	Limiting Viscosity at Infinite Shear Rate (Pa·s)
γ	Shear Strain
$\dot{\gamma}$	Shear rate (s^{-1})
γ_c	Critical Shear Rate
σ	Shear Stress (Pa)
ω_c	Critical Frequency
ϕ	Volume Fraction
MMA	Methyl Methacrylate
PMMA	Poly(Methyl Methacrylate)
PEG	Poly(Ethylene Glycol)
PEO	Poly(Ethylene Oxide)
PSAN	Poly (Styrene Acrylonitrile)
PVC	Poly (Vinyl Choloride)
SANS	Small Angle Neutron Scattering
SEM	Scanning Electron Microscopy
TPM	3-(trimethoxysily) Propyl Methacrylate
TGA	Thermal Gravimetric Analysis
THFFA	Tetrahydrofurfural Alcohol

CHAPTER 1

INTRODUCTION

Colloidal dispersions have been used in a wide variety of applications in food, paint and ceramic industries which are just few instances. In order to produce those dispersions, their flow behaviour is one of the most important properties that should be well understood. This is particularly related to concentrated dispersions. Since the beginning of this century, the rheological properties of concentrated dispersions have been the topic of the research. In recent years, interest in the rheology of suspensions has greatly increased and there have been more interest in the topic of shear thickening in concentrated dispersions (Boersma et al., 1990). In addition, the concentrated dispersions show widely varying rheological properties, which can define shear thinning, shear thickening, thixotropy and yield stress. There have been lots of investigations about these dispersions which were related to the steady shear properties (Boersma et al., 1992).

Shear thickening is non-Newtonian flow behaviour and defined in the British Standard Rheological Nomenclature as the increase of viscosity with increase in shear rate. This is distinguished from rheopexy which is described as the increase of viscosity with time while the shear rate in constant. Dilatancy is another term used to define shear thickening, however, it has been avoided since it typically implies an increase in the volume on deformation, which is not considered in this situation (Barnes, 1989).

There are many colloidal suspensions such as photographic dies, paints, coatings and lubricants and they are subjected to rapid shearing during processing. In some cases when the shear force become strong enough to drive shear thickening, which is indicated by a rapid, sometimes discontinuous in viscosity with small increases in shear rate. The dramatic viscosity increase in shear thickening fluids can damage processing equipment and induce dramatic changes in suspension microstructure such as particle aggregation, which causes in poor fluid and coating qualities. On the other hand, this shear thickening phenomenon can be utilized in the design of damping and control devices, whereby the fluid can limit the maximum rate of flow through a highly nonlinear response (Bender and Wagner, 1996).

Shear thickening fluids (STFs) are concentrated colloidal suspensions, which are composed of non-aggregating solid particles suspended in a carrier fluid and exhibit a marked increase in viscosity beyond a critical shear rate, which is defined as hydrodynamic clustering effects **(**Fischer et al., 2006).

Nanoparticles have been used for many industrial applications, which are faster, smarter, and more convenient communication components and devices. It was observed that dispersions, which are consisting of particles from micrometers to nanometers in size show, shear thickened state at properly high shear stresses (Lee and Wagner, 2006).

Highly concentrated suspensions show thickening behaviour at high shear rates, which increase in viscosity with increasing shear rate. On the other hand, viscosity can exhibit thickening behaviour with a large and discontinuous jump at critical stress. Conversely, at lower volume fractions and lower stresses opposite effect have been observed. These suspensions display thickening, involving colloids of monodisperse spherical particles. The microstructural origins of thickening are not resolved. Some have seen it as a general feature of nonequilibrium phase diagrams resulting from an increase in particle Reynolds number, others as a mechanical instability of layered flow. Some theories emphasize the competition between conservative repulsive forces and hydrodynamic forces. Some have speculated on the role of Brownian forces either as a source of mechanical instability of layer flow or as relaxation mechanisms for clusters. Thickening has been seen in a number of molecular dynamics simulations, but a simulation study of colloids showed thickening and clustering owing to different lubrication interactions (Melrose et al., 1996).

This phenomenon has been found in colloidal dispersions, which are related to strong viscous flow and observed by a rapid or even discontinuous increase in viscosity above a critical shear rate. In order to explain shear thickening behavior the order-diorder transition and “hydroclusters” mechanism have been proposed (Maranzano and Wagner, 2002).

The reversible shear thickening in concentrated colloidal suspensions was found to be owing to the formation of jamming clusters resulting from hydrodynamic lubrication forces between particles, often denoted by the term “hydroclusters”. Also, the mechanism of shear thickening has been studied extensively by rheo-optical experiments, neutron scattering and stress-jump rheological measurements. The onset of shear thickening was found to predict for colloidal suspensions of hard-spheres and electrostatically stabilized dispersions (Lee et al., 2003).

The shear thickening fluids have been used to improve the performance of the Kevlar woven fabrics for protective applications in ballistic and stab. The ballistic penetration resistance of Kevlar fabric is enhanced by impregnation of the fabric with a shear thickening fluid. Impregnated STF-fabric composites are indicated to provide superior ballistic protection as compared with simple stacks of neat fabric and STF. The shear thickening effect was found to be critical to achieving enhanced performance (Lee et al., 2003). The typical defence/protection materials applications of STFs are presented in Figure 1.1.

The stab resistance of shear thickening fluid impregnated fabrics is explored and found to show significant improvements over neat fabric of equivalent areal density. Impressive improvements in puncture resistance are observed (Decker et al., 2007; Hassan et al., 2010).

The objective of this study is to develop the shear thickening fluids, which are composed of nanoparticles in a carrier fluid. Fabrication of the Kevlar woven fabrics impregnated with a colloidal shear thickening fluids, characterization of their puncture resistance and evaluation of the ballistic performance of the liquid armor system are the objective of this study. Investigations of the rheological and thermal properties of the shear thickening fluids are also the aim of the present work.

Figure 1.1. Typical defence/protection applications of shear thickening fluids (STFs)

CHAPTER 2

SHEAR THICKENING FLUIDS

2.1. Mechanism of Shear Thickening

Concentrated colloidal suspensions at high shear rate demonstrate shear thickening effect, which is the increase of viscosity with increasing shear rate. At volume fractions approaching close packing, discontinuous thickening with a large jump in viscosity can occur at a critical shear stress. On the other hand, at lower volume fractions and lower stresses a more continuous rise is often reported. Many systems show thickening, including colloids of monodisperse spherical particles. The important parameters that control the shear thickening are particle size distribution, particle volume fraction, particle shape, particle particle interactions and viscosity of suspended phase and the type, rate, and time of deformation. All of these parameters have been studied to some extent (Barnes, 1989).

Altough the technological significance of controlling this phenomenon, there has been little attempt in order to investigate the microstructural origins of shear thickening in colloidal suspensions (Bender and Wagner, 1996).

Shear thickening of colloidal dispersions is of considerable scientific and technical importance. Experimental and theoretical investigations have provided insights into understanding the underlying mechanism of the shear thickening process (Krishnamurthy et al., 2005).

The onset of shear thickening transition is found to be related with a structural change within the suspension. Sometimes known as discontinuous or critical dilatancy, this phenomenon is characterized by the material displaying a sudden increase in the viscosity as a function of shear rate or shear stress. The change in microstructure at the onset of shear thickening has been observed in different types of suspensions. (Hoffman, 1972; Barnes, 1989; Boersma et al., 1991; Laun et al., 1992; Chow and Zukoski, 1995).

To predict the onset of thickening from colloidal parameters, micromechanical models have been developed by several researchers (Hoffman, 1974; Boersma et al., 1990).

To understand the mechanism of shear thickening a great number of work has been reported in the literature. To date, two different mechanisms have been proposed to explain these fluids behaviour: The order-disorder theory and ‘‘hydrocluster’’ theory. All of the mechanism involve structural transitions. In the case of extreme or discontinuous shear thickening behavior the fluid response at the critical shear rate has been difficult to study since most rheometer operated by controlling the imposed deformation rate. Recently, with the improvement of stressed controlled rheometers and with the help of additional techniques which can characterized microstructure of colloidal dispersions by small angle neutron scattering and rheo-optical devices. This has allowed for understanding shear thickening phenomenon and its microstructure (Frith et al., 1996). Stokesian Dynamics techniques are also commonly used to understand the behavior of shear thickening in the suspensions (Brady and Bossis, 1988; Melrose et al., 1996).

Hoffman was the first to propose a mechanism for shear thickening. He observed that monodisperse polyvinyl chloride spheres in dioctyl phthalate have shear thickening behavior in the apparent viscosity and he also obtained similar results with suspensions of (poly) styrene- acrylonitrile, polystyrene and polyvinyl toluene spheres in ethylene glycol. In this case the flow curve shows a sudden jump in viscosity at a certain critical shear rate. This increase could be as much as two orders of magnitude, and be either continous or discontinous. This transition occured from a two dimensional ordered state of hexagnally packed layers to a disordered state. Experimental evidence for an order–disorder transition accompanying shear thickening is provided by small angle light scattering (Hoffman, 1972).

This transition was considered to be shear rate dependent. At sufficiently high rates of shear, the shear stress between layers is sufficient over come the forces holding the sphere in layers (Hoffman, 1974).

Boersma et al. (1990) focused on the mechanism of the shear thickening to develop a new model. Based on the assumption that shear thickening is a consequence of a order-disorder transition, they proposed that the critical shear rate for thickening can be obtained from a balance between the electrostatic and shear forces acting on a pair of particles. They also simplfied Hoffman’s orginal analysis. This model provided a

correct estimate of the critical shear rate was considered evidence that an order-disorder transition drives shear thickening.

Another mechanism to explain shear thickening behaviour is ‘‘hydrocluster’’ theory. Evidence for the hydrodynamic basis of this phenomenon is provided by rheo-optical experiments and stress-jump rheological measurements. In addition, small angle neutron scattering (SANS) measurements of the shear induced microstructure support that shear thickening is accompanied by the formation of a microstructure qualitatively consistent with hydrocluster formation. This theory firstly suggested by Brady on the basis of Skosian Dynamics simulations (Bossis and Brady, 1989).

The state of shear thickening is found to be related with the formation of hydrodynamic clusters and hydrodynamic lubrication forces, which dominate all other colloidal forces in the shear thickening suspension. This is provided by rheo-optical experiments (Bender and Wagner, 1996). Small angle neutron scattering measurements were also used to investigate the fluid microstructure in both shear thinning and shear thickening region (Laun et al., 1992).

Bender and Wagner (1996) have proposed that altough order-disorder transition may occur during in some dispersions of charged particles, the order-disorder transitions are neither necessary nor sufficient to explain shear thickening. Both hydrodynamic cluster theory and Hoffman’s theory are the neccesary role of hydrodynamic interactions in driving the shear thickening transition.

Frith et al. (1996) showed that shear thickening is greatly affected by the nature of the particle surface. Particle-particle interactions depend on the nature of the particle surface. Shear thickening occurs when the hydrodynamic forces overcome the strongest stabilizing force, which may be a Brownian, steric or electrostatic force.

The shear thickening and strain thickening behavior of fumed silica suspensions under steady and oscillatory shear was provided to support to the cluster theory. The term strain thickening was presented to define an abrupt increase of the complex viscosity η^* at critical combination of strain amplitude and frequency. The combination of shear and strain thickening behavior was based on the temporary flow-induced clusters (Raghavan and Khan, 1997).

2.2. Order-Disorder Theory

Shear thickening and discontinuous viscosity behavior are observed in suspensions containing monosized spheres of polyvinyl chloride, (poly) styrene-acrylonitrile, polystyrene and polyvinyl toluene when the volume fraction of solids ranges from 0.46 to 0.60. The discontinuous viscosity behavior which occurs at solids concentrations above 0.50 is caused by a flow instability in which surfaces of spheres, packed in two dimensional hexagonal packing at low shear rates, break up into less ordered arrays of spheres.

The order-disorder transition was firstly proposed by Hoffman. According to this theory, Hoffman suggest that forces of attraction and repulsion acting between particles in the suspension interact with the forces of shear field to cause the formation of surfaces of two dimensional, hexagonally packed spheres which pass one over another in the direction of flow. As one increases the relative velocity of these neighboring surfaces of spheres the shear stress transmitted from one surface to the next through the interstitial fluid increased. Some critical value of the shear stress is finally reached at which the shear stress couple on the surfaces of hexagonally packed spheres is just sufficient to overcome the forces between the spheres which hold them in place. When this happens sections of the ordered flow occurs. The extra energy required by the spheres when they jam into one another during flow causes the discontinuous jump in the apparent viscosity at the instability point. In this theory evidence for the ordered arrangement of the spheres and the order-disorder transition is provided by white light diffraction (Hoffman, 1972).

2.3. Hydrocluster Theory

‘‘Hydrocluster’’ theory has been proposed to explain shear thickening behavior of concentrated suspension. This theory was attributed to a model that explains for the force balance between the hydrodynamic forces imposed by a shearing flow and forces arising by interparticle interactions. Based on this theory, at low stresses interparticle interactions, which are electrostatic and Brownian allow the particles to easily past each other. This occurs in low viscosity state. As the stress is increased the hydrodynamic lubrication forces between the particles dominate all the other colloidal forces. As the

lubrication and interparticle forces are of the same order of magnitude, the particles in suspension ‘jam’ into stress bearing cluster, often denoted by the term ‘‘Hydrocluster’’ (Bossis and Brady, 1989; Bender and Wagner, 1996).

2.4. Definition of Shear Thickening Phenomenon

Shear thickening fluid (STF) is a category of non-Newtonian fluid behavior in which the viscosity increases as a function of shear rate or shear stress at some critical parameter range. A particularly dramatic form, often called shear thickening, which occurs in many concentrated suspensions. These suspensions can be like a thin liquid when stirred slowly, then very thick like a solid when stirred harder and become thin again when the stress is removed. The rheology of a shear thickening fluid as function of the particle size, shape and size distribution, the particle density, charge, roughness, and in some cases the chemical interaction between the particle surface and carrier fluid. Furthermore, the important parameters control the shear thickening, which are size, size distribution, shape, particle-particle interaction and volume fraction of the particles and viscosity of suspended phase (Barnes, 1989). Maranzano and Wagner (2001) showed that the onset of reversible shear thickening depends on the particle size, concentration, polydispersity and interparticle interaction of dispersion at a critical stress.

2.4.1. Effect of Volume Fraction

The rheology of shear thickening fluids depends significantly on the volume fraction of the suspension. In order to observe shear thickening effects the volume fraction needs to be high enough that the particles feel each other’s presence, that is, the particle force field and behavior is affected by the presence of the surrounding particles. These interparticle forces depend on the particle charge as well as the polarity of the fluid. Because of this, it is difficult to define a critical volume fraction at which shear thickening is observed to occur. It should be noted that there has been found three different regions in the rheolgy of the suspension in terms of the volume fraction as shown in Figure 2.1.

1. An increase in the overall viscosity as volume fraction is increased.
2. The critical shear rate for the onset of shear thickening increases as the volume fraction decreases. As volume fraction increases the critical shear rate decreases.
3. An increase in the magnitude of the viscosity jump as the volume fraction increases.

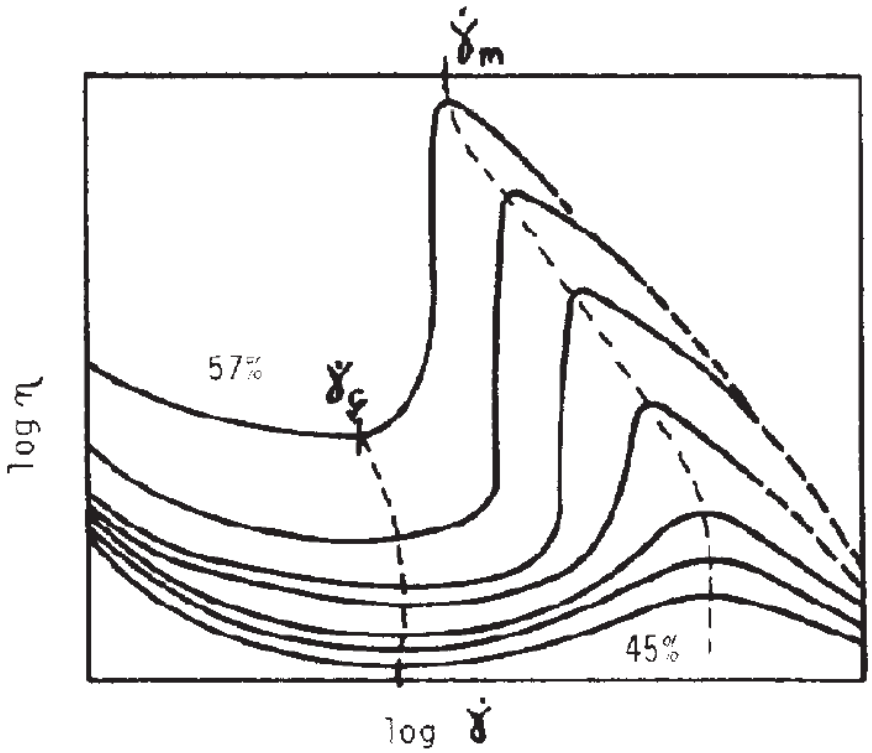

Figure 2.1. Shematic representation of viscosity versus shear rate for shear thickening systems, with approximate phase volume as parameter. Also shown are the loci of $\dot{\gamma}_c$ and $\dot{\gamma}_m$, the shear rates at the beginning and the end of the shear thickening region (Source: Barnes, 1989)

At high volume fractions the relation becomes more complex and even small changes in volume fraction result in large variation of viscosities. Furthermore, at very high volume fraction the viscosity becomes extremely sensitive to the roughness in homogeneity, shape of the particles.

It has also found that critical shear rate and shear stress for the onset of the shear thickening decreases with increasing volume fraction. As the number of the particles in suspension decreases the particles can be farther apart from each other, one needs to impose a greater stress to increase the size of the hydrocluster. This change in critical

stress is not linear in volume fraction. Barnes showed that the critical shear stress is very high at lower volume fraction (below ≈ 45%). The volume fraction around 50%, where the particles are very close to each other and it is easy to form hydrocluster. The critical shear stress decreases rapidly as the volume fraction greater than 50% (Barnes, 1989).

2.4.2. Effect of Particle Size

The rheology of shear thickening fluids depends on the particle size of the particles. Many studies have focused on the particle size dependence of the suspension rheology on the prediction of the critical stress. The values of the particle sized varied between 27 nm to 200 μmeter, while the corresponding critical shear rates varied between 5×10^{-3} to 1.5×10^{-4} s^{-1} (Barnes, 1989).

2.4.3. Effect of Particle Size Distribution

The particle size distribution of the particles in suspension also affects maximum value of volume fraction. The shear thickening effect strongly depends on the form of the particle size distribution. As the particles are of different size they can pack more efficiently because smaller particles can fit within the voids between the larger particles which allows for greater volume fractions. Two different suspensions, which are monodisperse and polydisperse particles in suspension with the same volume fraction can show different shear thickening effect. The monodisperse suspension will show a stronger shear thickening effect at a lower critical stress as compared to the polydisperse suspension. This relates to the fact that polydisperse suspension more efficiently. Because of that particles are farther from each other at constant volume fraction. Consequently, the broader the particle size distribution, the higher the critical shear stress and less severe shear thickening (Barnes, 1989).

Additionally, Bender and Wagner (1996) showed that they were able to control, and increase the critical stress by increasing the ratio of small to large particles. The particles used in their study were monodisperse silica spheres, which were elecrostatically stabilized.

2.4.4. Effect of Particle Shape

The shape of the particles in a suspension has also great influence on the resulting rheology. Non-spherical particles tend to align with the flow field and indicate greater elastic effect, which is including normal stress differences in spherical particles suspension.

Furthermore, suspension of anisotropic particles demonstrates non-Newtonian behavior. Shear thinning is related with low volume fraction as compared to the spherical particles suspensions. On the other hand, spherical particles suspensions begin to show shear thinning behavior at volume fractions above 30%. Additionally, the rheology of suspensions of anisotropic particles shows a smaller critical stresses for the onset of shear thickening and the thickening is also observable at lower volume fractions than for spherical particles suspensions (Barnes, 1989).

Egres and Wagner (2005) found shear thickening behavior using acicular precipitated calcium carbonate particles in poly(ethylene glycol) (PEG). The results showed that increase in particles aspect ratio (in ratio ranged between 2-7) improves shear thickening effect that can be observed at much lower volume fraction as compared to the spherical particles.

2.4.5. Effect of Particle-Particle Interaction

Interparticle interactions are extremely important in determining the shear thickening response of a suspension. The rheology of shear thickening fluids depends significantly on the particle-particle interaction of the suspension. Flocculated suspensions show high viscosity at low shear rate and at higher shear rates shear thinning. These suspensions indicate thixotropy. Conversely, deflocculated suspensions display shear thickening at high shear rate and low viscosity at low shear rates, which is rheopexy. To observe shear thickening, the particles in the suspension need to be neutral as Brownian, hard spheres or repel each other electrostatically charged particles. Suspensions of hard spheres tend to show less severe shear thickening as compared to electrostatically charged particles. The shear thickening effect is found to be much more severe at the higher the surface charge (Barnes, 1989; Maranzano and Wagner, 2001).

2.4.6. Effect on the Viscosity of Carrier Fluid

The overall viscosity is directly related with the continuous phase viscosity in suspensions. The rheology of shear thickening fluids is found to be strongly dependent with the viscosity of carrier fluid in suspensions. In order to understand the effect of the temperature on the carrier fluid viscosity heating has been used. Heating can cause not only a change in particle-particle interaction, but also decrease in the carrier fluid viscosity. The effect of Brownian motion is observed to increase with temperature (Barnes, 1989).

2.5. Rheology of Shear Thickening Fluids

2.5.1. Definition of Rheology

Rheology is a science dealing with deformation and flow of matter. Relationships between stresses and deformations are the fundamental concepts of continuum mechanics, which are related to the rheology. Becasue of the fact that rheology means the study of flow and deformation. Basically, rheology includes everything dealing with flow behavior: aeronautics, hydraulics, fluid dynamics, and even solid mechanics. On the other hand, in practice rheology has usually been restricted to the study of the fundamental relations, which are called constitutive relations, between force and deformation in materials, primarily liquids. Bingham observed unusual flow behavior in concentrated suspensions like paint. Because of this, the rheologist focuses on material behavior, using very simple deformations, while the mechanicist studies the forces developed in complex deformation, applying the constituve relations developed by the rheologist (Macosko, 1994).

The term “Rheology” was invented by Professor Bingham of Lafayette College, Indiana, on the advice of a colloeague, the Professor of Classics. It means *the study of the deformation and flow of matter***.** This definition was accepted when the American Society of Rheology was founded in 1929. That first meeting heard papers on the properties and behavior of such widely differing materials as asphalt, lubricants, paints, plastics and rubber, which gives some idea of the scope of the subject and also the numerous scientific disciplines which are likely to be involved. Nowadays, the scope is

even wider. Significant advances have been made in biorheology, in polymer rheology and in suspension rheology. There has also been a significant appreciation of the importance of rheology in the chemical processing industries. Opportunities no doubt exist for more extensive applications of rheology in the biotechnological industries. There are now national societies of rheology in many countries. The British Society of Rheology, for example, has over 600 members made up of scientist from widely differing backgrounds, including mathematics, physics, engineering and physical chemistry (Barnes et al., 1989).

In 1678, Robert Hooke developed his "*True Theory of Elasticity*". He proposed that "the power of any spring is in the same proportion with the tension thereof", *if you double the tension you double the extension*. This forms the basic premise behind the theory of classical (infinitesimal-strain) elasticity. At the other end of the spectrum, Isaac Newton gave attention to liquids and in the "Principia" published in 1687 there appears the following hypothesis related with the steady simple shearing flow shown in Figure 2.2. "The resistance which arises from the lack of slipperiness of the parts of the liquid, other things being equal, is proportional to the velocity with which the parts of the liquid are separated from one another" (Barnes et al., 1989).

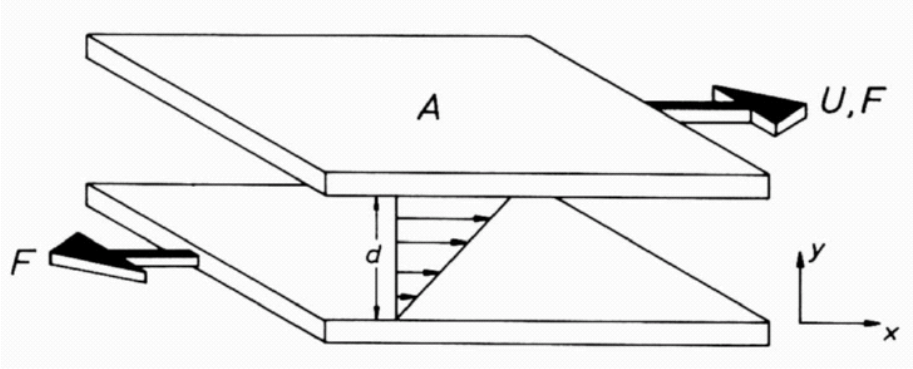

Figure 2.2. Showing two parallel planes, each of area A, at y = 0 and y = d, the intervening space being filled with sheared liquid. The upper plane moves with relative velocity U and the lengths of the arrows between the planes are proportional to the local velocity v_x in the liquid
(Source: Barnes et al., 1989)

This lack of slipperiness is defined as viscosity. It is synonymous with "internal friction" and is a measure of "resistance to flow". The force per unit area required to produce the motion is F/A and is denoted by a and is proportional to the 'velocity

gradient' (or 'shear rate') U/d, if you double the force you double the velocity gradient. The constant of proportionality η is described as the coefficient of viscosity,

$$\sigma = \eta U / d \tag{2.1}$$

In general, it can be written $\dot{\gamma}$ for the shear rate U/d. Although Newton introduced his ideas in 1687, it was not until the nineteenth century that Navier and Stokes independently developed a consistent three-dimensional theory which is defined as a Newtonian viscous liquid. For these fluids the equations, which are called the Navier-Stokes equations. For the simple shear illustrated in Figure 2.3. a 'shear stress' a results in 'flow'. In the case of a Newtonian liquid, the flow persists as long as the stress is applied. Conversely, for a Hookean solid, a shear stress a applied to the surface $y = d$ results in an instantaneous deformation as shown in Figure 2.2. When the deformed case is reached there is no further movement, but the deformed case continues as long as the stress is applied. The angle γ is called the 'strain' and the relevant 'constitutive equation' is as below;

$$a = Gy \tag{2.2}$$

where G is referred to as the 'rigidity modulus'.

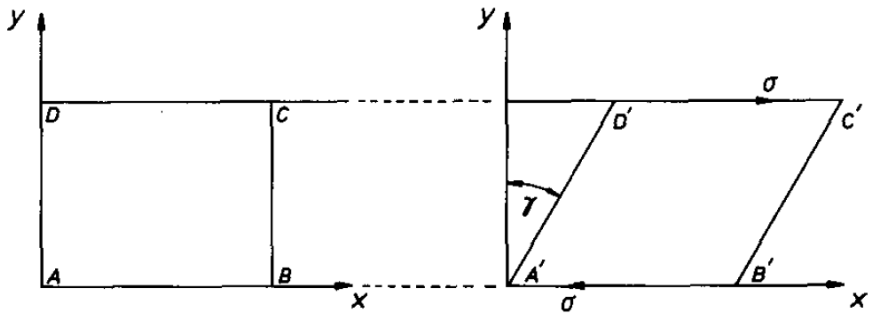

Figure 2.3. The result of the application of a shear stres σ to a block of Hookean solid. On the application of the stress the material section ABCD is deformed and becomes A'B'C'D' (Source: Barnes et al., 1989)

Rheology is the science associated with the deformation and flow of matter. Flow is a continuous irrevirsible deformation hindering by the external and internal friction of the flowing matter. The internal resistance to flow is showed as the viscosity, η, or fluidity, which is the reciprocal of viscosity, $1/\eta$. Viscosity is an internal friction, which is described as the retarding influence of a stationary layer on a moving paralel layer. As the shear stress, τ, which is defined as force per unit area, that is applied parallel to the imaginary layers in liquid system, each layer will move at a velocity which depends on the distance from the plane to which the force is applied. The velocity gradient dv/dx, perpendicular to the plane, which is called the shear rate, γ, or the rate of shear strain. According to the Newton's law the shear rate is proportional to the applied force:

$$\tau = \eta \frac{dv}{dx} = \eta\gamma \tag{2.3}$$

The proportionality factor, η, which is denoted as the viscosity coefficient. The liquids obeying Newton's law are called Newtonian liquids and η is then a constant. On the other hand, most practical dispersions and suspensions of technical ineterest do not obey Newton's law. The viscosities of non-Newtonian fluids are not independent of shear stress or, conversely, of the shear rate. Therefore, a one-point meausurement of their viscosity gives the apparent viscosity only for given shear rate or stress.

For many applications, the main interest is that the shear stress. Because shear stress can predict the force needed to move a fluid at the desired velocity. The primary importance of the shear stress may be practical reason for plotting the shear stress versus the shear rate. The shear stress versus shear rate curves are shown in Figure 2.4. that illustrate most common flow types. The slope of these flow curves, $\mathrm{d}\tau/\mathrm{d}\gamma$, is equal to the apparent viscosity at the corresponding shear rate. For Newtonian systems, the plot gives a straight line with a constant slope, which shows the viscosity. For non-Newtonian liquids the shape of the curve reveals the category of the flow. Some fluids indicate, in addition to viscous flow, elastic behavior. The viscosity depends on the shear rate (shear thinning or thickening or time-dependent (thixotropy or rheopexy) (Kissa, 1999).

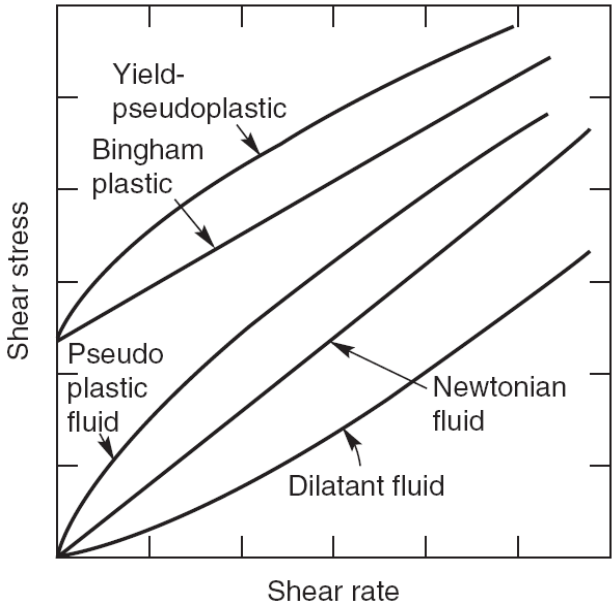

Figure 2.4. Flow curves shear stress versus shear rate representing different flow behavior (Source: Chhabbra, 2008)

When the viscometers became available to investigate the effect of shear rate on viscosity, investigations were found different from Newtonian behaviour for many materials, such as dispersions, emulsions and polymer solutions. In the most of cases, the viscosity was found to decrease with increasing the shear rate, which is generally called 'shear-thinning' behaviour although the terms temporary viscosity loss and 'pseudoplasticity'. For shear-thinning materials, the general shape of the curve representing the variation of viscosity with shear rate is shown in Figure 2.5 (Barnes, 1989).

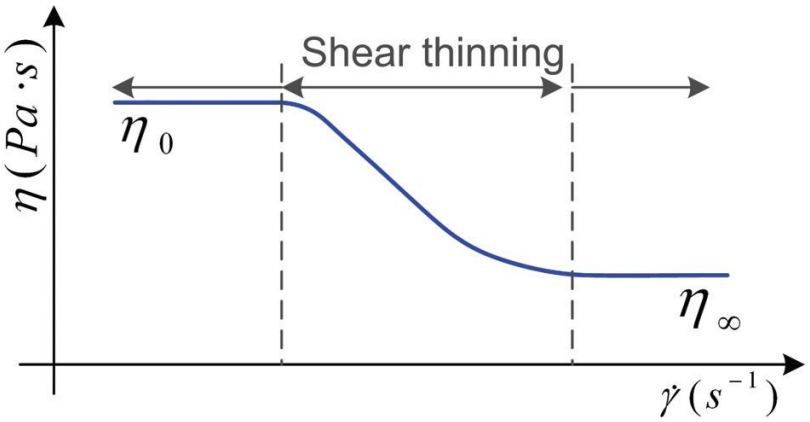

Figure 2.5. Typical viscosity curve for a shear thinning behaviour containing the three regions: The two limiting Newtonian viscosities, η_0 and η_∞, separated by a shear thinning region (Source: G-Rosales and R-Hernández, 2010)

Most of the non-Newtonian fluids, which are foods, biofluids, personal care products and polymers show shear thinnning behavior. Their viscosity decreases with increasing shear rates. These fluids indicate three distinct regions, which are a lower Newtonian, a middle and an upper Newtonian region (Galindo-Rosales and Rubio-Hernández, 2010).

The curve indicates that in the limit of very low shear rates (or stresses) the viscosity is constant, while in the limit of shear rates (or stresses) the viscosity is again constant, but at a lower level. These two extremes are sometimes known as the lower and upper Newtonian regions, respectively, the *lower* and *upper* referring to the *shear rate* and not the viscosity. The terms "first Newtonian region" and "second Newtonian region" have also been used to describe the two regions where the viscosity reaches constant values. The higher constant value is called the "zero-shear viscosity".

It is possible that the very act of deforming a material can cause rearrangement of its microstructure such that the resistance to flow increases with shear rate. Typical examples of the shear-thickening phenomenon are given in Figure 2.6. It can be observed that the shear-thickening region extends over only about a decade of shear rate. In this region, the power-law model can usually be fitted to the data with a value of ***n*** greater than unity. In almost all known cases of shear-thickening, there is a region of shear-thinning at lower shear rates (Barnes, 1989).

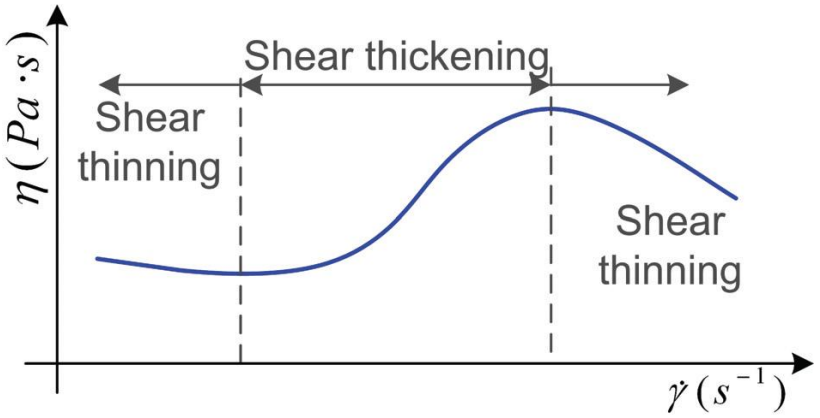

Figure 2.6. Typical viscosity curve for a shear thickening behaviour containing the three regions: The two limiting shear thinning behaviours separated by a shear thickening region (Source: G-Rosales and R-Hernández, 2010)

Figure 2.6. exhibits the viscosity curve for a STF, which include the three characteristic regions, which are slight shear thinning at low shear rates, followed by a sharp viscosity increase over a threshold shear rate value (critical shear rate), and a subsequent pronounced shear thinning region at high shear rates. The physics of the phenomenon is deeply understood through the use of modern rheometers, scattering techniques, rheo-optical devices and Stokesian dynamic simulations.

For shear thickening fluids only the power-law model, given by Equation 2.4, were commonly used (Galindo-Rosales and Rubio-Hernández, 2010).

$$\eta(\dot{\gamma}) = k\dot{\gamma}^{n-1} \tag{2.4}$$

This is the well known"*power-law*" model, which is called the power-law index k is a constant and called the 'consistency' index and n is termed the flow index, which indicates the degree of deviation from Newtonian behavior (n = 1). The system is shear thinning (pseudoplastic), if $n < 1$, and shear thickening, if $n > 1$ (Kissa, 1999).

2.5.2. Steady Shear Rheology

Hoffman (1972) investigated the rheological behavior of well-stabilized monodisperse polyvinyl choloride (PVC) dispersions in dioctyl phthalate (DOP). He used monosized spheres of polyvinyl chloride (PVC) and crosslinked (poly) styrene-acrylonitrile (PSAN) containing 68% styrene, 2% divinylbenzene and 30% acrylonitrile to obtain concentrated colloidal dispersions. The results clearly showed that dilatant and discontinuous viscosity behavior in suspensions when the volume fraction of solids ranges from 0.46 to 0.60. The viscosity versus shear rate curve is illustrated in Figure 2.7. It can be seen that the discontinuous viscosity behavior which occurs at solids concentration above 0.46.

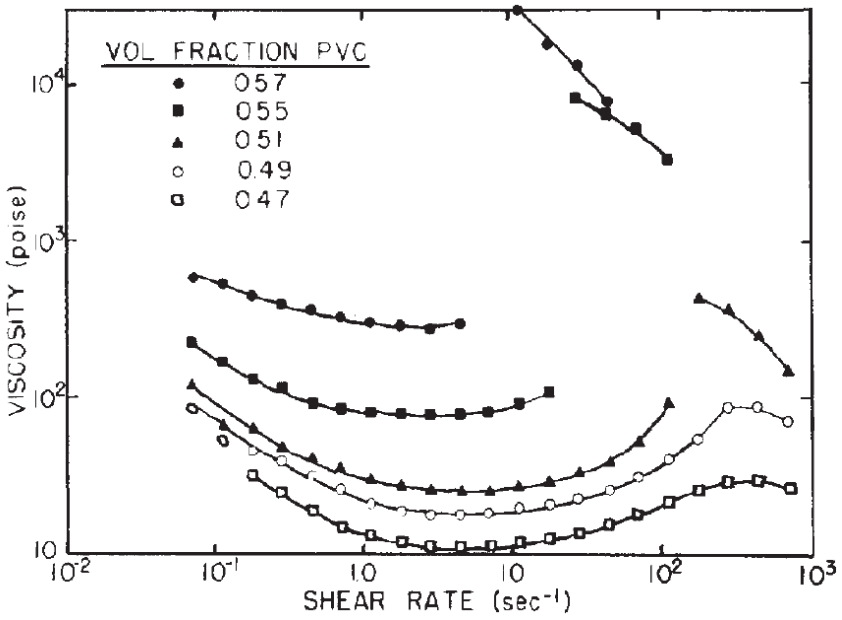

Figure 2.7. Effect of volume fraction of 1.25 μm PVC particles in dioctyl phthalate (Source: Hoffman 1972)

Boersma et al. (1990) studied the steady shear rheology in different suspensions. They used polyvinyl chloride (PVC) in dioctyphthalate (DOP), polystyrene in a glycerol/ water (86.1/13.9 w / w) mixture, silica (SiO_2) in glycerol / water (86.1/13.9 w / w), glass particles in glycerol / water (86.1/13.9 w / w) to achieve concentrated colloidal dispersions. It was found that with polydisperse dispersions the increase in viscosity at the critical shear rate is still drastic but less dramatic and more gradual than with monodisperse dispersions. On the other hand, the results at lower shear rates indicate a Newtonian region, absence of a yield stress with all dispersion system except the PVC in DOP system, for which the Newtonian plateau is not clear. Furthermore, it can be seen that concentrated dispersions often show shear thinning region at lower shear rates. At high shear rates it is difficult to see the existence of a Newtonian plateau due to excessively high stress levels. The viscosities as a function of shear rate are shown in Figures 2.8 to 2.11 for different dispersions. It can be seen that both the dispersions of monodisperse and the dispersions of polydisperse particles show strong shear thickening.

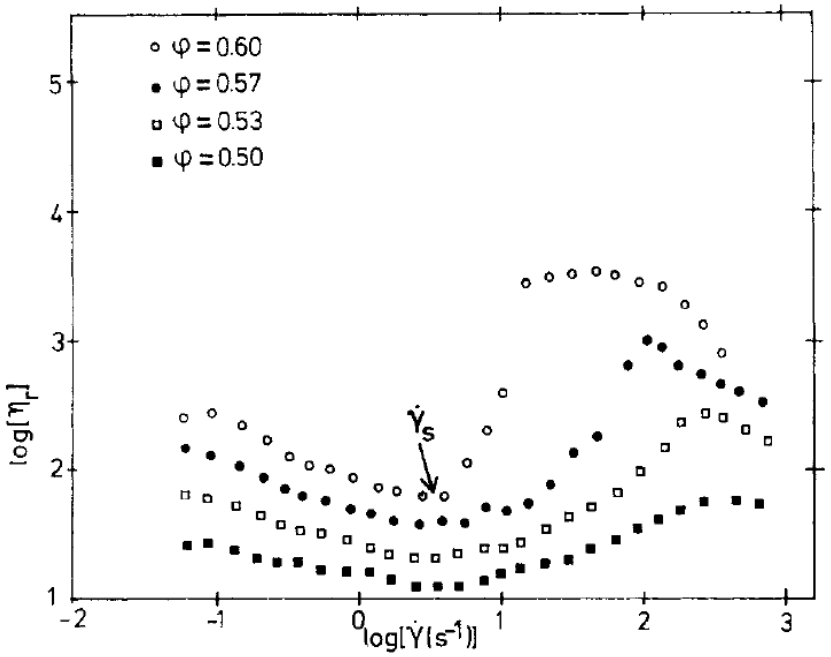

Figure 2.8. Viscosities as a function of shear rate for dispersions of PVC in DOP at 25°C (Source: Boersma et al., 1992)

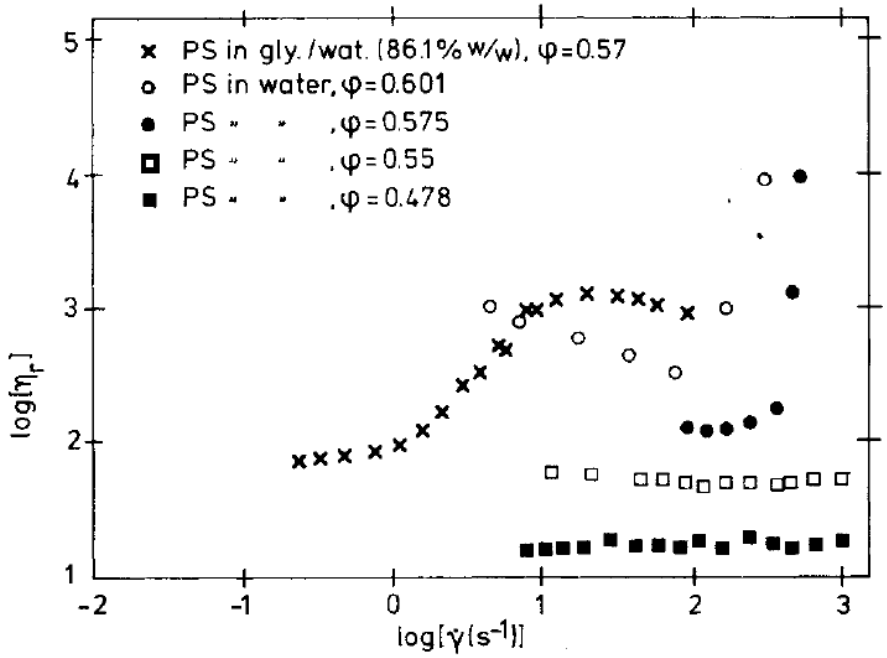

Figure 2.9. Viscosities as a function of shear rate for dispersions of PS in water and in glycerol/water (86.1% w / w) at 20 °C (Source: Boersma et al., 1992)

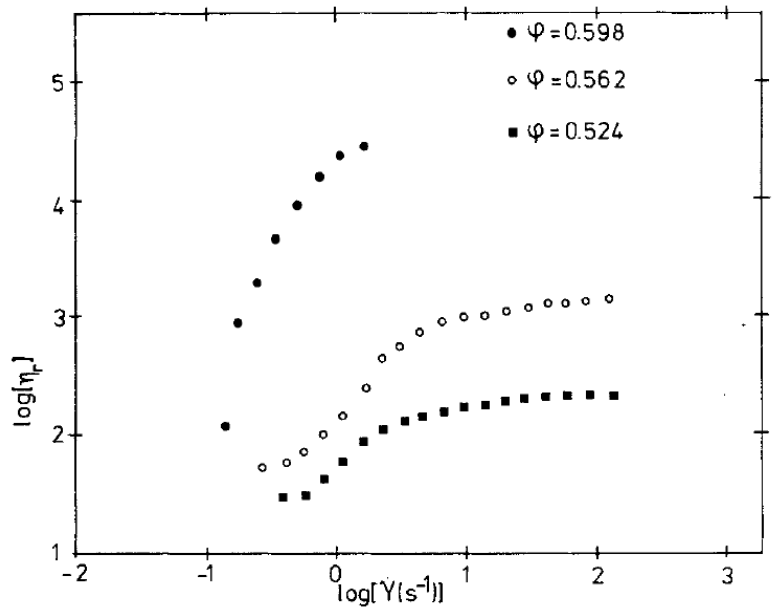

Figure 2.10. Viscosities as a function of shear rate for dispersions of SiO_2 glycerol / water (86,1% w / w) at 20 °C (Source: Boersma et al., 1990)

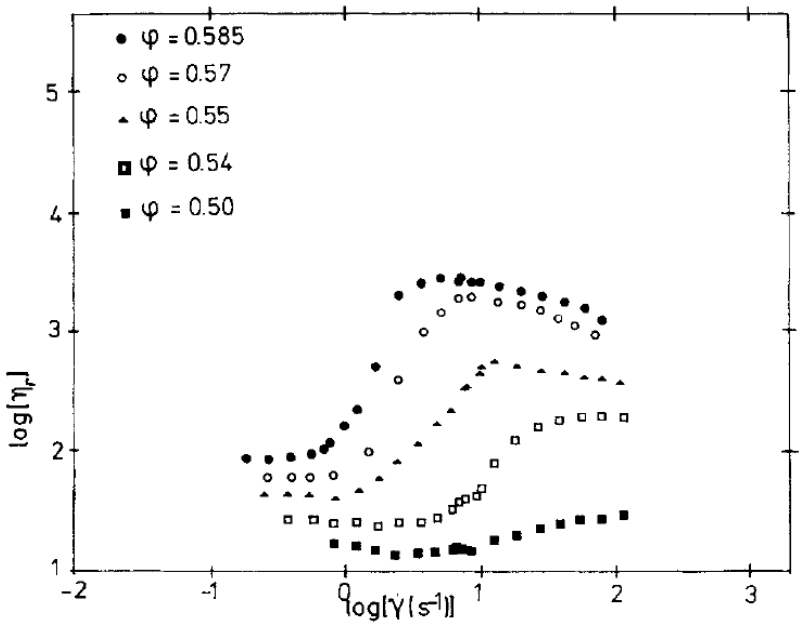

Figure. 2.11. Viscosities as a function of shear rate for dispersions of glass in glycerol / water (86,1% w / w) at 20 °C (Source: Boersma et al., 1990)

Concentrated dispersions of monodisperse electrostatically stabilized polymer spheres in polar dispersants like water or glycol indicate different regimes in the shear viscosity function. In the region of low shear rates pronounced shear thinning was observed, wheresas at high shear rates strong shear thickening was found (Laun et al., 1991).

Laun et al. (1992) investigated shear-induced particle structures of rheologically well-chracterized concentrated polymer dispersions in a wide range of shear rates. The dispersions consist of electrostatically stabilized styrene-ethylacrylate-copolymer spheres in glycol or water. Their viscosity functions show pronounced shear thinning and strong shear thickening versus shear rate as measured by various rotational rheometers and by capillary rheometry. The particles were prepared by aqueous emulsion polymerization of (predominantly) styrene and ethylacrylate. Small amounts of mono and dicarboxylic acids were added to the monomers to incorporate carboxyl groups. Due to partial dissociation of the COOH groups in polar fluids electrostatic stabilization of the dispersions is obtained.

Chow and Zukoski (1995) explored the rheological and microstructural properties of dense suspensions of uniform, charge stabilized colloidal spheres with diameters greater than 200 nm at volume fractions just below the ordering transition up to 0.6. Shear thickening behavior is only observed above a volume fraction of 0.4-0.5, depending on particle size and shear rate. Additionally, it was found that the shear rates at the stress where discontinuous shear thinning occurs also increase exponentially with volume fraction. On the other hand, shear rates characteristic of changes in flow properties and microstructure increase exponentially with volume fraction. Shear thickening was found to be strongly correlated only above a critical volume fraction of ϕ_c (≈ 0.5 for the small particles and ≈ 0.4 for large particles).

Frith et al. (1996) investigated the onset of shear thickening (dilatancy) in submicron model suspensions of sterically stabilized spherical particles. They focused on the effect of particle size, particle concentration, and the nature of the suspending medium on the onset of shear thickening. They found that the critical shear rate changes inversely proportional with medium viscosity. They used sterically stabilized poly (methyl methacrylate) (PMMA) suspensions. Suspensions were prepared by the process known as nonaqueus dispersion polymerization. This process involves polymerizing the MMA in a hydrocarbon medium in which the MMA is soluble but the resulting polymer

will form precipitate. As the polymerization proceeds, the newly formed polymer precipitates out to form particles. Monomer then migrates into the polymer particles, swelling them, so that after an initial nucleation stage all polymerization occurs within the particles, and no new particles are formed. This nucleation and growth mechanism results in the formation of uniformly sized particles, and standard deviations of as little as 5% of the mean diameter can be achieved. Particle size is controlled by varying the number of nuclei formed, which is achieved by altering the solvency of the polymerization medium, and the monomer concentration. Five different particle sizes were studied. Their sizes as measured by electron microscopy are listed in Table 2.1 along with polydispersity.

Table 2.1. Characteristics of PMMA particles
(Source: Frith et al., 1996)

Sample	Particle diameter (nm)	Standard deviation (%)
A	341	5.8
B	690	5.1
C	890	3.9
D	370	6
E	797	4

Four different suspension media were studied. These were decalin (a mixture of cis and trans), di-octyl phthalate (DOP), a blend of 30% decalin and 70% DOP by weight and di-dodecyl phthalate (DDP). Since two of the dispersion media used were viscous, it proved to be impossible to use centrifugation to transfer the particles into them directly, instead two methods were used to achieve the transfer. In both approaches the samples were initially transferred into a highly volatile, low viscosity medium (hexane) by centrifugation. At this point the two preparations differ, in one, the suspension in hexane was dried in a vacuum oven and the required amount of medium added to the resulting powder. This method was used for the suspensions in DOP and the blend of decalin and DOP. In the other method, used for the DDP, the medium was added to the suspension in hexane that was then stripped off in a vacuum oven to produce the final suspension at the desired concentration.

The results showed that a region of essentially constant average shear rate develops suddenly at some stage, when the particle concentration is high enough. At lower concentrations ($\phi < 0.53$) there is no discontinuous change in response, the slope $d\dot{\gamma}/d\sigma$ then decreases smoothly with increasing shear stress. Shear rate as a function of applied stress curve is illustrated in Figure 2.12.

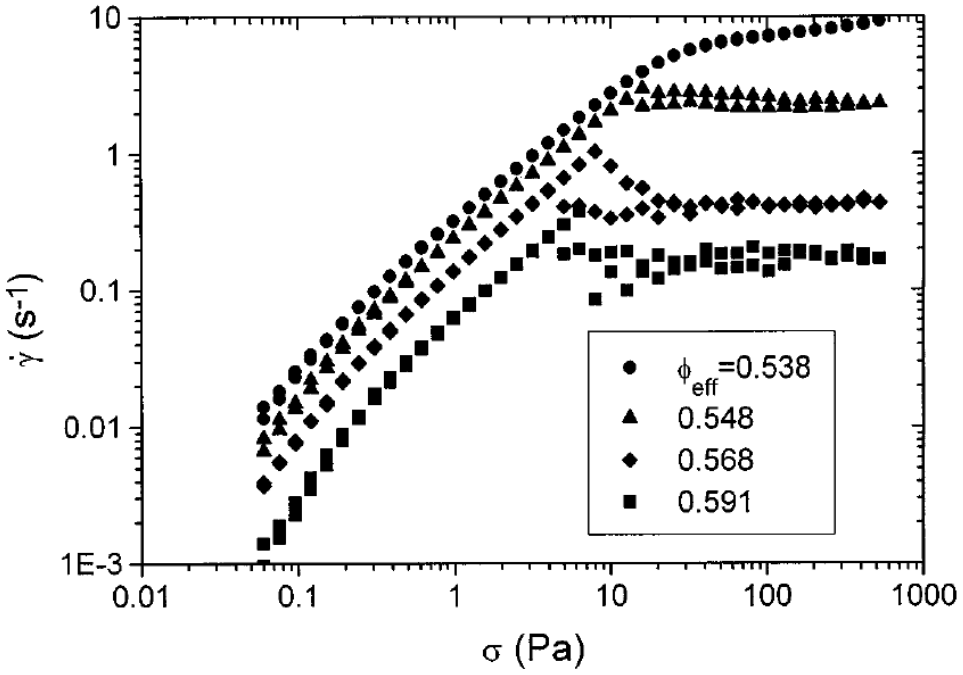

Figure 2.12. Measured shear rate as a function of applied shear stress
(Source: Frith et al., 1996)

When the stress is gradually increased there is a region around the shear thickening transition in which a certain amount of hysteresis can be observed. Beyond the transition the shear rate drops to a value that is independent of stress. When the stress is subsequently decreased again through the transition region, the shear rate rejoins the curve of increasing stress at some lower value. If the sample is conditioned at some low stress level before applying a higher stress, obviously no hysteresis will be seen. It can be seen that the sample no longer shows steady flow behavior in the shear thickening region.

In order to study the effect of changes in medium viscosity and particle size on the shear thickening transition, the phenomenon was characterized in terms of a critical shear stress (σ_c) or a critical shear rate ($\dot{\gamma}_c$). It has been demonstrated that there is unique relation between these two parameters for suspensions of particles

approximating to hard spheres. Consequently, they found that in sterically stabilized suspensions a change in suspending medium changes not only the viscosity but also the solvency for the stabilizer layer. The resulting effects of changes in thickness of the stabilizer have been observed, they correspond to subtle changes in rheological behavior, including a reduction in the critical shear rate in media that are better solvents for the stabilizer. The concentration dependence of the critical shear stress also varies depending on the solvency of the medium (Frith et al., 1996).

Bender and Wagner (1996) investigated reversible shear thickening behavior in monodisperse and bidisperse colloidal dispersions. They also focused on the mechanism of the shear thickening to elucidate the origins of the shear thickening in dense colloidal suspensions. Rheology, flow dicroism and the stress optical rule are used to determine which colloidal force drives shear thickening between the two postulated mechanisms for shear thickening. Turbidity and SANS are used to determine the microstructure of the shear thickening state, as well as to detect any shear-induced ordering of particles.

It was found that hydrodynamic interactions cause the shear thickening transition. Turbidity and flow-small angle neutron scattering (flow-SANS) results showed that particles cluster reversibly in the shear thickening state. Additionally, SANS measurements indicate that the shear thickening occurs without any shear-induced order-disorder transition, in contrast to observations for dispersions of charged colloids. For this purpose, they used monodisperse, near hard-sphere silica particles of diameters 160, 330, 400 nm. The particles were coated with (3-trimethoxysilypropyl)-methacrylate (TPM) to remove surface charges and suspended in a near-index matching solvent (tetrahydrofurfural alcohol) to remove van der Waals interactions and render the suspension translucent. The bimodal suspensions were formulated by mixing the concentrated monodisperse suspensions in appropriate amounts, striring vigorously until homogeneous. It should be noted that these particles have no strongly steric or electrostatic stabilization. They observed that the shear thickening appeared discontinuous, characterized by a sudden jump to a higher viscosity as the shear rate increased. The viscosity and shear thickening behavior of a suspension of nearly monodisperse 330 nm diameter particles, as well as mixtures with 160 nm diameter particles, depends on the choice of either controlled stress or controlled shear rheometry as shown in Figure 2.13. The viscosity was found to be time dependent, apparently switching between low and high viscosity states as shown in Figure 2.14.

They also found that bidisperse suspensions provide insight into controlling the onset and severity of shear thickening. Viscosity versus shear stress for a variety of volume fractions of small (160 nm) to large (330 nm) silica particles, all the same total volume fraction of 0.64 as shown in Figure 2.15. The onset of shear thickening is a smooth, increasing function of the ratio of smaller/larger particles. Additionally, the shear stress required for the onset of thickening is observed to increase with the ratio of small to large particles. Including a few smaller particles greatly increase the shear rate neccessary for thickening.

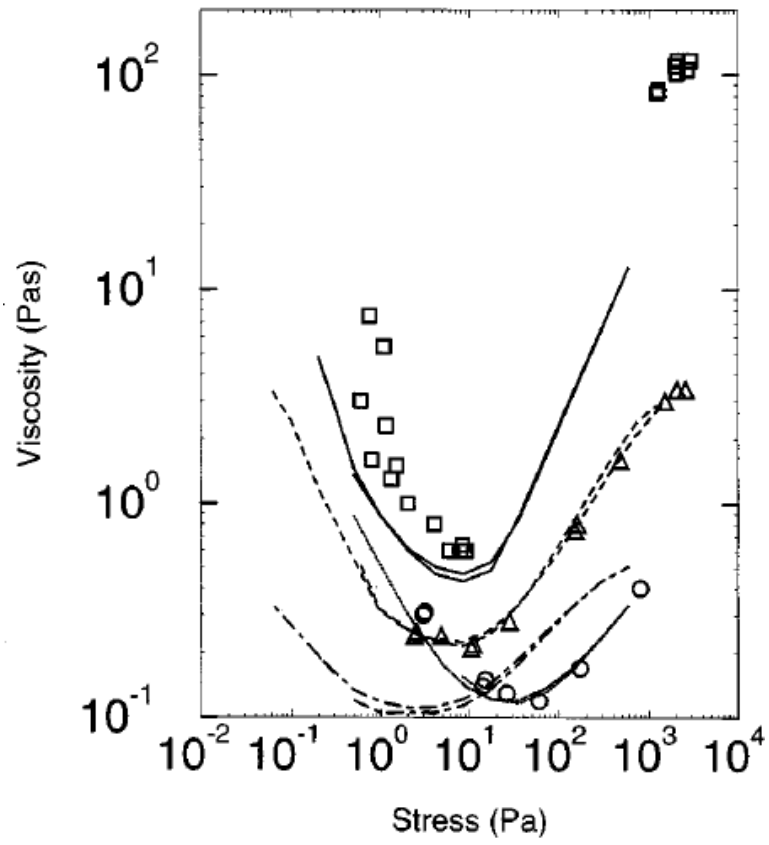

Figure 2.13. Comparison of the viscosities obtained from a controlled shear rheometer (symbols) and control stress rheometer (—). Symbols: (□), (–) 330 nm, ϕ=0.64; (Δ), (- - -) 10% 160 nm 90% 330 nm ϕ=64 mixture; (○), (….) 50% / 50% ϕ=64 mixture, (- · -) 330 nm ϕ=64 (Source: Bender and Wagner, 1996)

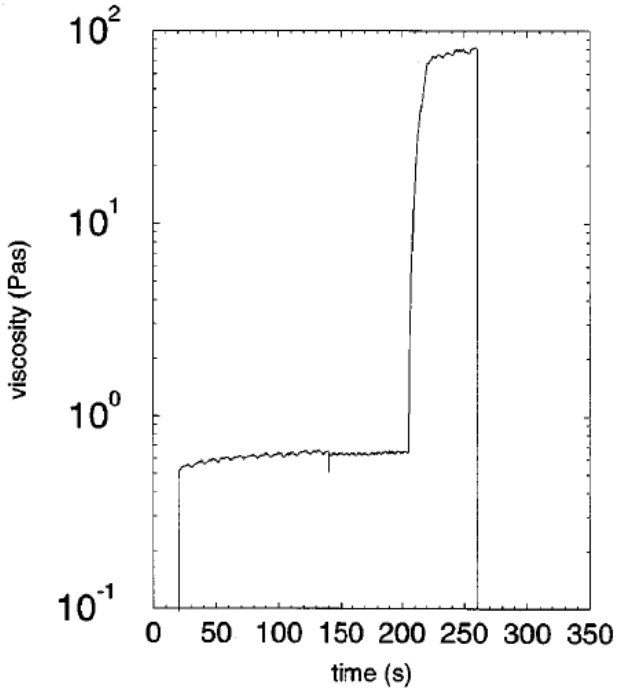

Figure 2.14. Time dependence and relaxation of the viscosity of 330 nm particles ϕ=64 at a shear rate of of 15 sec^{-1}. Flow started at 20 sec and stopped at 260 sec. The blip at 140 sec indicates the point of flow reversal (Source: Bender and Wagner, 1996)

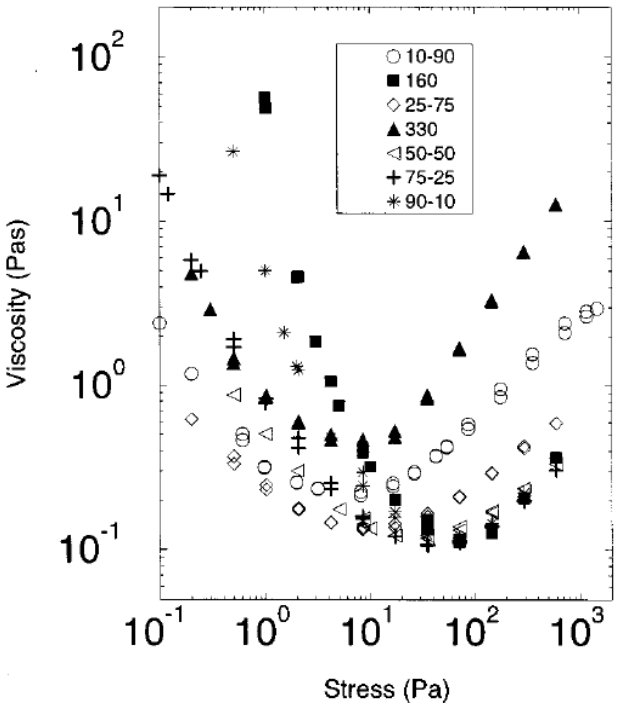

Figure 2.15. Viscosities as a function of shear stress for two monodisperse suspension and the bimodal mixtures at ϕ=0.64. The labels indicate the mixing of small (160 nm) to large (330 nm) particles by volume percent (Source: Bender and Wagner, 1996)

It can be concluded that the state of the shear thickened sample is consistent with the formation of hydrodynamic cluster and hydrodynamic lubrication forces dominate all other colloidal forces in the shear thickened suspension. Furthermore, no shear induced, order-to-disorder transition is observed for these hard-spheres suspensions. ODT is neither neccessary nor sufficient for shear thickening. Shear thickening is thus a transition from distorted colloidal fluid or shear ordered structure to a state of hydrodynamic clustering.

Maranzano and Wagner (2001) explored the reversible shear thickening transition in concentrated colloidal suspensions. For this purpose, they used five suspensions of monodisperse silica. These are synthesized via the Stöber synthesis and dispersed in an index matched organic solvent to minimize van der Waals interactions. The residual surface charge is neutralized with nitric acid ($c_{HNO_3} \approx 0.1$ M) resulting in a near hard-sphere interaction that is confirmed by small angle neutron scattering across a range of volume fractions. They focused on the dependence of the shear thickening rheology and the critical stress for the onset of shear thickening on dispersion concentration and particle size for nearly monodisperse, near hard-sphere suspensions. They found that for both dispersions at equal particle concentration after the charge neutralization the low shear rheology changes qualitatively and Newtonian low-shear plateau is evident as shown in Figure 2.16. This indicate that the extreme sensitivity of the low shear viscosity in concentrated dispersions to relatively weak, short-range electrastatic forces. Furthermore, the high shear rheology of the dispersions are also significantly altered by neutralization of the residual surface charge as illusturated in Figures 2.16 and 2.17.

Additionally, the shear thickening behavior in both dispersions was found to be reversible, with hysteresis evident only at low applied stresses and at the highest particle concentrations for the charge-neutralized dispersions. They observed that there is qualitative difference in the viscosity in the shear thickened state between the two types of dispersions, which are for the charge-neutralized and original as shown in Figure 2.17. The viscosity for the original dispersions increases more sharply at the shear thickening transition, whereas the viscosity response on the charge-neutralized dispersions increases more gradually upon shear thickening.

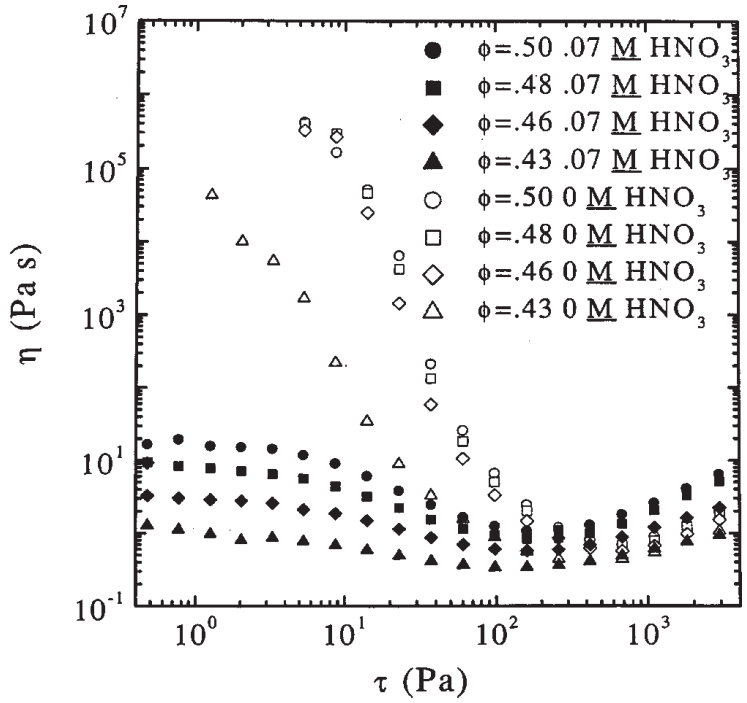

Figure 2.16. Comparison of viscosity data between the HS75 dispersions with 0.066 M HNO_3 (filled symbols) and 0 M HNO_3 (open symbols) plotted against applied shear stress (Source: Maranzano and Wagner, 2001)

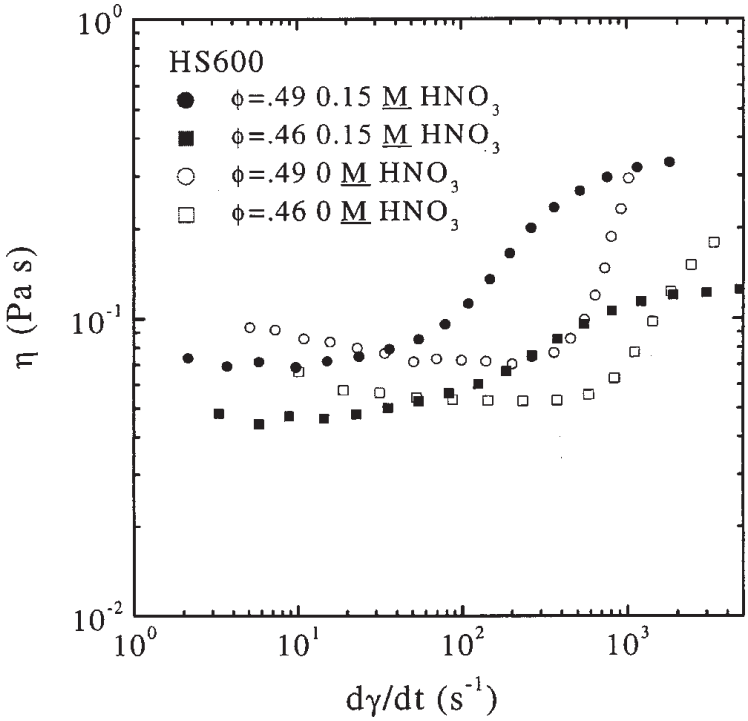

Figure 2.17. Comparison of viscosity data between the HS600 dispersions with 0.066 M HNO_3 (filled symbols) and 0 M HNO_3 (open symbols) plotted against applied shear rate (Source: Maranzano and Wagner, 2001)

It was concluded that the addition of small amount of nitric acid to a dispersion TPM coated silica in an index matched organic solvent (THFFA) is sufficient to suppress the electrophoretic mobility and lead to paucidisperse hard-sphere SANS spectra. The charge-neutralized dispersions exhibit rheology consistent with that predicted for hard spheres. Comparison between charge-neutralized and electrostatically stabilized dispersions qualitatively validates model predictions that additional, conservative forces act to suppress the onset of shear thickening in concentrated, stable dispersions. The critical stress for the onset of reversible shear thickening for the hard-sphere dispersions is shown to scale with the inverse particle size cubed, which is in agreement with predictions for hard spheres.

Mewis and Biebaut (2001) investigated the phenomenon of shear thickening in sterically stabilized colloidal suspensions. The results showed that in a lower viscosity in the shear thinning region but also in lower critical shear rate and shear stress at the onset of shear thickening. They also found that when the critical shear stress increases the increase in particle volume fraction. The viscosity versus shear rate curve at different temperatures for two volume fractions is illustrated in Figure 2.18. It is observed that particularly in the more concentrated system a higher temperature causes an increase in the viscosity at low shear stresses but a decrease in the shear thickening region. The shear thickening was found to be gradual, continuous for all volume fractions.

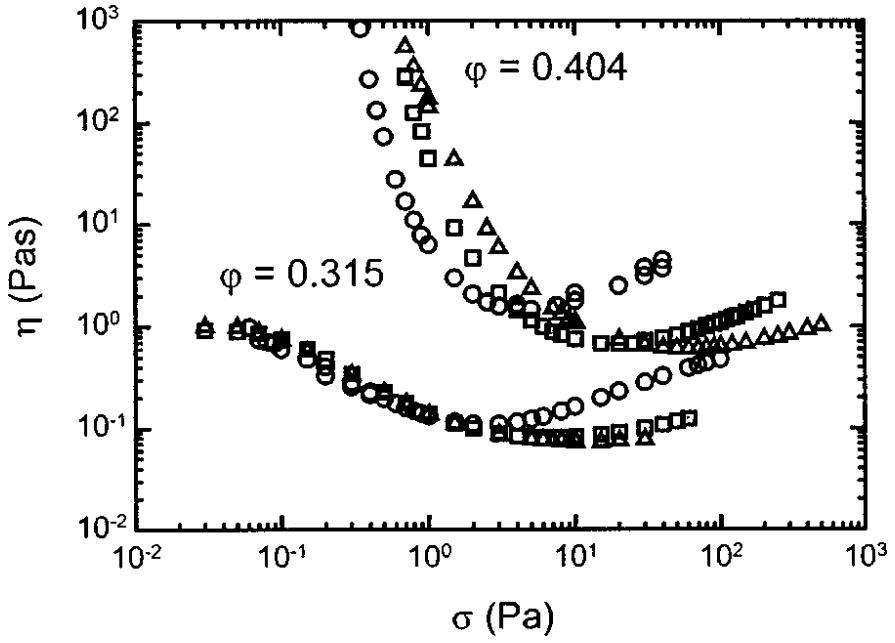

Figure 2.18. Effect of temperature on the viscosity curves for two volume fractions (circles: 293 K; squares: 298 K; triangles: 303 K) (Source: Mewis and Biebaut 2001)

Maranzano and Wagner (2002) studied shear thickening transition in the dispersions consist of 75 nm Stöber silica coated with 3-(trimethoxysily) propyl methacrylate (TPM) and have a zeta potential of – 42.6 ± 4.7 mV. To neutralize the surface charge of the stable hard-sphere dispersions 0.066 M nitric acid was used. They also explored the order-disorder transition and hydrocluster mechanism for shear thickening with SANS. The viscosity as a function of shear rate curve is illustrated in Figure 2.19. This curve compares the reversible shear thickening of the unneutralized and charge-neutralized dispersions at two particle concentrations $\phi = 0.5$ and $\phi = 0.43$. It is observed that there is a Newtonian low-shear plateau and upon charge neutralization the low-shear rheology changes. This is related to decreasing the effective particle concentration because of the removal of the weak electrostatic interactions. Additionally, the shear thickening in both dispersions was found to be reversible. In the hydrocluster mechanism for shear thickening, the formation of hydrocluster is predicted to occur when the compressive hydrodynamic forces dominate over the stabilizing repulsive forces. Consequently, they found that reversible shear thickening in dense, colloidal suspensions due to the hydrodynamic interactions. The charge-stabilized dispersions indicated much higher low shear rate viscosities proportionally larger microstructure deformations than the charge-neutralized dispersions.

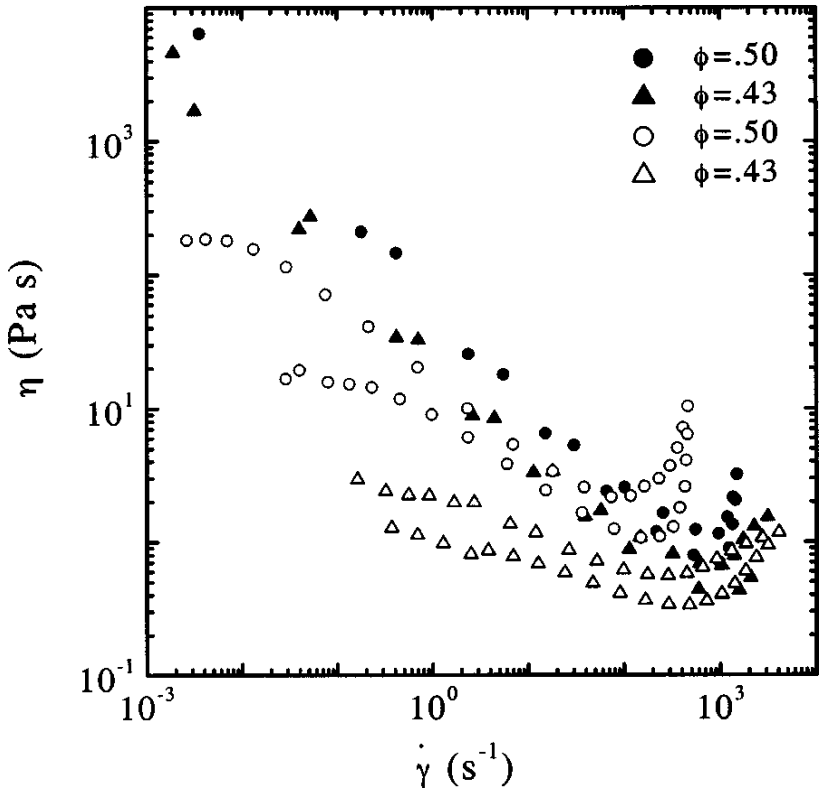

Figure 2.19. Viscosities plotted against applied shear rate for the unneutralized (filled symbols) and neutralized (open symbols) dispersions at two particle concentrations $\phi = 0.5$ and $\phi = 0.43$. Each viscosity measurement consists of data recorded during ascending shear stress (upper curve) and descending shear stress (lower curve)
(Source: Maranzano and Wagner 2002)

Lee et al. (2003) invistigated that the colloidal silica particles in etylene glycol show shear thickening behavior. They used colloidal silica an aqueous suspension at a particle concentration of about 40 wt%. The average particle diameter was found to be 446 nm by dynamic light scattering. The steady shear viscosity as a function of the steady shear for the etylene glycol based silica suspension at volume fracitons of $\phi = 0.57$ and $\phi = 0.62$ as shown in Figure 2.20. It was observed that there are both shear thinning and shear thickening behavior. The shear thickening transition is found at high particle concentrations and low shear rates. Furthermore, strong shear thinning is observed due to the yield stress. As the shear rate increases the viscosity show strong shear thinning until a critical shear rate. At a critical shear rate the shear thickening transition occur. It was observed that the shear thickening transition for the concentrated dispersions having a particle volume fraction of $\phi = 0.62$ occur at shear rate 10 s^{-1} and 300 s^{-1} for the particle volume fraction of $\phi = 0.57$. At high shear rates in the shear

thickening region, the high volume fraction dispersion indicates a greater increase in viscosity. It should be noted that the shear thickening transition is found to be reversible.

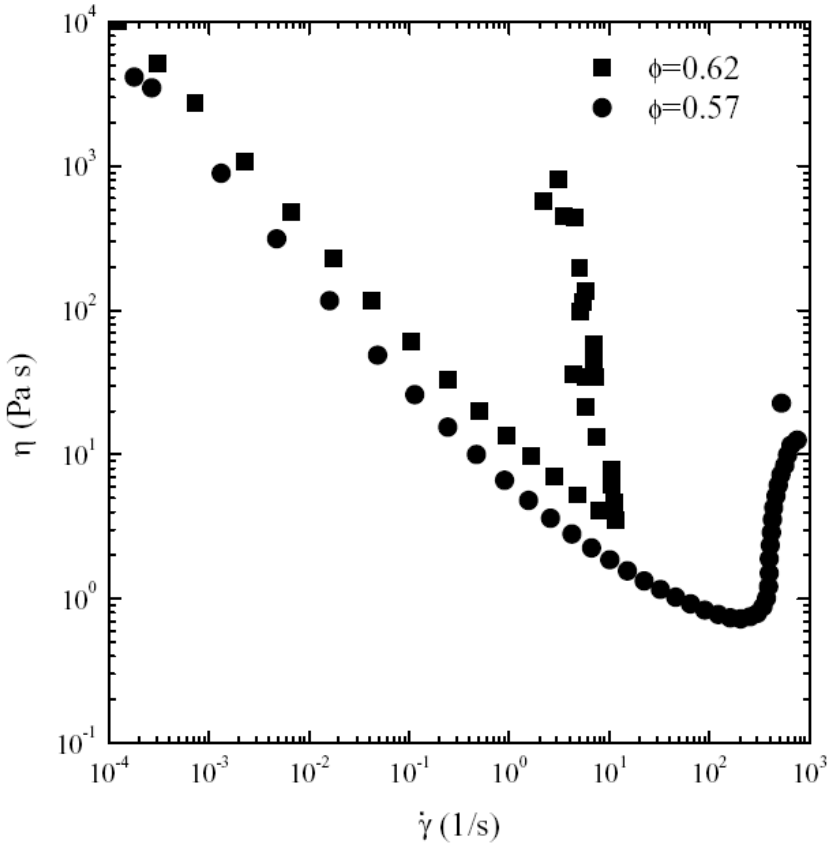

Figure 2.20. Shear thickening behavior of 57 and 62 volume % colloidal silica dispersed in etylene glycol for steady shear flow (Source: Lee et al., 2003)

Muñoz et al. (2003) investigated the rheological behavior of the solution of poly(2-hydroxyethyl methacrylamide) in glycerine. The rheological results showed that when the shear rate increased the increase in viscosity is observed. According to the results, the shear thickening transition without occurring any shear thinning region is observed. On the other hand, at the highest shear rate values the onset of shear thinning is noted as shown in Figure 2.21. It should also be noted that there is a Newtonian plateau until the shear thickening transition.

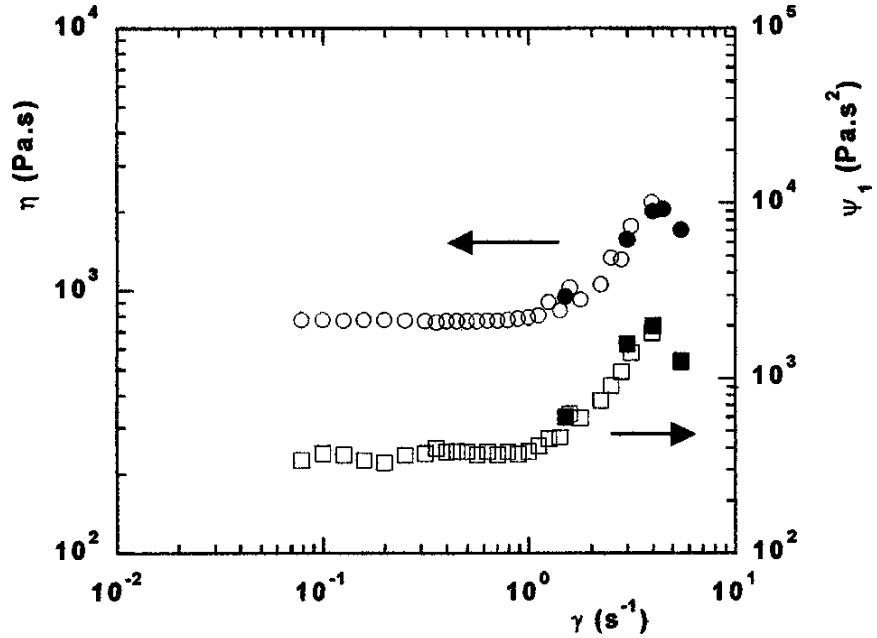

Figure 2.21. Viscosity and first normal coefficient as a function of shear rate. Open symbols correspond to a continuous increase of shear rate at rate of 0.4 s 21/min. Filled symbols correspond to steady state viscosities obtained from shear rate jump experiments (Source: Muñoz et al., 2003)

Egres and Wagner (2005) investigated the shear rheology and shear-induced microstructure of poly(ethylene glycol) (PEG)-based dispersions of acicular precipitated calcium carbonate (PCC) particles of different particle aspect ratio (nominal $L/D \approx 2$, 4, 7). According to the rheological results, these particles in PEG show both continuous and discontinuous reversible shear thickening with increasing applied shear rate or stress. It was observed that when the average particle aspect ratio is increased the critical volume fraction for the onset of discontinuous shear thickening decreases. On the other hand, they found that the critical stress for the shear thickening transition is independent of particle anisotropy and volume fraction. They also explored the reason of the shear thickening transition with small angle neutron scattering (Rheo-SANS). The results showed that reversible shear thickening is a consequence of lubrication hydrodynamic interactions and the formation of transient hydrocluster of flow-aligned particles.

Lee and Wagner (2006) focused on the rheological properties and flow microstructure of a stable dispersion of spherical nanoparticles. The shear rheology and flow-small angle neutron scattering of charge-stabilized silica dispersed in etylene glycol are investigated as a function of shear stress and particle volume fraction. According to the rheological results, the steady shear viscosity of the 32 nm

nanoparticle dispersions with different particle volume fractions demonstrate at low shear rate or stress Newtonian plateau for all colloidal dispersions. Significant shear thinning is also observed until the shear thickening occurs. This transition was found to be reversible. Furthermore, reversible shear thickening is found at very high shear rates. Consequently, the shear thickening in nanoparticle dispersions is related with hydrocluster mechanism which is confirmed by Flow-small angle neutron scattering measurements.

Zhang et al. (2008) studied the rheological properties of the fumed silica nanoparticles suspensions in ethylene glycol. They achieved the shear thickening fluid, which consist of nanosize silica particles in ethylene glycol at high volume fractions. The results showed that the viscosity of the STF increases with increasing volume fractions. At low shear rates, slight shear thinning is observed. The viscosity display a sharp increase at a crtical shear rate. It should also be noted that at higher shear rates strong shear thinning occurs. Furthermore, they found the critical shear rate is dependent on the volume fractions. When the volume fractions increase with decreasing critical shear rate.

Kamibayashi et al. (2008) investigated the steady shear rheology of the suspensions of silica nanoparticles with diameters of 8-25 nm dispersed in aqueous solution of poly(ethylene oxide) (PEO). The rheological results exhibited the additions of silica nanoparticles cause the viscosity increase over the entire range of shear rates. When the shear rate is increased, the viscosity suddenly starts to increase then reach a maximum value and then decreases at high shear rates. The shear rate at which the shear thickening transition begins decreases with increasing particle concentration.

Additionally, the results showed that there is a Newtonian behavior at low shear rates. When the particle concentration is increased, the viscosity quickly increases. The drastic increase in viscosity indicates that the silica suspensions are highly flocculated by PEO polymer. With increasing polymer concentration, the Newtonian viscosity at low shear rates quickly increases and the shear rate at the onset of shear thickening flow decreases.

Kalman and Wagner (2009) investigated the microstructre of reversible shear thickening in colloidal suspensions using a new method of flow-ultra small angle neutron scattering under steady state flow conditions. In order to obtain colloidal suspensions they used silica nanoparticles in poly(ethylene glycol). The steady state shear viscosity as a function of shear rate is shown in Figure 2.22. The lowest

concentrations show only slight shear thinning and thickening, only noticeable on the expanded linear viscosity scale. The higher concentrations show significant amounts of shear thinning and thickening. The results clearly show that the shear thickening transition is reversible. Additionally, microstructure of colloidal suspensions at shear thinning and shear thickening transition is observed owing to formation of hydrocluster.

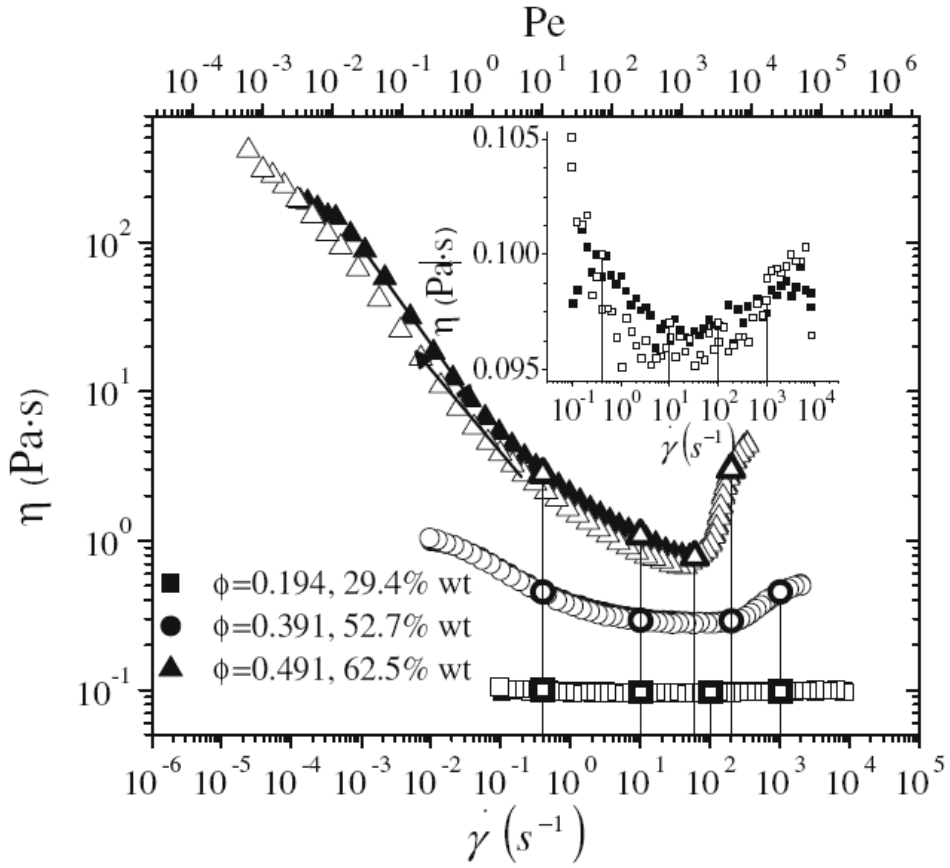

Figure 2.22. Steady-shear viscosity of a suspension of silica in PEG as a function of shear rate (Source: Kalman and Wagner, 2009)

Chellamuthu et al. (2009) explored the extensional rheology of shear thickening nanoparticle suspensions. They used fumed silica nanoparticles in polypropylene glycol to obtain colloidal suspensions. The shear rheology of these suspensions was found to show dynamic shear thickening behavior because of the formation of large hydrodynamic clusters. The shear rheology of a series of suspensions of concentrations 17.5 wt%, 25 wt% and 30 wt% indicated a shear thinning behavior at low strain and strain rates and shear thicken at high strain and strain rates. The shear thickening transition was observed to be initiated at lower frequencies when the strain amplitude was high. The critical value of angular frequency for the onset of shear thickening was

found to increase monotonically with decreasing strain amplitude. The steady state extensional viscosity as a function of extension rate shows sharp extensional thickening transition. At a critical extension, a dramatic increase in both the speed and magnitude of the strain-hardening is observed for both the 25 wt% and 30 wt% suspensions with increasing extensional rate.

Galindo-Rosales and Rubio-Hernández (2010) showed the shear thickening behavior suspensions of hydrophilic fumed silica in polypropylene glycol. At lower shear rates the slight shear thinning behavior is observed. Furthermore, it was found that this suspension shows time dependent behavior within its reversible shear thinning region, which is related to thixoelasticity. On the other hand, at higher shear rates reversible shear thickening is observed as shown in Figure 2.23.

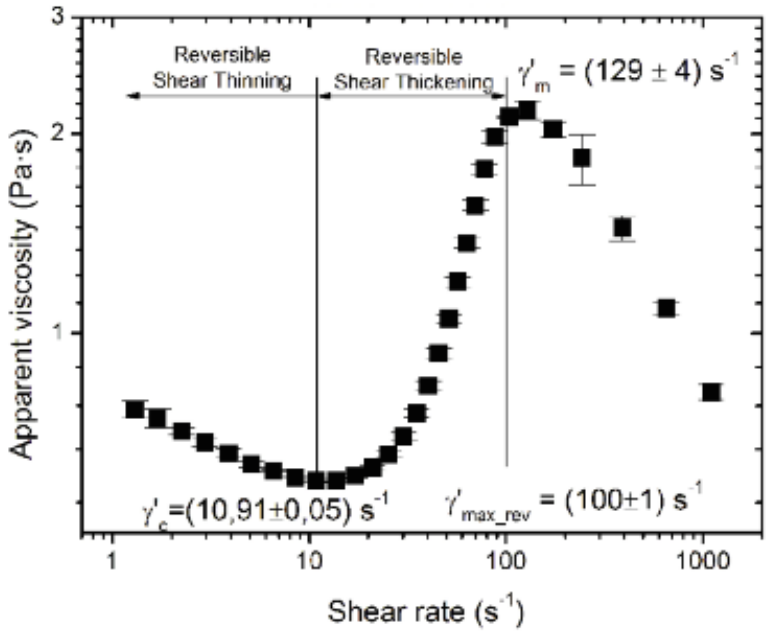

Figure 2.23. Steady state viscosity as a function of shear rate of a suspension of fumed silica in PPG (Source: Galindo-Rosales and Rubio-Hernández, 2010)

Amanda et al. (2010) investigated the transient response of a shear thickening fluid using the split Hopkinson pressure bar technique. They used the hard-sphere colloidal suspensions consist of 40% , 45%, 50%, 52%, 54% volume fraction (ϕ) silica particles in polyethylene glycol. The silica nanoparticles are nearly monodisperse with a hydrodynamic diameter of 520 nm with less than 10% polydispersity. They found that the steady state shear viscosity of these STFs exhibit a discontinous transition from fluid-like (shear thinning) to solid-like (shear thickening) behavior when the shear stress

increased. Steady state shear viscosity as a function of shear stress curve is illustrated in Figure 2.24. At low shear rates (1-200 s^{-1}) shear thinning behavior is observed. When shear stress reached the critical value a strong shear thickening behavior occured. It should be noted that at lower volume fractions, the suspension shows slight shear thinning and shear thickening. On the other hand, the shear thickening response was found to be revesible. Additionally, they showed that there is a minimum strain required for shear thickening at high Peclet numbers.

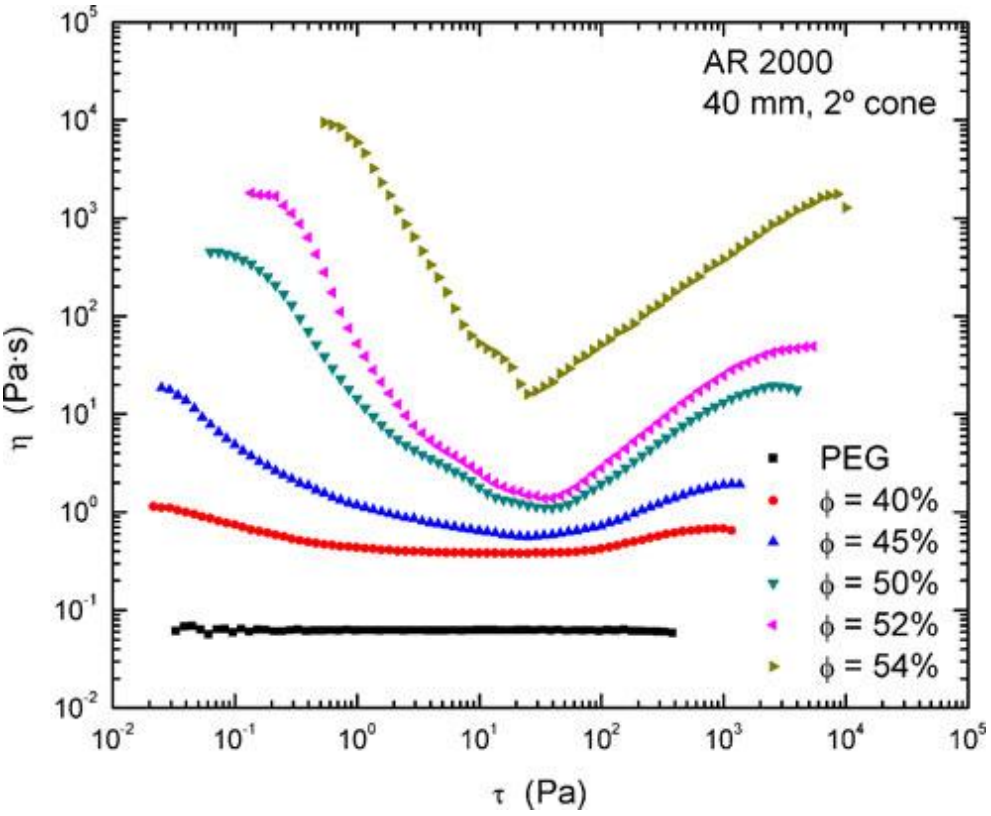

Figure 2.24. Steady state shear viscosity of the colloidal dispersions at varying volume fractions and the suspending medium (PEG) (Source: Amanda et al., 2010)

Hassan et al. (2010) used different technique to synthesize shear thickening suspensions. They used the sonochemical method to prepare shear thickening suspensions. Colloidal silica and dry powder silica nanoparticles have been used for this study. Polyethylene glycol was used to as the liquid polymer in the STFs synthesis process. The rheological properties show the shear thickening behavior at low shear rates. They found that the shear thickening response increases as particle loading increases, with discontinous shear thickening at the highest particle loadings. It should

be noted that the shear rate at which shear thickening behavior is first observed decreases as particle loading increases.

2.5.3. Dynamic Shear Rheology

Boersma et al. (1992) studied the viscoelastic properties of electrostatically stabilized concentrated dispersions of silica and glass particles in a glycerol / water mixture under steady and oscillatory shear conditions. They found that these dispersions show shear thickening behavior under steady shear. They also observed the increase in the viscosity much more clear at the higher volume fractions. On the other hand, the shear rate at which shear thickening begins is lower for the higher volume fractions. The shear thickening transitions for glass dispersions are found at higher shear rates, whereas for the silica dispersions occured at lower shear rates. Elastic modulus G' and viscous modulus G'' increase when the strain amplitude of the deformation is kept constant and the frequency is increased. Furthermore, they observed the viscous modulus G'' higher than the elastic modulus G' at higher volume fractions. Additionally, in the linear region the loss modulus is found to be dominant than the storage modulus. This behavior shows that these dispersions have viscous character.

Raghavan and Khan (1997) investigated the shear thickening response of fumed silica suspensions under steady and oscillatory shear. They used fumed silica in polyproylene glycol. They found that suspensions of fumed silica in polypropylene glycol show shear thickening under steady state and ‘‘strain thickening’’ under oscillatory shear. Strain thickening behavior with a sharp increase in the complex viscosity η^* is observed at critical combinations of strain amplitude and frequency. Strain thickening behavior has been found different conditions. One of them occured at high critical strains and low frequencies, whereas the another one occured at high critical frequencies and a constant lower strain. The steady shear response of the glycol based suspension over a range of silica weight fractions (3-10%) is shown in Figure 2.25. At low shear rates, slight shear thinning is observed. When the shear rate increased the viscosity begins to increase upright until reversible transition occur.

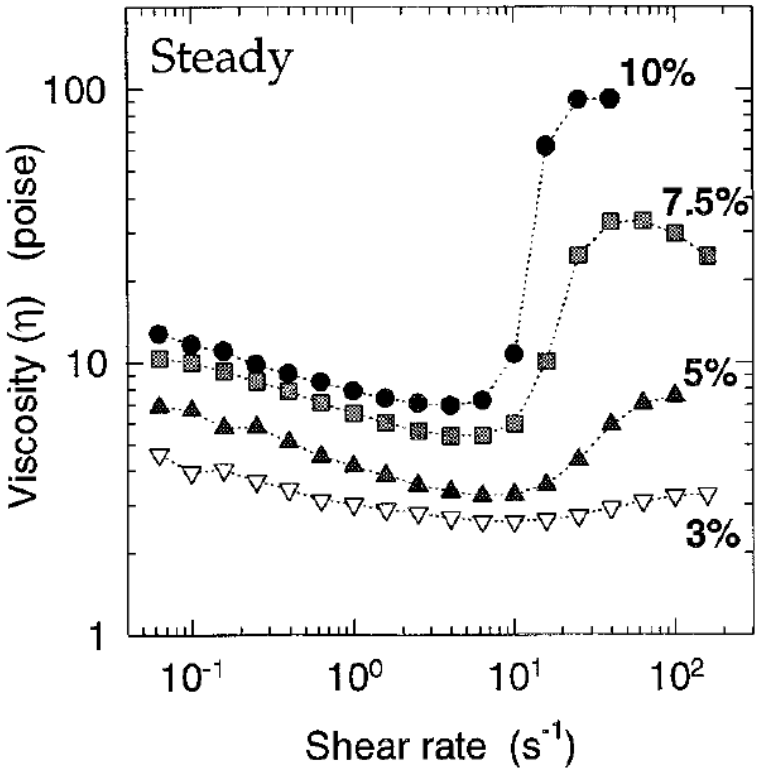

Figure 2.25. The steady shear viscosity as a function of shear rate
(Source: Raghavan and Kahn, 1997)

In order to understand the dynamic response of the suspensions strain sweep and frequency sweep experiments were performed. Strain sweeps were performed at different frequencies. The results show that the transition to strain thickening behavior occured at smaller strains as the frequency of the deformation is increased. The same strain thickening behavior is observed when the strain amplitude of the deformation is kept constant and the frequency is increased. Elastic and complex modulus as a function of strain amplitude for 10% fumed silica suspension in PPG as shown in Figures 2.26 and 2.27, respectively (Raghavan and Kahn, 1997).

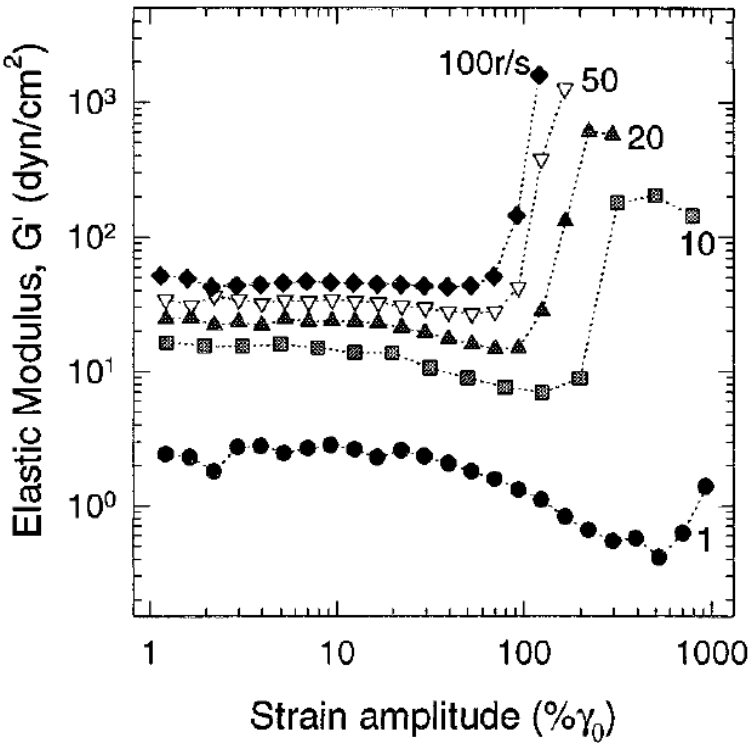

Figure 2.26.The elastic modulus G' as a function of strain amplitude for a 10% fumed silica suspension in PPG (Source: Raghavan and Kahn, 1997)

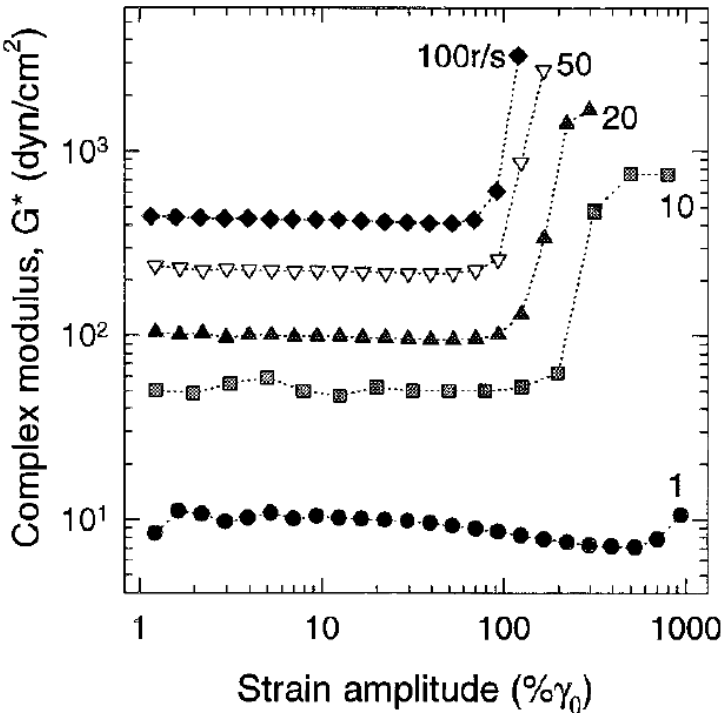

Figure 2.27. The complex shear modulus G^* as a function of strain amplitude for a 10% fumed silica suspension in PPG (Source: Raghavan and Kahn, 1997)

The suspension indicated strain thickening at high strain amplitudes for both modulus G' and G^* at different frequencies. When the strain reached the critical value the strain thickening behavior occured. On the other hand, the same strain thickening transition is observed when the strain amplitude of the deformation is kept constant and the frequency is increased. The storage G' and loss G'' modulus as a function of frequency curve at a strain of 750% as shown in Figure 2.28.

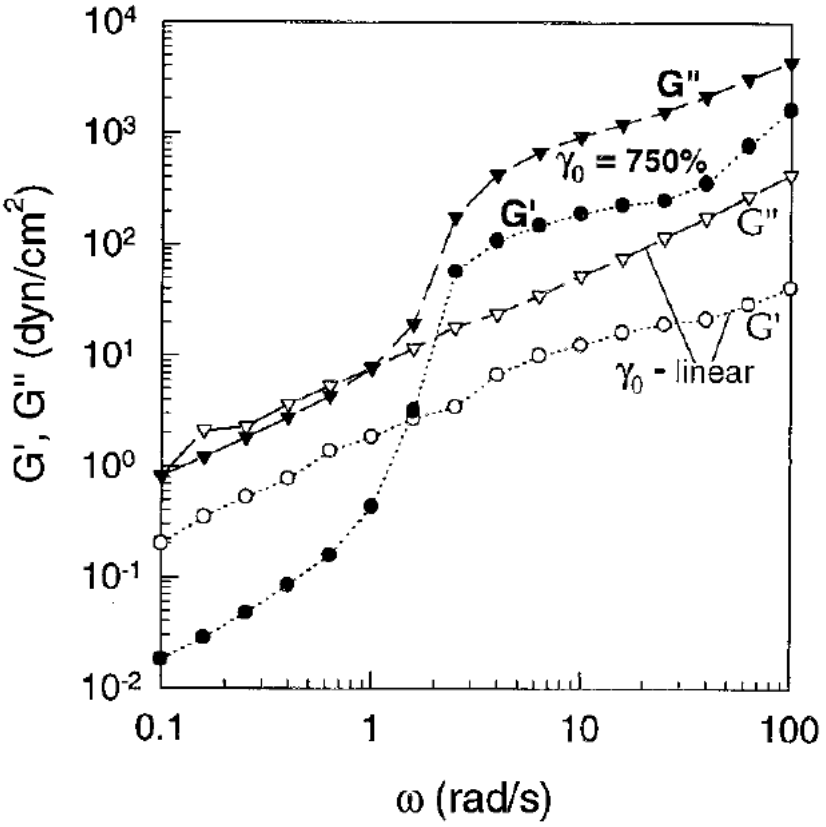

Figure 2.28. The elastic G' and viscous G'' modulus as a function of frequency at a strain amplitude of 750% (Source: Raghavan and Kahn, 1997)

Additionally, the increase in complex viscosity owing to shear thickening transition at higher concentrations was most noticeably. The complex viscosity as a function of frequency at a fixed strain of 750% is shown in Figure 2.29. It should be noted that there are important parameters to occur shear thickening transition in steady and dynamic shear which are the critical shear rate ($\dot{\gamma}_c$) and the critical frequency (ω_c). They found that these parameters decrease with increasing concentration.

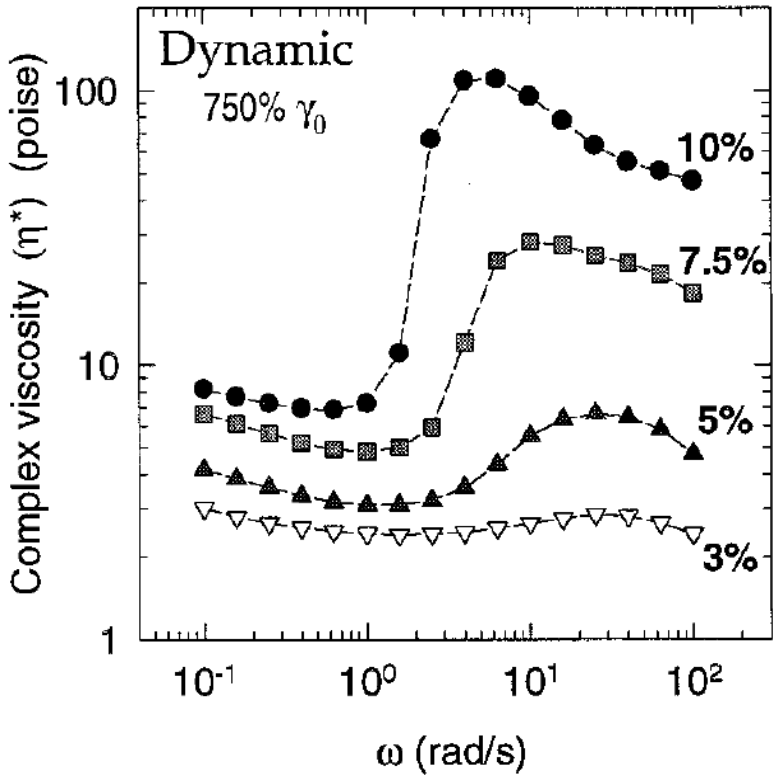

Figure 2.29. The complex viscosity as a function of frequency for a strain amplitude of 750% (Source: Raghavan and Kahn, 1997)

Mewis and Biebaut (2001) investigated the shear thickening behavior of sterically stabilized colloidal suspensions under steady and oscillatory shear flow. The results showed that the critical strain decreases with increasing frequency, whereas the degree of shear thickening increases. The critical shear stress increases with increasing particle volume fraction. Furthermore, the shear thickening occured at lower shear rates with increasing volume fractions. On the other hand, the values of the storage and loss modulus increased with increasing the frequency. The shear thickening suspensions are found to indicate strain hardening. Elastic and viscous modulus as a function of strain amplitude for the colloidal suspension at volume fraction of $\phi = 0.438$ as shown in Figure 2.30.

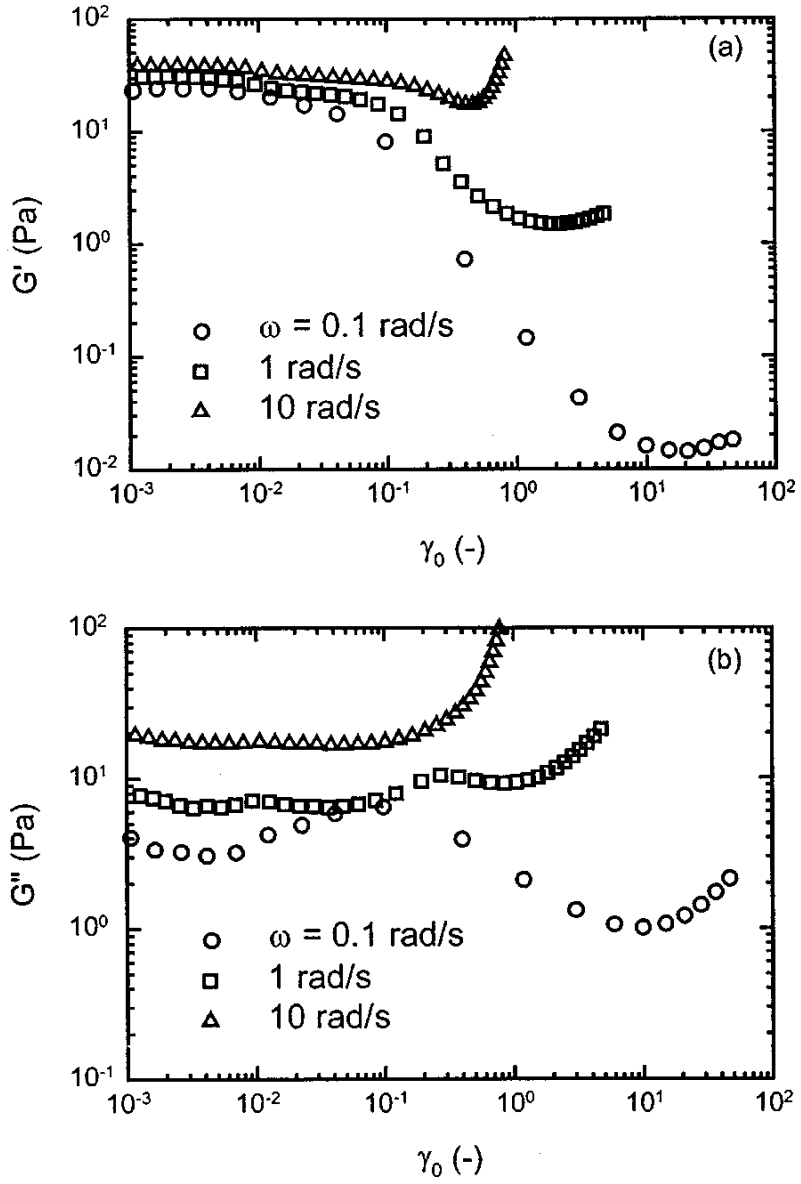

Figure 2.30. Modulus as a function of strain aplitude for colloidal suspension at different frequencies (a) storage modulus (b) loss modulus (Source: Mewis and Biebaut, 2001)

Lee and Wagner (2003) investigated dynamic properties of shear thickening in colloidal suspensions. They showed the reversible shear thickening in both steady and dynamic shear. In order to verify the reversibility of shear thickening both ascending and descending stress sweeps were conducted. The steady shear and the complex viscosity as a function of the steady shear stress curve for the suspension at volume fractions of $\phi = 0.55$ and $\phi = 0.60$ as shown in Figure 2.31. They found that the critical strain amplitude is required for shear thickening. Moreover, the critical strain for shear thickening depends inversely on the frequency at fixed applied stress for low frequencies.

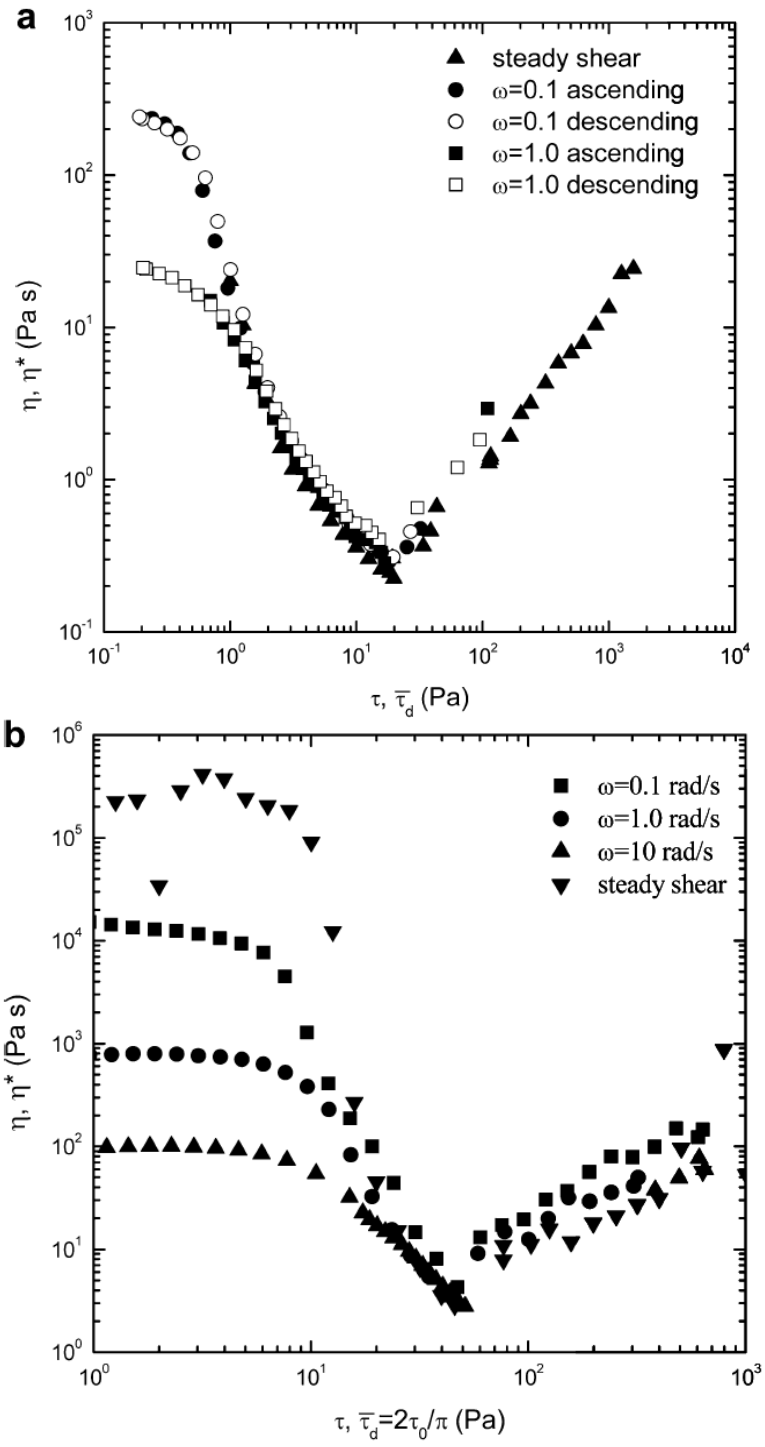

Figure 2.31. Reversible shear thickening behavior of colloidal silica dispersed in water for both steady and dynamic shear as a function of the average applied dynamic shear stress (a) at volume fraction of $\phi = 0.55$ (b) at volume fraction of $\phi = 0.60$ (Source: Lee and Wagner, 2003)

2.6. Shear Thickening Fluids (STFs) Impregnated Fabric Composites

Shear thickening fluids (STFs) have been used to improve the performance of woven fabrics for protective applications in ballistics, stab and puncture. The addition of colloidal shear thickening fluids (STFs) to Kevlar fabrics has been found to enhance the ballistic penetration resistance of the fabric, under conditions of low velocities and small target sizes. Furthermore, the stab resistance of shear thickening fluid (STF)-Kevlar and STF-Nylon fabric composites were found to indicate significant improvements over neat fabric targets of equivalent areal density. This improvement in ballistic properties is related to the resistance of the STF to deformation at high strain rates. Additionally, impressive improvements in puncture resistance for both the spike and knife threats under high and low speed loading conditions were observed. Dynamic stab test results showed a significant improvement of target stab resistant and protection in STF/fabric composite targets as compared to neat fabric targets for the both spike and knife threats (Lee et al., 2003; Decker et al., 2007; Kalman et al., 2009; Hassan et al., 2010).

2.6.1. Methods of STFs/Fabric Composite Production

Shear thickening fluids have been used in generally to impregnate into the Kevlar fabrics. To facilitate impregnation of the STF into the Kevlar fabric, an equal volume of ethyl alcohol was added to the original ethylene glycol based STF. This diluted STF was observed to spontaneously impregnate the fabric. Then, the composite material was heated at 80 ºC for 20 minutes in convection oven to remove the ethyl alcohol from the composite material (Lee et al., 2003).

To fabricate the STF-fabric composites, the STF was first diluted in ethyl alcohol at a 3:1 volume ratio of ethyl alcohol:STF. Then, individual fabric layers were soaked in the solution for 1 min, squeezed to remove excess fluid, and dried at 65 ºC for 30 minutes. (Decker et al., 2007)

The STF was diluted with ethyl alcohol in order to facilitate the impregnation to the Kevlar fabrics and individual fabric sheets were dipped and held in the solution for at least 1 min before being squeezed through rubber-coated nip rollers and hung to dry at room temperature. After air-drying for at least 10 minutes, the fabric was dried in an

oven 60 ºC for 30 min to remove ethyl alcohol and/or water co-solvents (Kalman et al., 2009).

The STF/fabric composite materials were prepared by Hassan et al. using the solution of STF/ethyl alcohol (40:60). 381mm × 381 mm layers of Kevlar and Nylon fabrics were cut and impregnated individually into STF/ethyl alcohol solution. Each sheet of Kevlar or Nylon fabric was soaked in an aluminium container filled with STF/ethyl alcohol solution for 1 min and then squeezed using an 11.34 kg steel cylinder to get rid of the excess amount of the solution and then hanged for 48 h at room temperature to remove the solvent. The steps of the fabric impregnation procedure are illustrated in Figure 2.31 (Hassan et al., 2010).

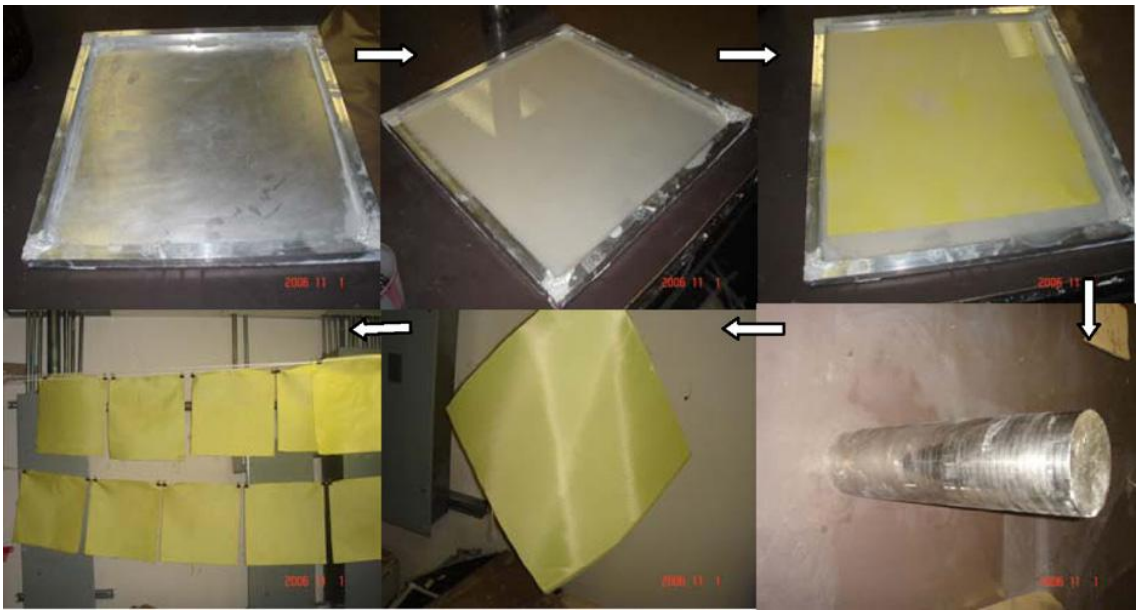

Figure 2.32. The steps of the fabric impregnation procedure
(Source: Hassan et al., 2010)

2.7. Test Techniques for Evaluating Effectiveness of Shear Thickening Fluids

To investigate the properties of woven Kevlar fabrics impregnated with the shear thickening fluids, the ballistic tests were performed by Lee et al. For this pupose, a smooth bore helium gas gun was used. The gun was sighted on the target center and the impact velocity was adjusted to approximately 244 m/s (800fps). The projectile was a NATO standard fragment simulation projectile, consisting of a chisel-pointed metal

cylinder of 1.1 grams (17 grains) and 0.56 cm diameter (22 caliber). The ballistic test apparatus used in their study is illustrated in Figure 2.33 (Lee et al., 2003).

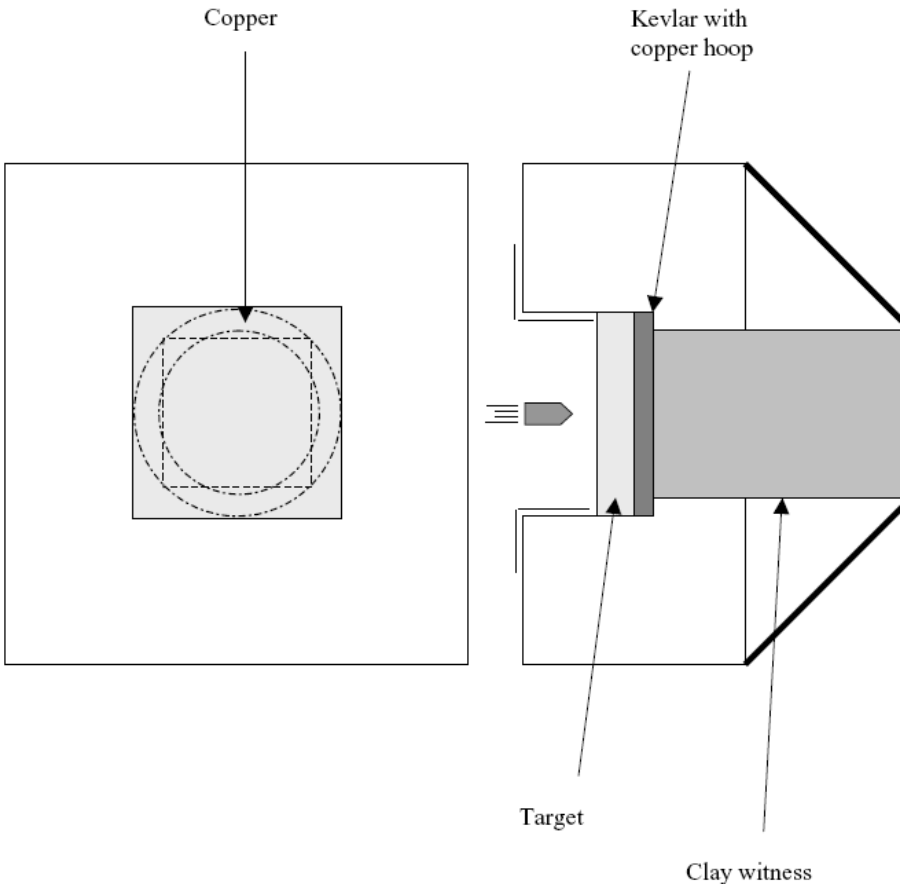

Figure 2.33. Schematic diagram of test apparatus and helium gun target
(Source: Lee et al., 2003)

The stab tests were conducted using the National Institute of Justice (NIJ) standard 0115.0 for stab resistance of body armor to understand the effect of the shear thickening fluids on the Kevlar fabrics. Two NIJ-specified impactors were used: the "S1" knife, and the "spike" and the stab targets were placed on a multi-layer foam backing as specified by the NIJ standard as shown in Figure 2.34.

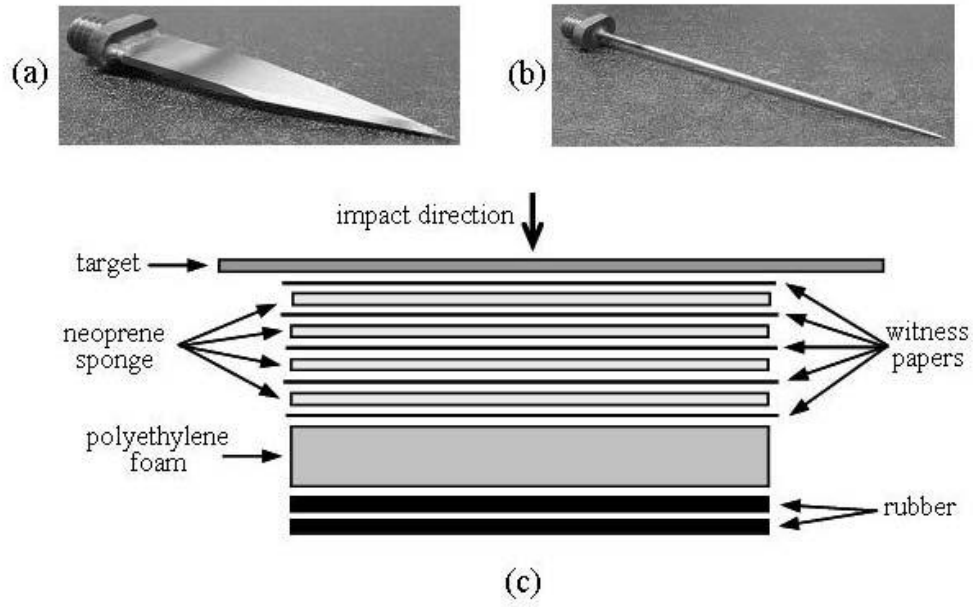

Figure 2.34. a) Knife impactor, b) Spike impactor, c) Multi-layer foam backing construction (Source: Decker et al., 2007)

Flexibility tests and thickness measurements were conducted for both neat fabric and STF/fabric composite samples to understand the effect of STF addition on the fabric flexibility and thickness. To measure the flexibility, neat fabric and STF/fabric were cut into 51mm×51mm square layers, 2 test specimens were prepared by stacking 4 layers for the first specimen and 10 layers of second specimen of the square layers. A 20 g weight was then attached to the test specimens according to the geometry as shown in Figure 2.34 and the bending angle θ was measured and recorded for each specimen (Lee et al., 2003; Hassan et al., 2010).

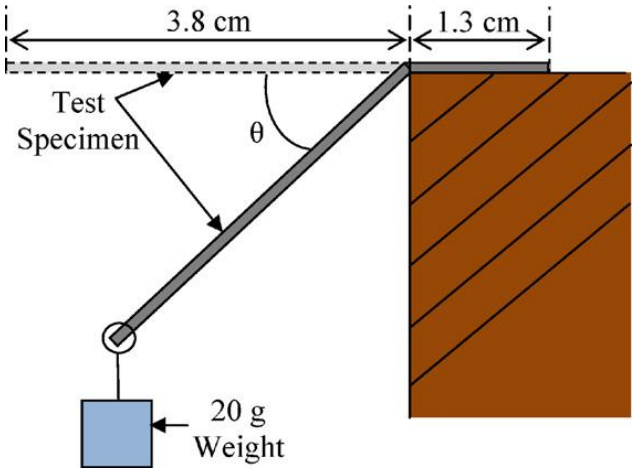

Figure 2.35. Flexibility test geometry (Source: Hassan et al., 2010)

2.7.1. Drop Tower Tests

Decker et al. (2007) investigated the stab resistance of shear thickening fluid (STF) impregnated fabrics. They found that the stab resistance of shear thickening fluid (STF) impregnated Kevlar and Nylon fabrics indicate remarkable improvements over neat fabric targets of equivalent areal density. An impressive improvement was observed in puncture resistance (spike threat) under high and low speed loading conditions. The drop tower stab result of the Kevlar and STF-Kevlar composite material against the knife impactor is shown in Figure 2.36. The impact energy increases with increasing the depth of penetration into the backing material. The STF-Kevlar targets indicated less penetration depth as compared to the Kevlar target. At higher energy levels for all targets the maximum penetration depth is observed. The drop tower stab result of the Kevlar and STF-Kevlar composite target against the spike impactor is shown in Figure 2.37. The STF-Kevlar composite target exhibited significantly better stab resistance as compared to those of Kevlar fabric. The Kevlar target showed the maximum penetration, five witness layers at an energy of only 4 J. Conversely, the STF-Kevlar composite target showed the maximum penetration, three witness layers, at the highest energy level of 17 J.

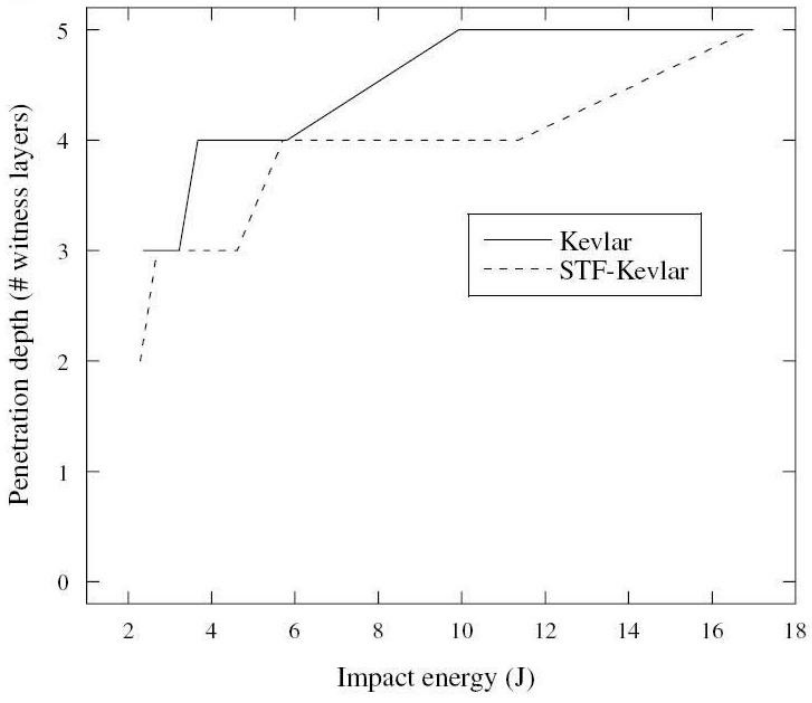

Figure 2.36. Knife drop tower results for Kevlar and STF-Kevlar fabric (Source: Decker et al., 2007)

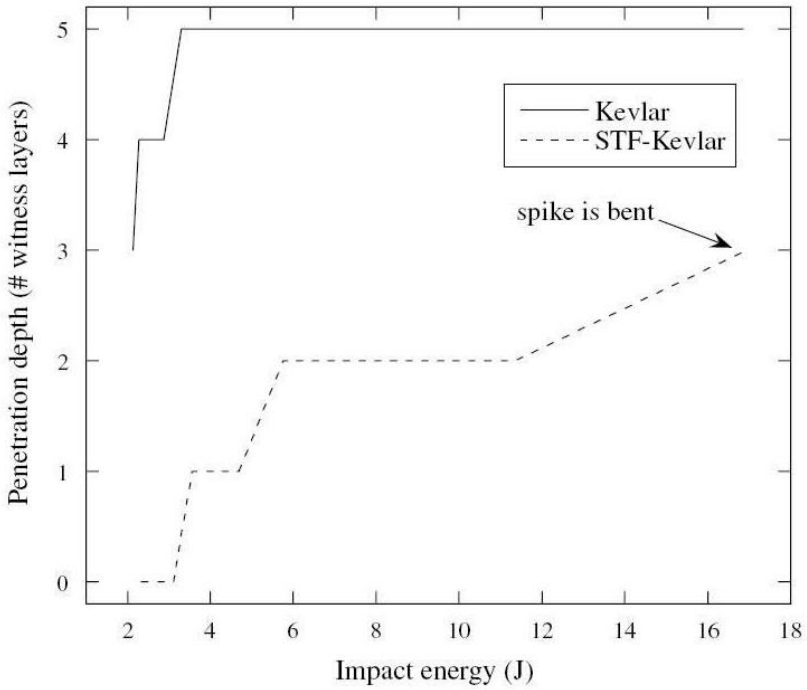

Figure 2.37. Spike drop tower results for Kevlar and STF-Kevlar fabric
(Source: Decker et al., 2007)

Hassan et al. (2010) explored the drop tower stab resistance of neat Kevlar, STF-Kevlar composite, neat Nylon and STF-Nylon composite target against the knife and spike threats. The drop tower stab performance of neat Kevlar and STF-Kevlar targets against the knife and spike threats is shown in Figure 2.38. It can be seen that the impact energy increases with increasing the penetration depth for the knife threat. STF-Kevlar target exhibited less penetration depth and better stab resistance as compared to the neat Kevlar for low values of impact energy. The maximum penetration depth of five witness papers was observed at impact energy of 8 J for both targets. Furthermore, the impact energy increased with increasing the depth of penetration into backing material for the spike threat. The STF-Kevlar targets showed significantly higher stab resistance as compared to the neat Kevlar targets. The neat Kevlar targets exhibited maximum penetration of five witness papers at all impact energy levels. Conversely, the STF-Kevlar composite target was penetrated through one witness paper at an impact energy of 2.7 J. Furthermore, the maximum penetration of five witness papers was observed at an impact energy of 8 J.

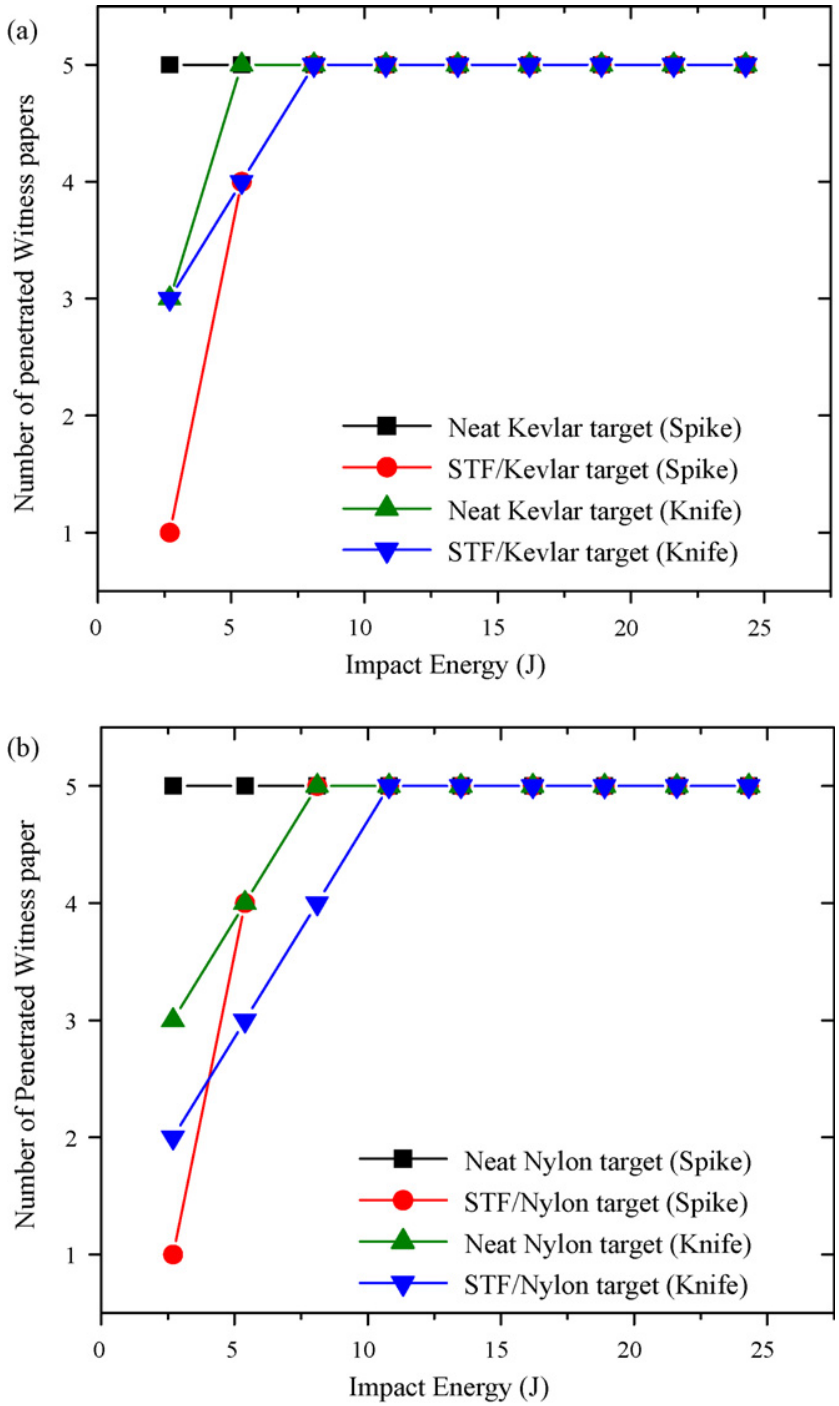

Figure 2.38. Dynamic stab test results for (a) neat Kevlar and STF/Kevlar composite (b) neat Nylon and STF/Nylon composite (Source: Hassan et al., 2010)

It was observed that STF-Nylon composite targets showed the same behavior with the STF-Kevlar composite targets against the knife and spike threats. The impact energy was measured to be increased with increasing the depth of penetration into the backing material. The STF-Nylon composite target showed less penetration depth as

compared to the neat Nylon target for the knife threats. Additionally, the maximum penetration of five witness papers for the neat Nylon target was observed at impact energy of 8 J. Conversely, the STF-Nylon composite target resulted with only two penetrated papers at impact energy of 2.7 J. For the same materials, at impact energy of 5.4 J three witness papers were found to be penetrated. The maximum penetration (five witness papers) was observed at higher energy levels. On the other hand, the maximum penetration of 5 witness papers for the neat Nylon target was observed at an impact energy of about 8 J. The STF/Nylon composite target exhibited a significant stab resistance against the spike threat. The neat Nylon target did not show any resistance against the spike stab testing, i.e; maximum of 5 witness papers were penetrated for all impact energy levels.

2.7.2. Quasistatic Tests

Decker et al. (2007) investigated the quasistatic stab performance of shear thickening fluid (STF) impregnated fabrics against the knife and spike impactors. The STF-Kevlar target showed significantly higher load than the neat Kevlar target against both impactors as shown in Figure 2.39. It should also be noted that there is a better penetration resistance for the spike threat than for the knife threat. This behavior correlated with the appearance of the targets after testing. For the spike impactor, all five witness papers under the neat Kevlar target were penetrated, whereas none of the witness papers for the STF-Kevlar target were penetrated. Conversely, four witness papers were penetrated for both Kevlar and STF-Kevlar targets against the knife impactor.

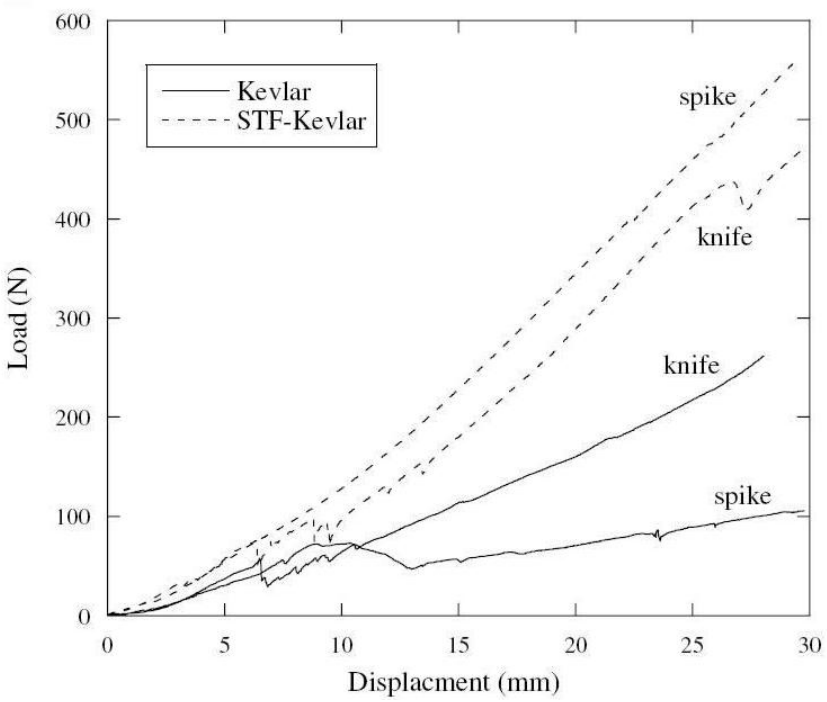

Figure 2.39. Load-displacement curve for quasistatic loading of Kevlar and STF-Kevlar target against both impactor (Source: Decker et al., 2007)

Hassan et al. (2010) explored the quasistatic performance of shear thickening fluid (STF) impregnated fabrics to implement the drop tower tests againts both knife and spike impactors. The load against displacement curve for quasistatic loading of neat fabric and STF-Fabric composite as shown in Figure 2.40. It can be seen that STF-Kevlar composite target exhibited significantly higher load 530 N, whereas the neat Kevlar target showed 286 N against the knife impactor. Furthermore, the neat Kevlar target showed 85 N load and also the STF –Kevlar composite target exhibited a high load of 575 N against the spike impactor. Additionally, the STF-Nylon composite target indicated higher loading 406 N than the neat Nylon target 284 N against the knife impactor. On the other hand, the neat Nylon target exhibited only 100 N of load. Conversely, STF-Nylon composite target showed higher load 548 N against the spike impactor. The quasistatic loading results showed a great improvement in loading resistant in STF/fabric composite targets as compared to the neat fabric targets for both the spike and knife threats. It was observed that this behavior is owing to the addition of STF to the fabrics.

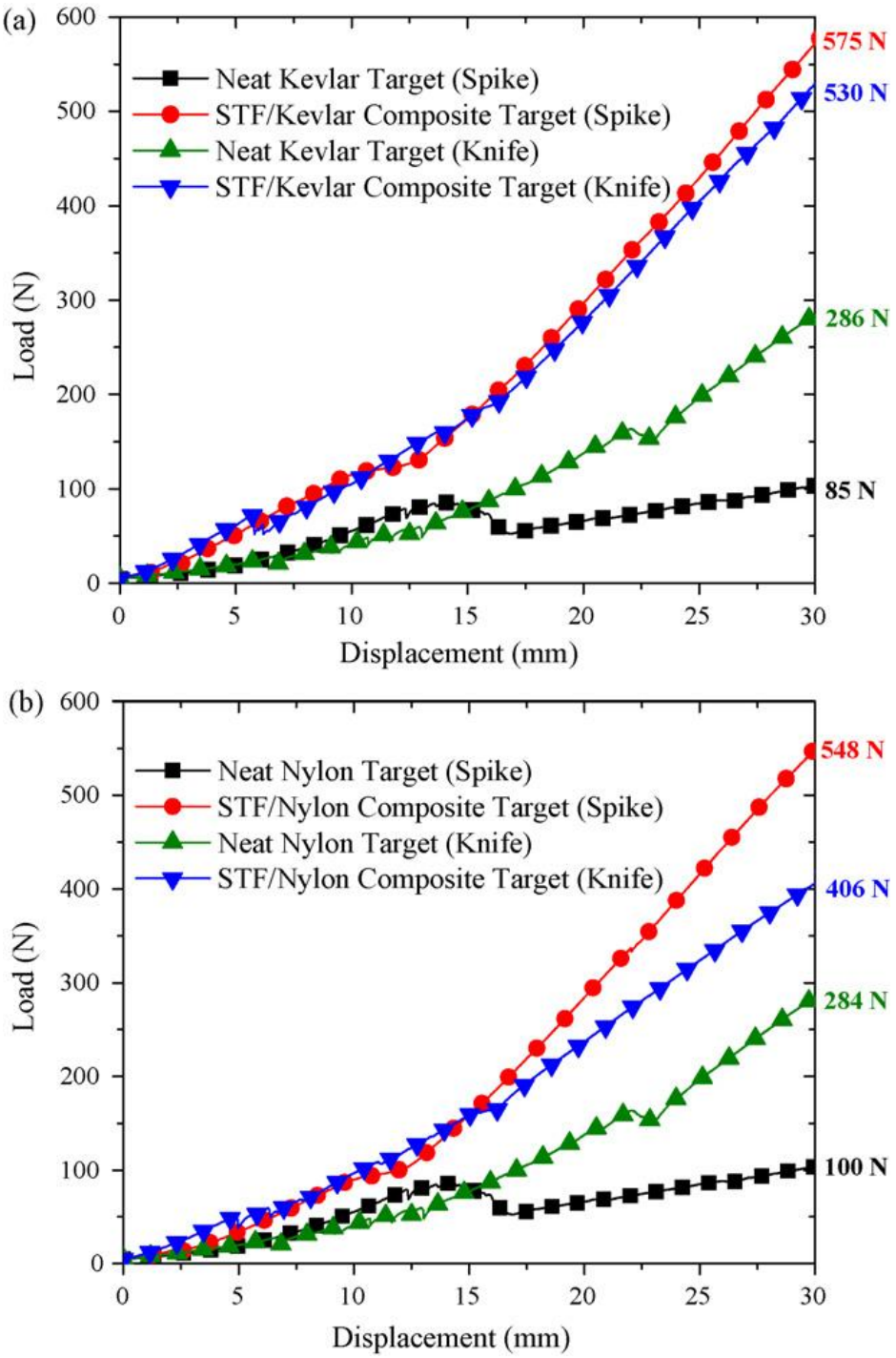

Figure 2.40. Quasistatic results for neat and STF/fabric composite targets (Source: Hassan et al., 2010)

2.7.3. Flexibility and Thickness Tests

The flexibility and thickness properties are investigated to understand the effect of the STF addition for both neat Kevlar and STF-Kevlar composites. The results showed that the weight of the 4-layer STF-impregnated Kevlar is found to be the same

with the 10-layer unimpregnated Kevlar. On the other hand, the 4-layer STF-impregnated Kevlar indicated more flexibility as compared with the 10-layer unimpregnated Kevlar. It was observed that there is no difference in terms of flexibility between the neat Kevlar and STF-impregnated Kevlar fabrics. The addition of STF caused no change in the flexibility of Kevlar fabrics as shown in Table 2.2 (Lee et al., 2003).

Table 2.2. Flexibility and thickness values for neat Kevlar and STF-impregnated Kevlar (Source: Lee et al., 2003)

Target	Description	Sample weight (g)	Penetration Depth(cm)	Dissipated energy (Joule)	Bending angle, θ (°)	Sample Thickness (mm)
G	4 layers of Kevlar	1.9	2.12	25.1	50	1.4
J	10 layers of Kevlar	4.7	1.55	28.6	13	3.0
H	2 ml STF impregnated in 4 layers of Kevlar	4.8	1.23	28.6	51	1.5

Hassan et al. (2010) showed the effect of the addition STF on the fabric flexibility and thickness for both neat fabric and STF-fabric composite samples. The thickness of 4 layers of STF impregnated Kevlar fabric is found to be almost the same with the neat Kevlar fabric. Furthermore, the 4-layers of STF-impregnated Kevlar showed the same flexibility and thickness with the 4 layers of unimpregnated Kevlar. The 10 layers of neat Kevlar and STF-Kevlar composite indicated almost the same values in terms of flexibility and thickness as shown in Table 2.3.

Table 2.3. Flexibility and thickness values for neat fabric and STF-impregnated fabrics (Source: Hassan et al., 2010)

Sample	Number of layers	Sample weight (g)	Sample thickness (mm)	Bending angle (°)
Neat Kevlar	4	1.90	1.03	50
Neat Kevlar	10	5.02	2.52	13
STF/Kevlar composite	4	2.25	1.08	51
STF/Kevlar composite	10	5.63	2.70	13
Neat Nylon	4	4.34	2.34	62
Neat Nylon	10	10.86	5.88	32
STF/Nylon composite	4	5.17	2.83	63
STF/Nylon composite	10	12.92	6.84	34

It can be seen that the neat and STF-impregnated Nylon fabrics showed slightly different results as compared to the Kevlar fabrics in terms of flexibility and thickness. The results indicated that the addition of STF caused no change in the flexibility and thickness of fabrics.

2.7.4. Ballistic Tests

Lee et al. (2003) investigated the ballistic performance of Kevlar woven fabrics impregnated with a colloidal shear thickening fluid. The results showed that a significant enhancement in ballistic resistance owing to the addition of shear thickening fluid to the fabric, without any loss in material flexibility. The ballistic test results of STF impregnated Kevlar targets are shown in Table 2.4. It should be noted that energy absorption by the STF-fabric composite was found to be proportional to the volume fraction. The STF-impregnated Kevlar fabric supplied almost the same ballistic protection as compared with neat Kevlar fabrics of equivalent weight. Furthermore, STF-impregnated Kevlar composites were found to be much thinner and more flexible.

Table 2.4. Test results of STF impregnated Kevlar fabrics with different conditions (Source: Lee et al., 2003)

Target	Description	Sample weight (g)	Impact velocity (m/s)	Penetration depth	Dissipated energy (Joule)
A	8 ml STF-K-K-K-K	13.9	247	1.72	27.8
B	KK-8ml STF-K-K 4 ml STF	13.9	249	1.36	29.8
C	KK-8ml STF-K-K	13.9	244	1.22	28.9
D	K-K-K-K-8 ml STF	13.9	253	1.19	31.5
E	K-K-8 ml STF impregnated in 2 layers of Kevlar	13.9	242	0.787	29.7
F	8 ml STF impregnated in 4 layers of Kevlar	13.9	253	0.673	32.9

CHAPTER 3

EXPERIMENTAL

3.1. Materials

The polyethylene glycol (PEG) was used as the liquid polymer (oligomer) in the STFs synthesis process. The average molecular weight of the PEG used in this study was 200 g/mole and it was purchased from Acros Organics, Belgium. The PEG had a density of 1.125 g/cm^3, a melting point (Tm) of – 65°C, a flash point of 171°C and a refractive index of 1.458-1.461 (20°C, 589 nm). The fumed amorphous silica nanoparticles were used as dry particles in this study. These nanoparticles were purchased from Cabot Corporation, USA. The properties of the nanoparticles are given in Table 3.1. Ethyl alcohol was used as the solvent in the mechanical mixing process in order to synthesize STF. Ethyl alcohol was purchased from Merck Chemicals, Germany.

Table 3.1. Properties of the fumed amorphous silica nanoparticles (dry powder) used in this study (Source: Cabot Corporation, 2004)

B.E.T. Surface Area	200 m²/g
pH (4% aqueous slurry)	3.7–4,3
325 Mesh Residue (44 microns)	0.02% max.
Bulk Density (Pour Density)	3.0 lb/ft3 max. (50 g/l Tap Density)
Loss on Heating	< 1.5% max.
Loss on Ignition (1000ºC)	< 2 wt. %
Specific Gravity Wt. per gallon	2.2 g/cm^3 18.3 lb
Refractive Index	1.46
X-ray Form	Amorphous
Assay (% SiO_2)	> 99.8
Oil Adsorption	~350 g/100 g oil
Average Particle (Aggregate) Length	0.2–0.3 microns

The Kevlar fabrics were also used in this study to prepare the STF/Kevlar fabric composite materials. The Kevlar fabrics used in all composite targets was plain-woven Hexcel Aramid (polyparaphenylene terephthalamide), Fabric Style 140 with an areal density of 110 g/m^2. The Kevlar fabrics were purchased from C. Cramer GmbH & Co. KG, Germany.

3.2. Synthesis of Shear Thickening Fluids

The STF synthesis procedure is schematically illustrated in Figure 3.1. The polyethylene glycol (PEG) and fumed amorphous silica nanoparticles were mixed in excess amount of ethyl alcohol (20:80 STF:ethyl alcohol ratio was used) in order to produce stable dispersions. A variety of weight fractions of nanoparticles were added to PEG and they were blended in excess amount of ethyl alcohol at a temperature of 25 ºC for 5 hours by mechanical mixing method. After obtaining the solution of the STF, the solution was dried and held in an air-circulating oven for 12 hours in order to remove ethanol from the reaction mixture. The evaporation temperature of ethanol was set around 79 ºC. After being held for 12 hours in an oven, STF was grinded in a agate mortar. The grinding was applied until homogeneous dispersion was obtained. In order to eliminate the bubbles, STF was placed in a vacuum oven at room temperature for several hours until no bubbles were observed. The concentrations of STF samples prepared are listed in Table 3.2. The STF samples produced are also shown in Figures 3.2 to 3.4.

Table 3.2. The concentrations of STF samples produced in this study.

Sample ID	Silica weight fraction (%)	PEG weight fraction (%)
%5	5	95
%7.5	7.5	92.5
%10	10	90
%15	15	85
%20	20	80
%25	25	75

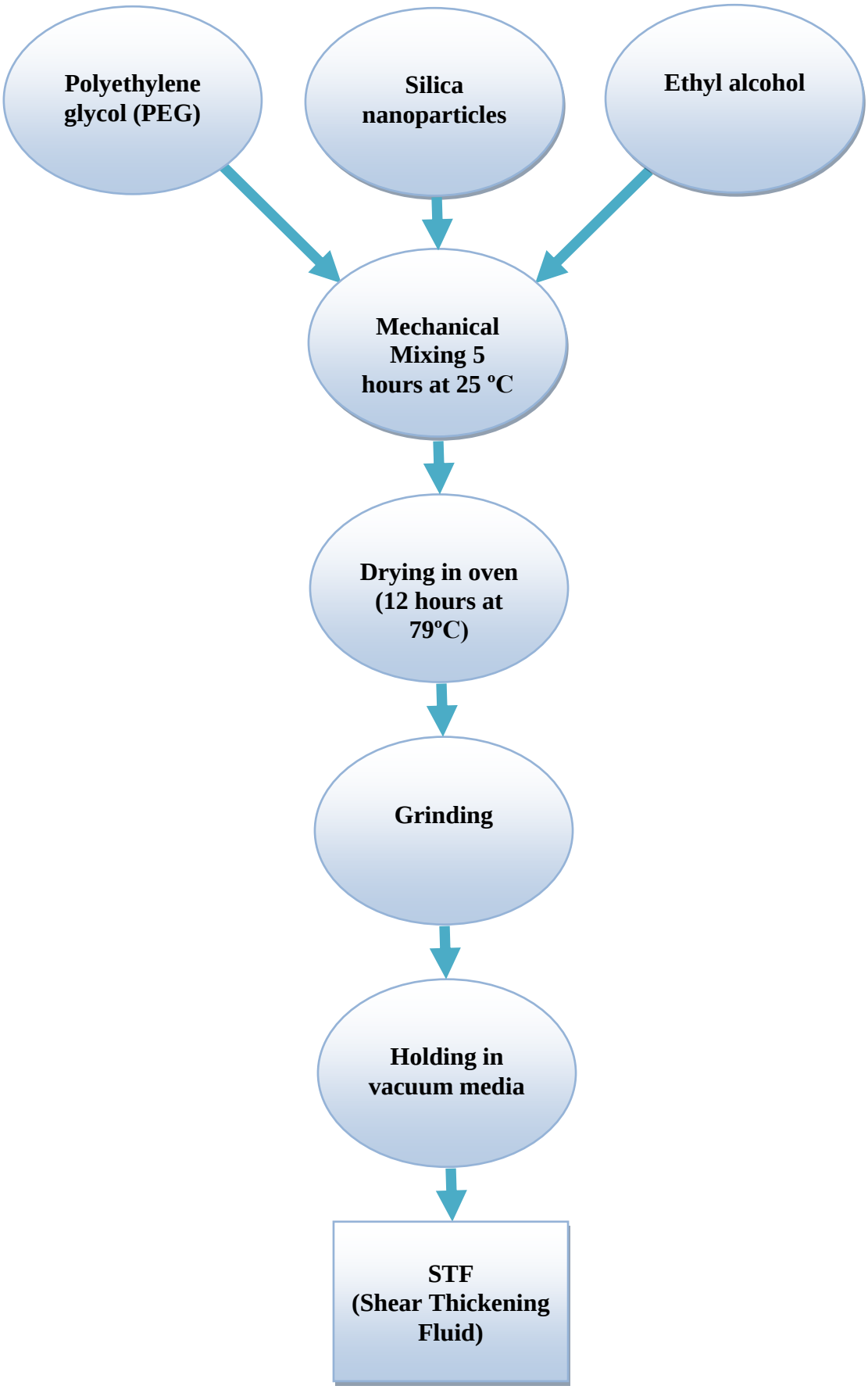

Figure 3.1. Processing stages of shear thickening fluid (STF)

Figure 3.2. The STF sample produced in this study after drying process.

Figure 3.3. The STF sample produced in this study after grinding process.

Figure 3.4. The STF sample produced in this study after completion of the synthesis process.

3.3. Fabrication of STF/fabric Composites

The STFs/fabric composite materials were prepared for testing based on to the following procedure. To produce STF/fabric composites various impregnation procedures were applied. Based on the experiments to obtain rheological properties, STF concentration with 25 wt% silica and 75 wt% PEG was selected to prepare STF/fabric composite materials in the further experiment. The STF/fabric impregnation stage is schematically illustrated in Figure 3.5.

To prepare STF/fabric composites, 200 mm×200 mm layers of Kevlar fabrics were cut and individual layers were impregnated by STF solution. Each sheet of Kevlar fabrics was soaked in a plastic container filled with STF solution for 5 min and then hanged vertically to remove the excess amount of the STF solution. The impregnated fabrics were hold at room temperature for 24 h to remove the solvent.

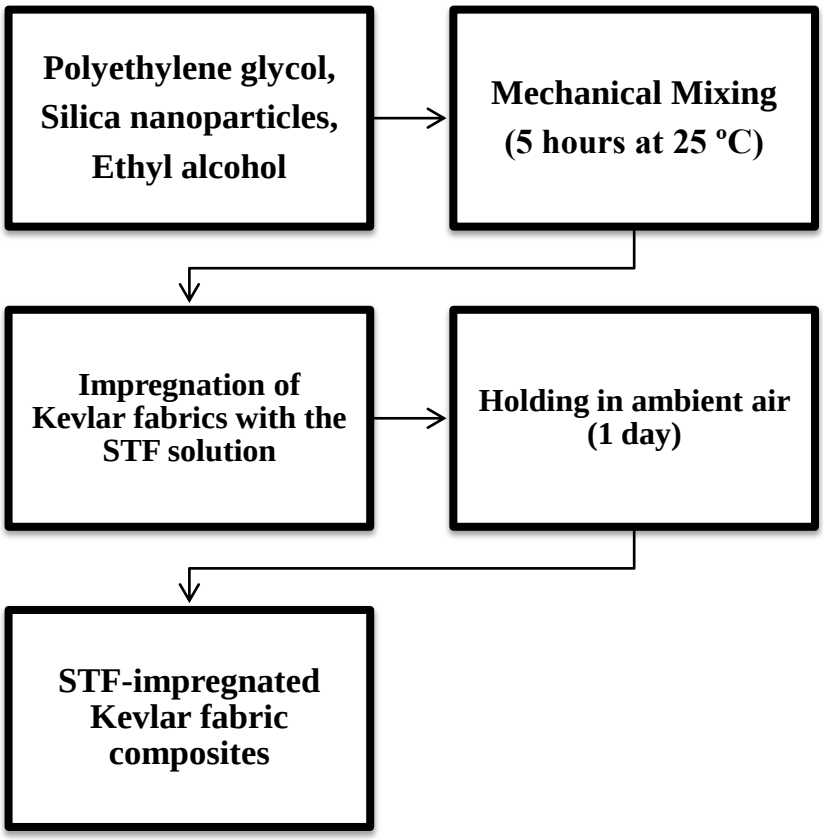

Figure 3.5. Stages of the fabric impregnation by STF

As a second alternative route, the STF was prepared as described in Figure 3.1 and in the next step ethyl alcohol was added to the original STF solution to reduce the viscosity. The diluted STF/fabric impregnation procedure is schematically illustrated in Figure 3.6. Individual fabric layers each has about 200mm×200mm dimensions were soaked in the STF/ethyl alcohol solution for 5 minutes and slightly pressed to get rid of the excess amount of the fluid. It was observed that the diluted STF was spontaneously impregnated into the fabric. STF impregnated Kevlar fabrics were dried in an air-circulating oven at 79 ºC for 12 h. This drying process was applied to remove the ethyl alcohol co-solvent, and to leave STF behind in the fabric.

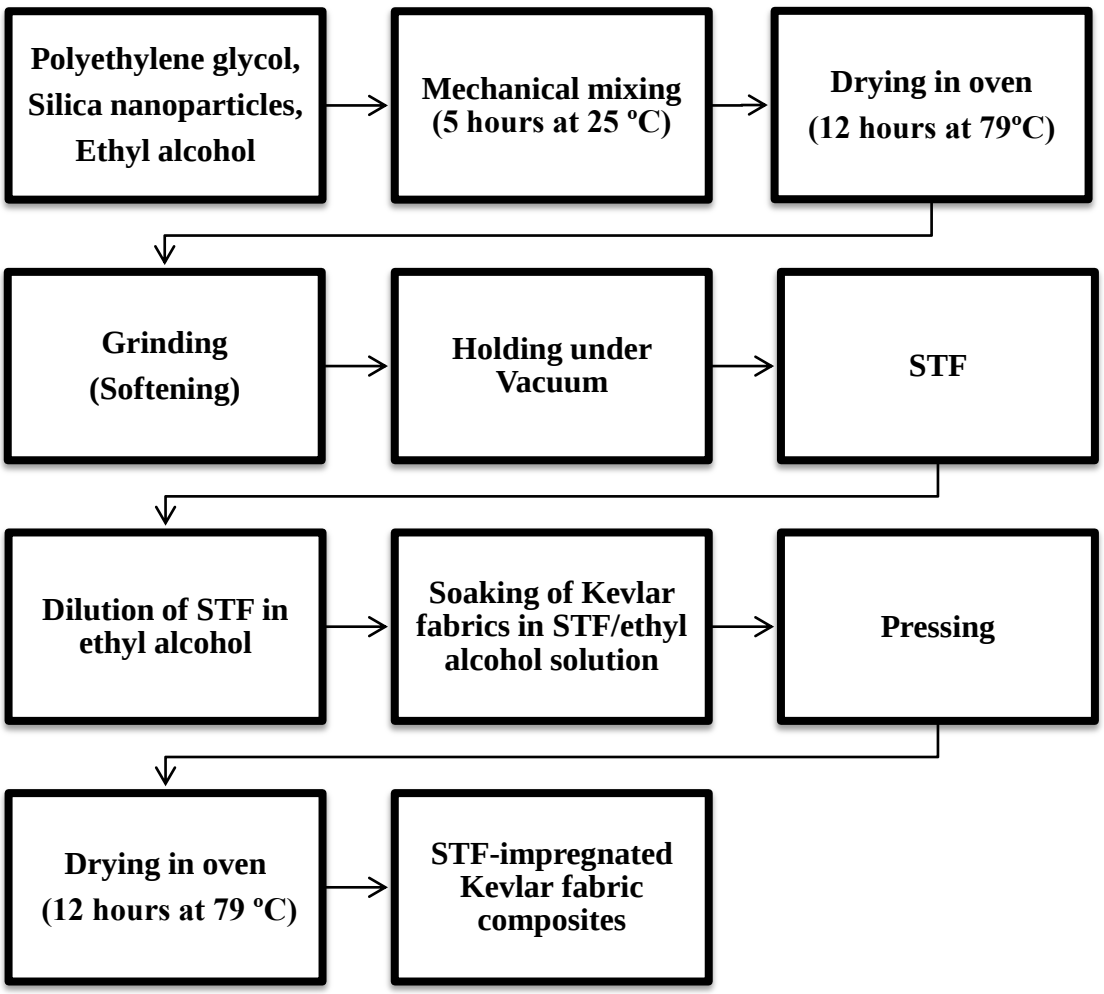

Figure 3.6. Shematic of the fabric impregnation procedure with diluted STF

As a third approach, the grinded (softened) STF were used immediately to fabricate the STF/fabric composites after the grinding process. This third STF/fabric impregnation procedure is schematically given in Figure 3.7. In this procedure, ethyl alcohol was not used to dilute the STF unlike the one described in the second approach given in Figure 3.6. To easily impregnate fabrics with STF, the STF was applied immediately after grinding process. Each fabric layer was soaked in the softened STF for 5 minutes and squeezed by pressing them between rigid Al panels to spread the solution homogeneously into the Kevlar fabrics.

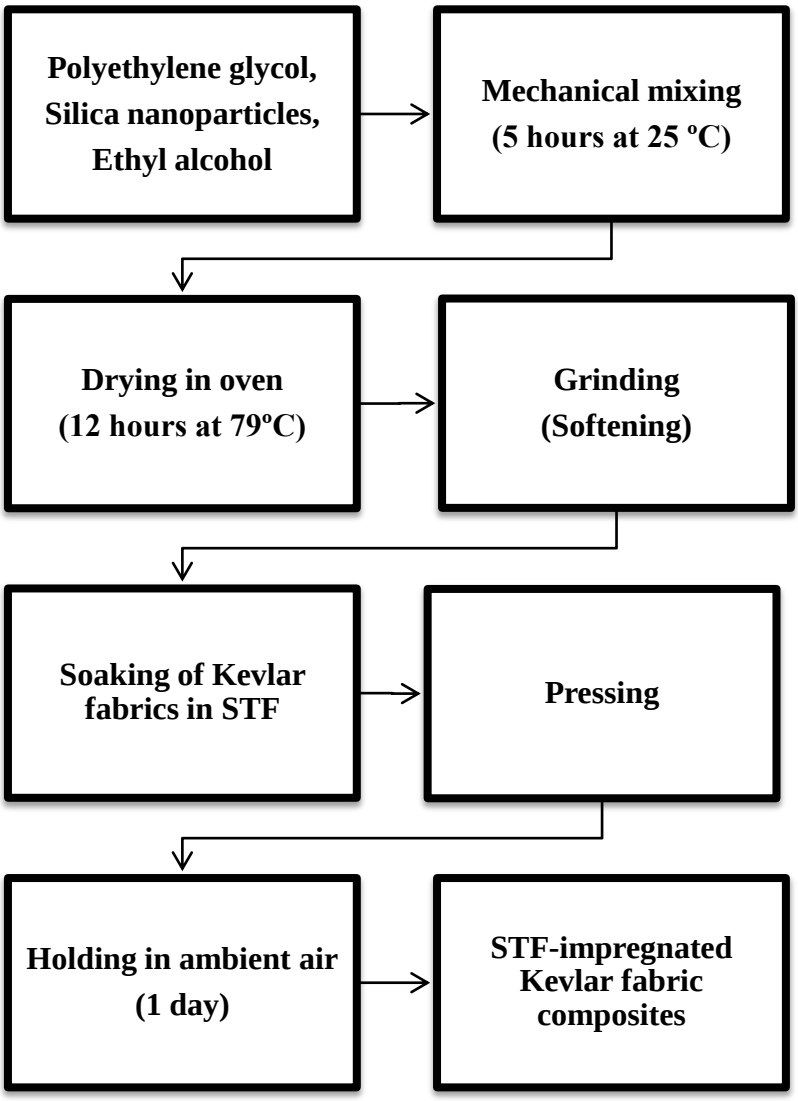

Figure 3.7. Shematic of the fabric impregnation procedure with grinded (softened) STF

After completion of impregnation procedures, in all cases, puncture targets consisting of ten layers of Kevlar were prepared. The weight of the fabric sheets was measured before and after the impregnation to ensure that the fabric layers have been equally impregnated with the STF and STF/ethyl alcohol solution. The STF/fabric composites were also arranged into multilayer targets. The STF/fabric composite materials prepared are listed in Table 3.4. Figure 3.8 also shows STF/fabric composite materials processing with the second approach.

Table 3.3. Chracteristics of STF/Kevlar fabric prepared in this study. The fabric material used is Kevlar fabric style 140

Sample ID	**STF wt% Impregnated into fabric**	**Number of layers in target**	**Sample weight (g)**	**Areal density (kg/m^2)**
Neat Kevlar	0.0	10	47	1.175
STF impreganated Kevlar	25	10	65	1.625
Diluted STF impregnated Kevlar	25	10	133	3.325
Softened STF impregnated Kevlar	25	10	250	6.25

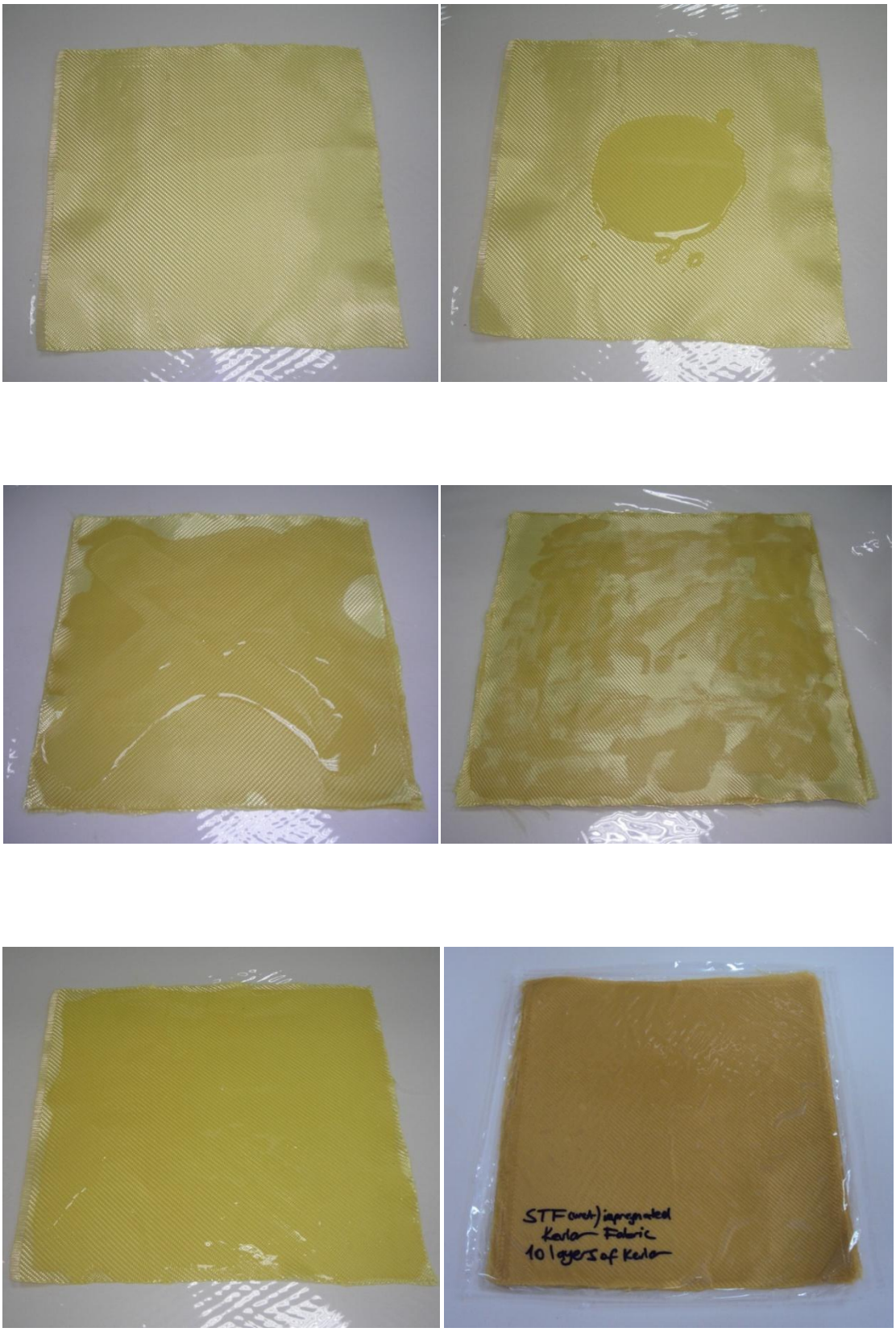

Figure 3.8. Photos showing the steps of the preparation of STF-impregnated Kevlar fabric composites

3.4. Characterization of Nanoparticles

3.4.1. Size Distribution of Particles with Dynamic Light Scattering (DLS)

The average particle size and size distribution based on intensity, volume and number of silica nanoparticles were measured with Zetasizer 3000HS by using Dynamic Light Scattering (DLS) technique. The wavelength of the laser light employed in the instrument was 633 nm, which can detect a minimal particle size 2 nm. Measurements for each sample were repeated at least three times. To investigate the particle size distributions, silica nanoparticles were dispersed in water. For this purpose, dry powder silica nanoparticles were dispersed in water and mixed for about 30 minutes until obtaining stable dispersion.

3.4.2. X-ray Diffraction (XRD)

X-ray Diffraction (XRD) analysis was performed using a Phillips™ XPert diffractometer with CuKα radiation source (λ=0.1541nm) operated at 40 kV and 30 mA over a 2θ-range of 5º - 70º for silica nanoparticles. The silica nanoparticles were analyzed to identify the crystallinity.

3.4.3. Fourier Transform Infrared Spectroscopy (FTIR)

Fourier transformed infrared (FTIR) was used with Spectrum 100 FTIR spectrometer (Perkin Elmer, Waltham, MA) to identify the molecular functional groups. The spectrum was collected in absorption mode from 400 to 4000 cm^{-1} at room temperature. FTIR spectrum was recorded using the KBr pellet technique.

3.4.4. Thermogravimetric Analysis (TGA)

Thermogravimetric analysis (TGA) is a technique which analyses the weight alteration as a result of heating. Thermal gravimetric analysis was performed with Perkin Elmer Diamond Thermo Gravimetric Analyzer to analyze the weight loss as a

function of temperature. The silica nanoparticles were heated at a rate of 10 ºC per minute from 30 ºC to 1200 ºC.

3.4.5. Scanning Electron Microscopy (SEM)

The silica nanoparticles were investigated with Phillips™ XL-30S FEG Scanning Electron Microscopy (SEM). All the sample surfaces were gold-coated by a sputtering apparatus before SEM examination. For SEM analysis, three types of silica nanoparticles were prepared. Silica nanoparticles-water suspension, silica nanoparticles-ethyl alcohol suspension and only silica nanoparticles without using any solvent. For the preparation of the suspension, silica nanoparticles were dispersed in distilled water and ethyl alcohol followed by a mixing for 1 hour using a magnetic stirrer in order to obtain homogeneous suspensions. Then, silica nanoparticles suspensions were coated as a thin layer and dried to remove the solvent.

3.5. Characterization of Shear Thickening Fluids

3.5.1. Scanning Electron Microscopy (SEM)

Dispersion of the silica nanoparticles in polyethylene glycol (PEG) was investigated using SEM (Phillips™ XL-30S FEG-SEM) from the STFs surface. For this purpose, STFs solutions were coated as a thin film. The sample surface was gold-coated by a sputtering apparatus before SEM examination.

3.5.2. Fourier Transform Infrared Spectroscopy (FTIR)

Fourier transformed infrared (FTIR) was used with Spectrum 100 FTIR spectrometer (Perkin Elmer, Waltham, MA) to identify the molecular functional groups in the STFs. The spectrum was collected in absorption mode from 400 to 4000 cm^{-1} at room temperature. FTIR spectrum was recorded using the KBr pellet technique.

3.5.3. Thermogravimetric Analysis (TGA)

Thermal Gravimetric analysis (TGA) was performed with Perkin Elmer Diamond Thermo Gravimetric Analyzer (TGA) to analyze the weight loss in STFs. The experiments were carried out from 30 ºC to 800 ºC.

3.6. Rheological Property Characterization of STFs

The steady and dynamic rheological behaviour of silica nanoparticle suspensions in PEG were investigated using a (TA AR2000ex) rheometer as shown in Figure 3.9. Experiments were conducted under both steady state as well as dynamic oscillatory shear. Dynamic oscillatory shear experiments were conducted at constant strain amplitude and constant frequency, respectively. Strain sweeps, where the frequency was held fixed and the strain amplitude increased in different steps, and frequency sweeps performed at a constant strain, with the frequency being increased in different steps. Rheological experiments were carried out at room temperature under both steady state as well as dynamic oscillatory shear mode. A cone plate having a cone angle of 2º and diameter of 40 mm was used. At higher fumed silica concentrations and dynamic oscillatory shear mode different cone plate geometry having a cone angle of 0.1 radians and a diameter of 25 mm was used. To remove loading effects, a preshear of 1 s^{-1} was applied for 60 s prior to further measurement.

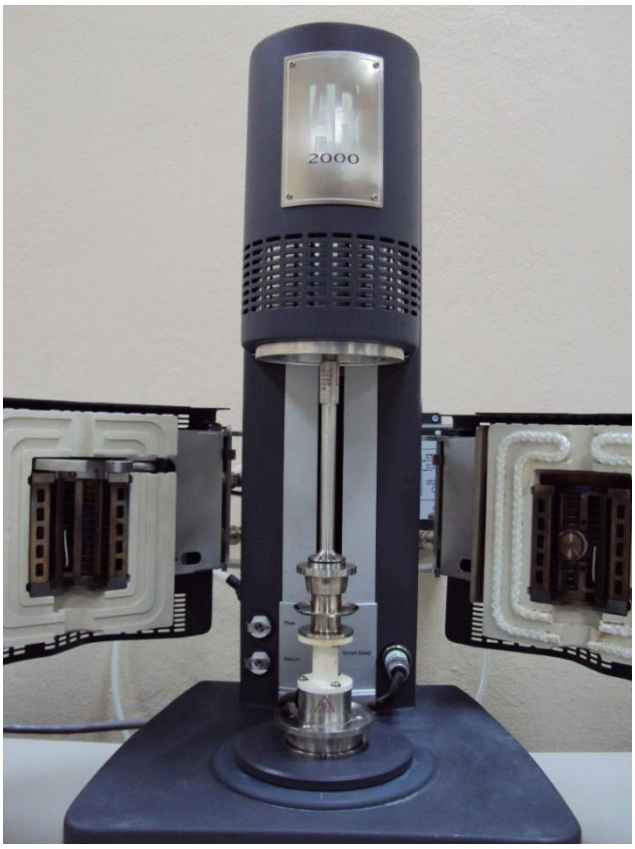

Figure 3.9. The STF sample in TA instruments Rheometer AR2000ex

3.7. Mechanical Property Characterization

3.7.1. Stab Testing

Quasistatic stab tests were performed for neat Kevlar and STF/Kevlar fabric composite targets to evaluate the fabric resistance against the spike threats. Tests were applied using the Schimadzu AGI universal test machine with a 5 kN load cell. Tests were performed by mounting a spike impactor into the crosshead of the load cell. The stab performed is based on the NIJ Standart 0115.0 for stab resistance of personal body armor. The stab targets were placed on a multi-layer foam backing as specified by the NIJ Standard. This backing consists of four layers of 5.8 mm-thick neoprene sponge, followed by one layer of 31 mm-thick polyetylene foam, backed by two 6.4-mm-thick layers of rubber, which is placed between the target and foam backing and behind each layer of neoprene sponge.

All quasistatic testing was conducted on ten-layer targets using a spike as the threat. The targets were located below the spike impactor and then the spike impactor was pushed into the target at a rate of 5 mm/min for low rate to a total depth of 30 mm. Quasistatic test configuration with the Schimadzu AGI universal test machine is shown in Figure 3.10.

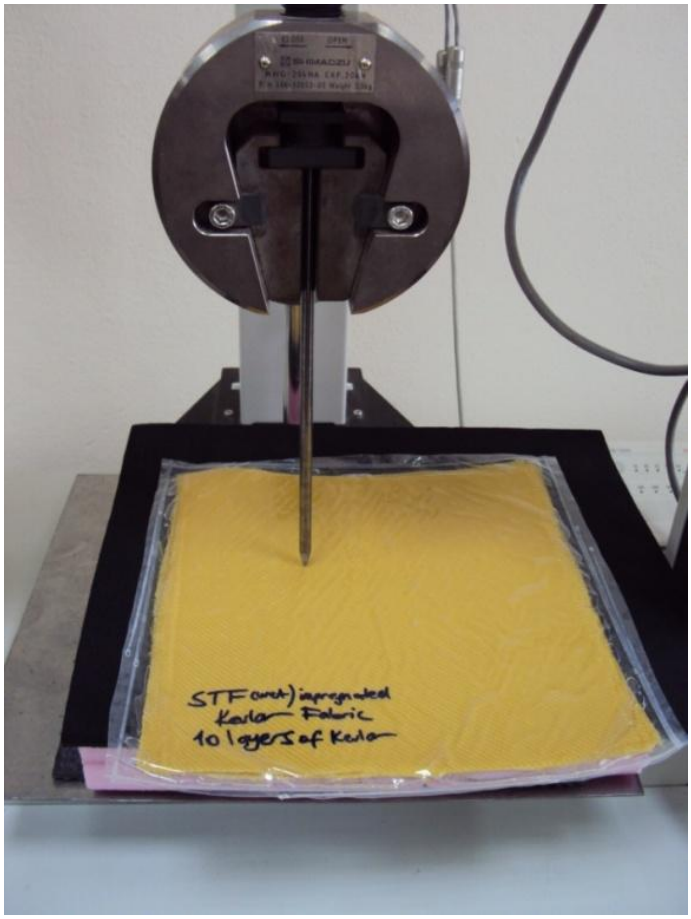

Figure 3.10. Stab test sample (STF/Kevlar fabric composite) under the Schimadzu AGI universal test machine

3.7.2. Ballistic Testing

The ballistic tests were performed for neat Kevlar and STF/Kevlar fabric composite targets to understand the effects of the STFs impregnation on the ballistic resistance of Kevlar fabrics. The ballistic testing was performed based on the NIJ standard 0101.03 (Ballistic Resistance of Police Body Armor). The configuration of the ballistic test is shown in Figure 3.11. Also, the photos of the ballistic test configuration are shown in Figure 3.12. All the tests were performed at room temperature. The gun was sighted on the target center and the impact velocity was adjusted to approximately 380 m/s. The exact impact velocity of each projectile was measured with a chronograph immediately before impacting the target. To produce the STF/fabric composites for ballistic testing various impregnation procedures were applied. The Kevlar layers were cut to 30 cm × 30 cm, impregnated with STF. The STF/fabric composites were also arranged as multilayer targets. The STF/fabric composites prepared are listed in Table 3.4.

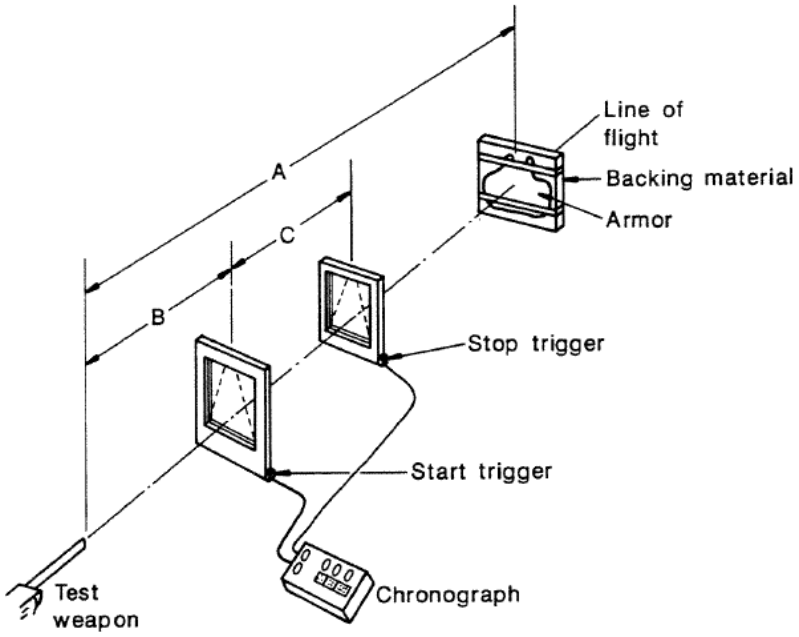

Figure 3.11. Ballistic test setup
(Source: NIJ Standard 0.101.03 Ballistic Resistance of Police Body Armor)

Figure 3.12. Photos showing the ballistic setup at Sarsılmaz Fişek San. A.Ş. a) the test gun,b) the projectile velocity measurement device for 15 m (type III and IV armors), c) the projectile velocity measurement device for 5m (type I, II-A, II and IIIA armors)

Table 3.4. Kevlar (STF unimpregnated) and STF/Kevlar (STF impregnated) fabric composites produced in this study for ballistic testing.

Sample ID	STF wt% impregnated into fabric	Number of layers in target
Unimpregnated Kevlar-1	0	10
Unimpregnated Kevlar-2	0	20
STF impregnated Kevlar-1	25	20
STF impregnated Kevlar-2	25	30
Diluted STF impregnated Kevlar-1	25	10
Diluted STF impregnated Kevlar-2	25	20
Softened STF impregnated Kevlar-1	25	10
Softened STF impregnated Kevlar-2	25	10

3.7.3. Microstructure Characterization

Scanning Electron Microscope (SEM) was performed on the neat Kevlar fabric and STF-impregnated Kevlar surfaces in order to investigate the impregnation quality of STF within the fabrics. For this purpose, Phillips™ XL-30S FEG-SEM was used. The surfaces of the samples were coated with a very thin layer of gold by a sputtering unit to obtain an electrically conductive surface to prevent charging.

CHAPTER 4

RESULTS AND DISCUSSION

In this chapter, the results and discussion on the expermental investigation of silica based shear thickening fluids (STFs) and their application onto the commercial fabrics are presented. Rheological and thermal properties of the STFs were determined and the results were given. In order to understand the effect of the STFs on the Kevlar fabrics a number of tests were performed and the experimental findings were reported.

4.1. Properties of Silica Nanoparticles

4.1.1. Size Distribution of Particles Determined by Dynamic Light Scattering (DLS)

The average particle size and size distributions based on intensity, volume and number of silica nanoparticles were obtained using DLS technique. Measurements were repeated three times for silica dispersions in water. For this purpose, dry powder fumed silica nanoparticles were mixed in water until homogeneous dispersion was obtained. DLS result is given in Figure 4.1. Based on this result, the silica nanoparticles were found to have particle sizes between 90 and 250 nm. On the other hand, polydispersity of the particle size distribution resulted in the broadening of the peaks due to aggregation of silica nanoparticles.

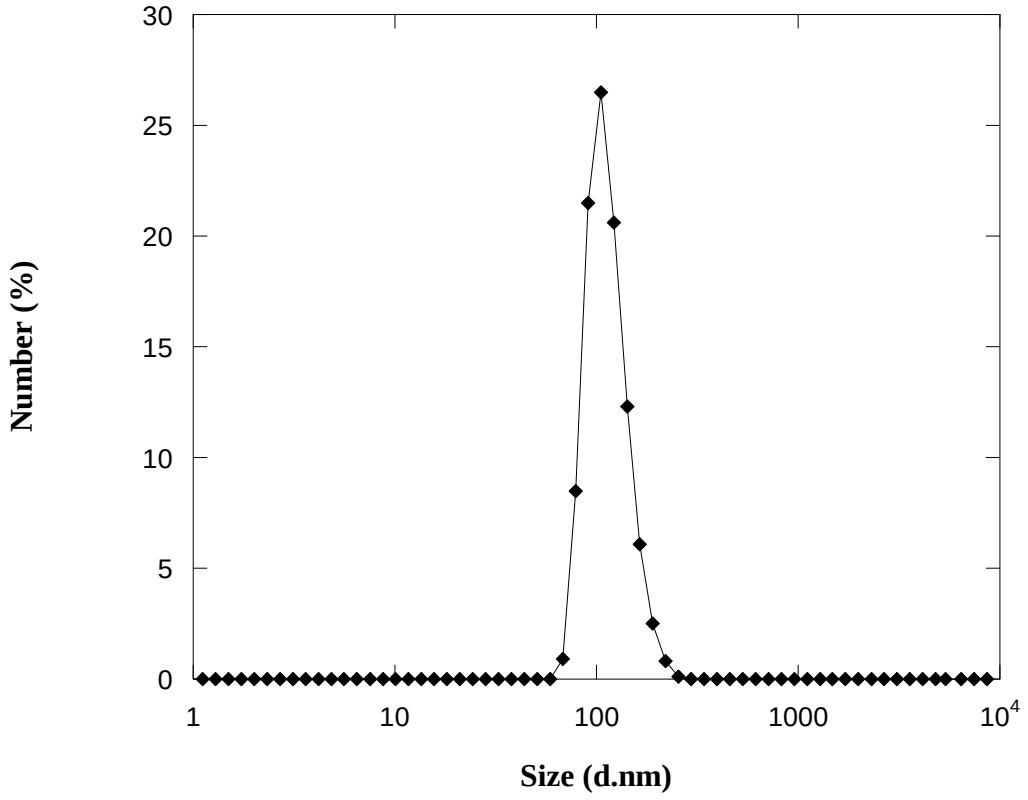

Figure 4.1.Size distributions of silica nanoparticles based on number percentage

4.1.2. X-ray Diffraction (XRD)

The XRD pattern of the dry powder fumed silica nanoparticles is shown in Figure 4.2. The characteristic peak for silica was revealed at the diffraction angle of about 23 ºC. As seen in the figure, silica shows a broad peak that indicates a relatively high fracture of amorphous phases with the silica structure.

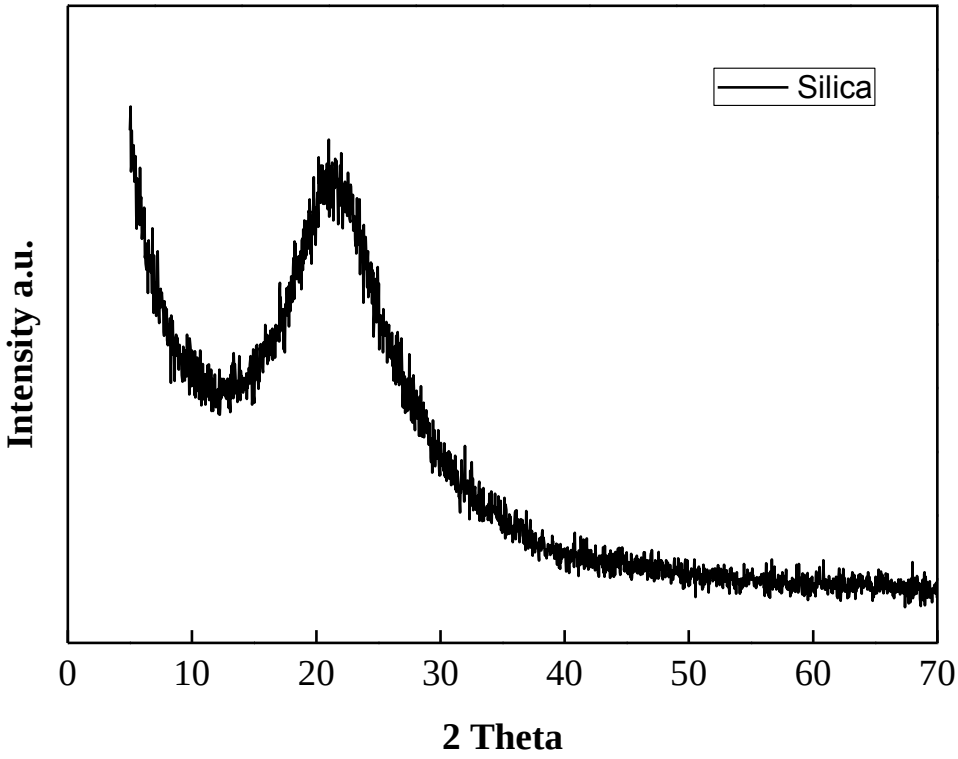

Figure 4.2. XRD pattern of dry powder fumed silica nanoparticles

4.1.3. Fourier Transform Infrared Spectroscopy (FTIR)

The FTIR spectrum of dry powder fumed silica nanoparticles is given in Figure 4.3. Typically, silanol and silicon alkoxides groups appear in the range from 1400 cm^{-1} to 400 cm^{-1}. According to spectra, the band at 800 cm^{-1} which is attributed to silicon alkoxides (Si-O-Si stretching) and the band at 940 cm^{-1} which is attributed to the bending modes of Si-O-H and Si-O are observed. The strongest band is observed in the asymmetric siloxane stretch (Si-O-Si) region, from about 950 to 1250 wavenumbers. In this region, the strongest band is at about 1090 cm^{-1}, and it is present for the sample. An adsorption peak around 1640 cm^{-1} is also visible in the spectra, which is assigned to the bending mode of physically absorbed water molecules. The other important infrared vibrations of silica that are the band at 1250-1020 cm^{-1} which is attributed to asymmetric stretching of Si-O-Si and at 3400-3500 cm^{-1} which belongs to stretching of Si-OH are also visible. The broad band in the range of 2800-3600 cm^{-1} is attributed to the stretching modes of hydroxyl groups and molecular water.

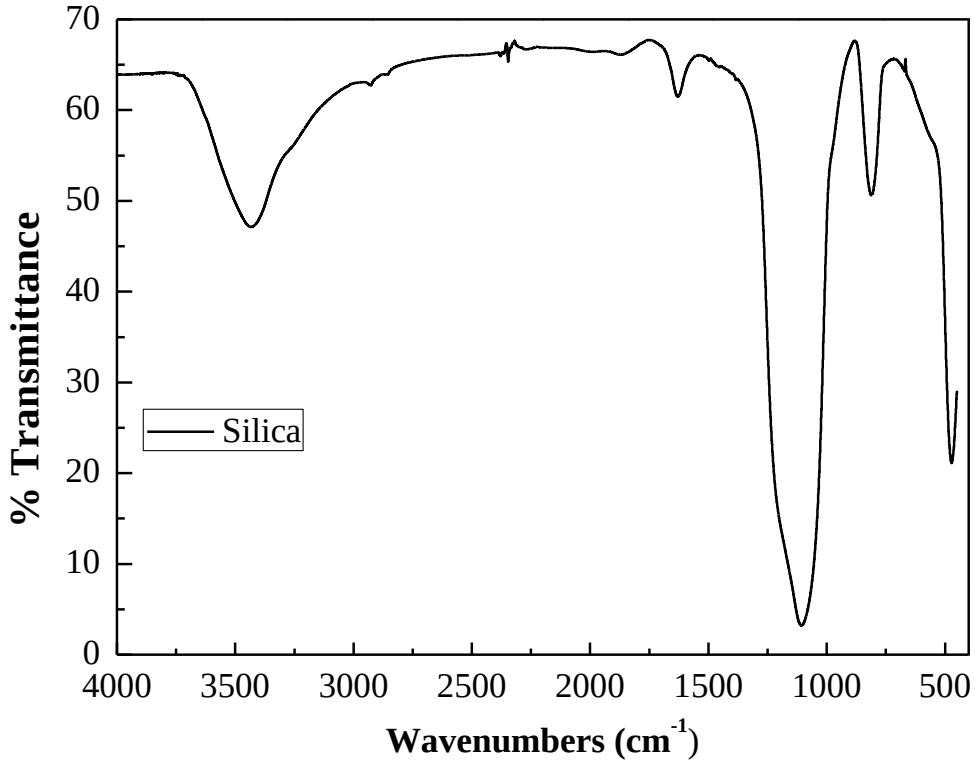

Figure 4.3. FTIR spectrum of dry powder fumed silica nanoparticles

4.1.4. Thermogravimetric Analysis (TGA)

The result of the thermal analysis of silica nanoparticles is given in Figure 4.4. The weight loss of silica nanoparticles continues with increasing temperature. Based on the TGA curves, from the room temperature to 800 °C, the total weight loss was found to be 12%. The weight loss from the room temperature to 270 °C may be due to the removal of the chemically bond water. It was observed that there is a gradual weight loss up to 800 °C.

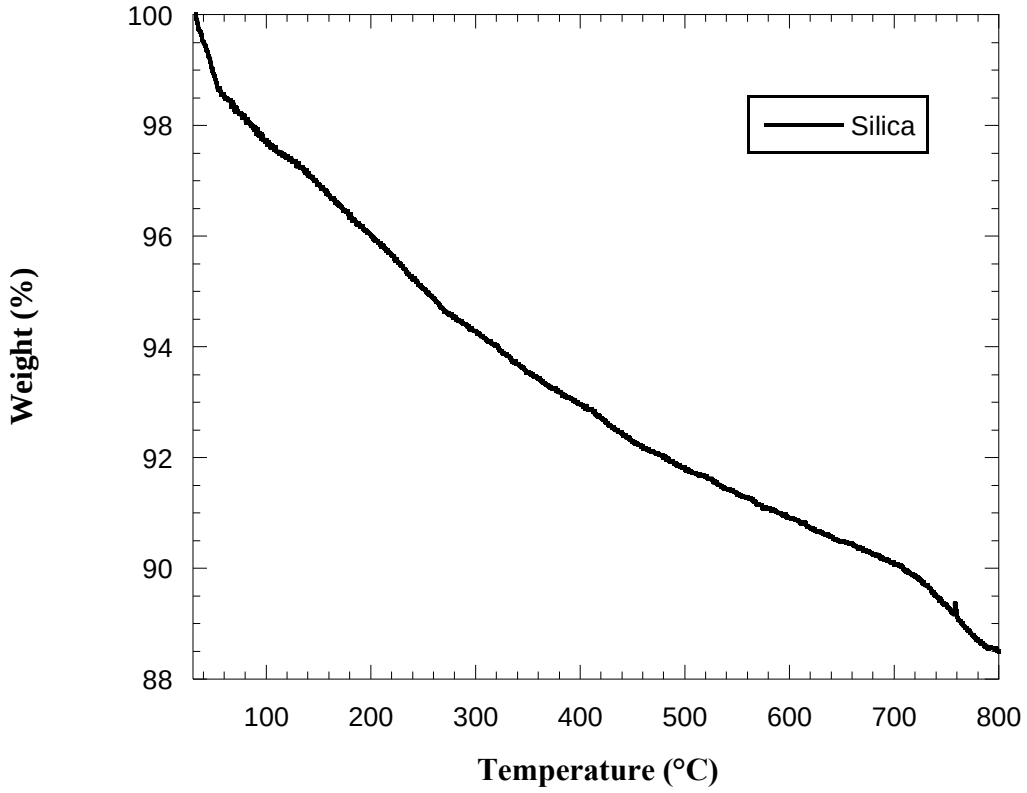

Figure 4.4. TGA curve of dry powder fumed silica nanoparticles

4.1.5. Scanning Electron Microscopy (SEM)

SEM was conducted to characterize the morphology and structure of the silica nanoparticles at different magnification. The SEM images of silica nanoparticles prepared with different methods; dry powder, dispersed in ethyl alcohol and dispersed in water, respectively are shown in Figure 4.5. The particles seems to be nearly spherical in shape and the size distribution was assumed to be around 50-200 nm agglomerates.

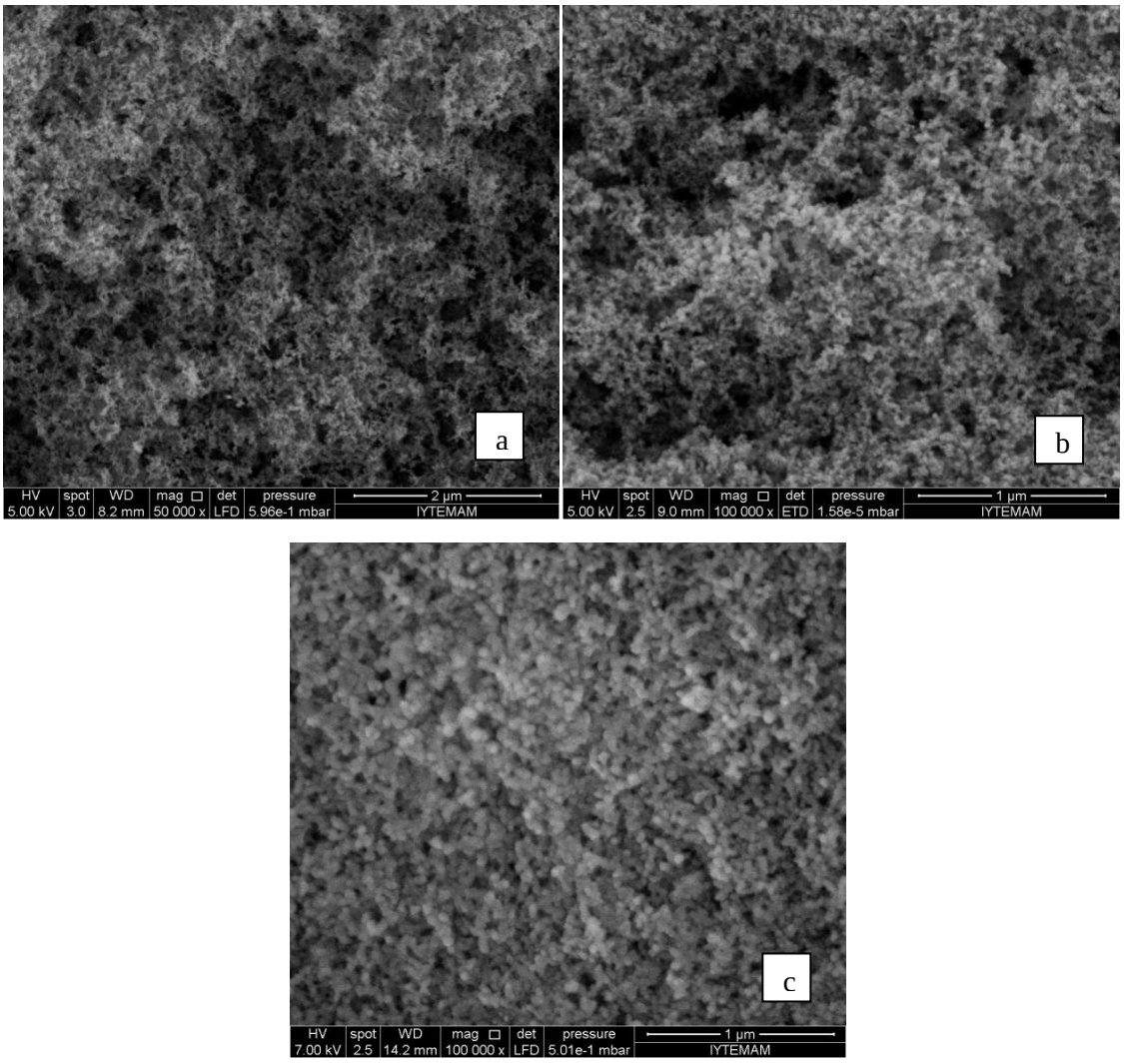

Figure 4.5. SEM images of dry powder fumed silica nanoparticles
a) dry powder, b) dispersed in ethyl alcohol and dried,
c) dispersed in water and dried

4.2. Properties of Shear Thickening Fluids

4.2.1. Scanning Electron Microscopy (SEM)

To further study the dispersion of silica nanoparticles in PEG, SEM analyses were carried out on the STF sample. Figures 4.6 and 4.7 show the SEM micrographs of STF sample at different magnifications. It was observed that the silica nanoparticles are well coated with PEG. The high magnification of SEM images (Figure 4.7) of STF sample clearly show the perfect blend of silica and PEG.

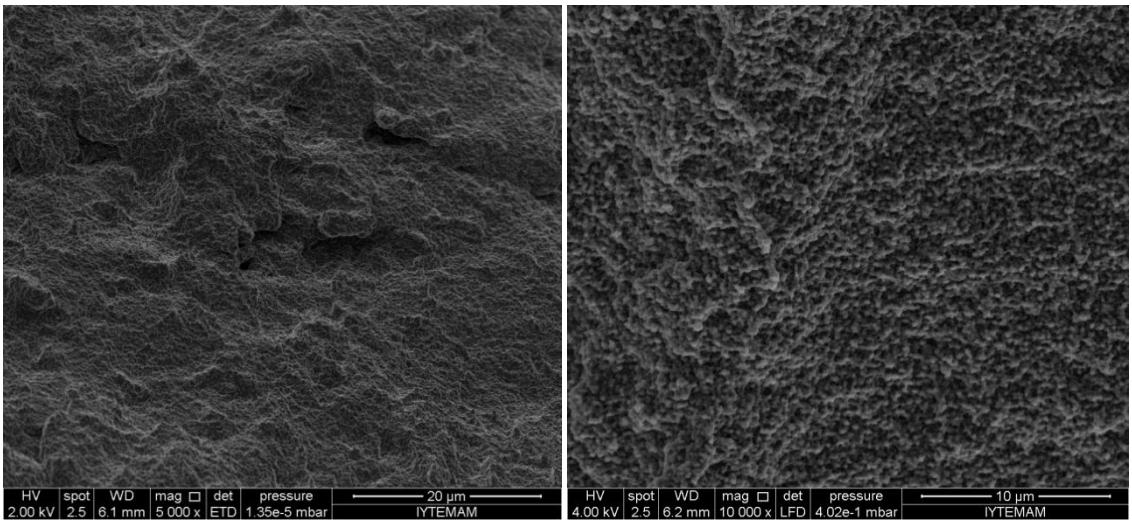

Figure 4.6. SEM images of STF at different magnifications

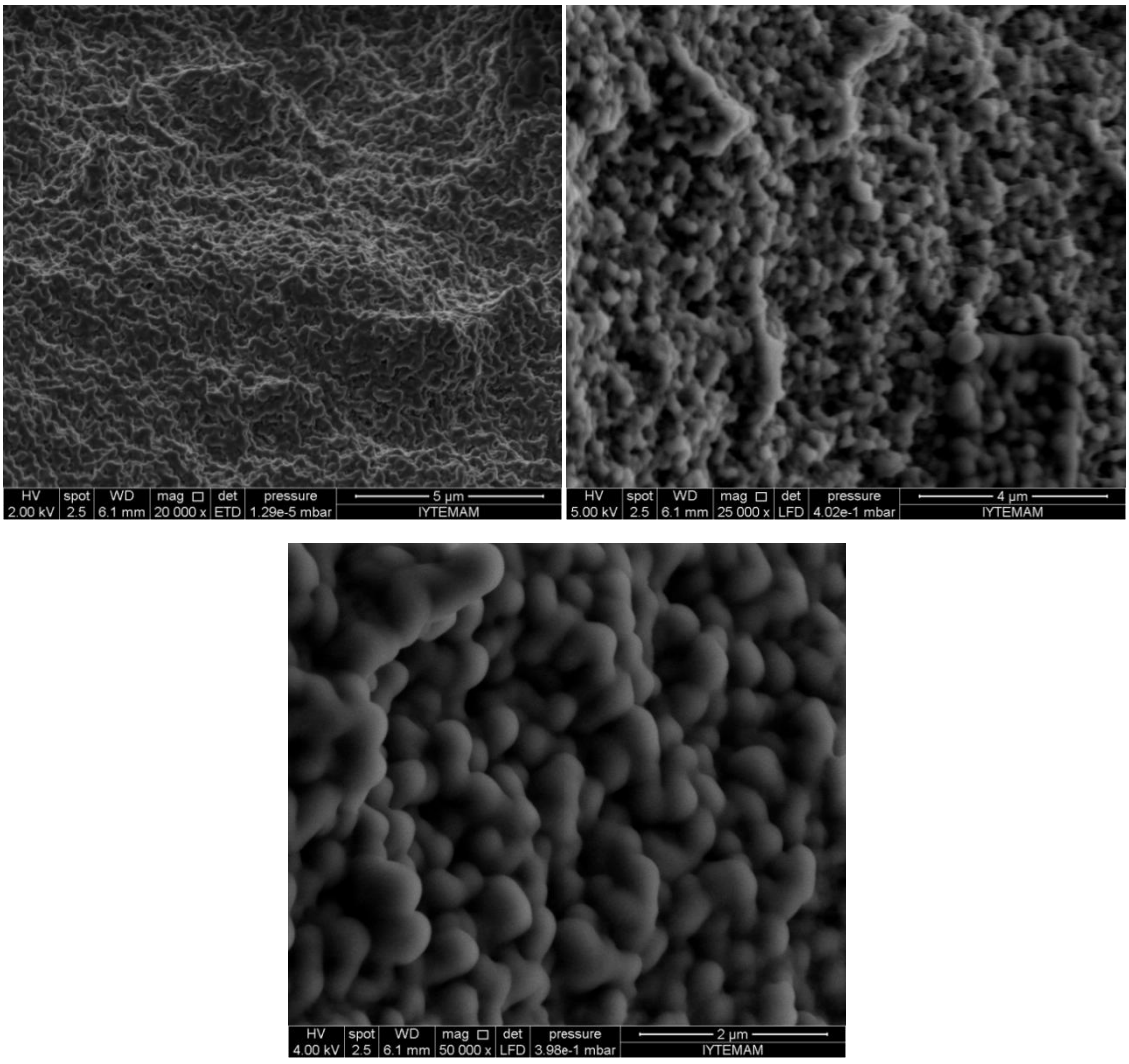

Figure 4.7. SEM images of STF at different magnifications

4.2.2. Fourier Transform Infrared Spectroscopy (FTIR) of STF

The FTIR spectrum of STF sample was recorded using KBr pellet method as shown in Figure 4.8. Typically, the two characteristic bands at 3391 and 1099 associates with the STFs-related groups, the stretching vibration of O-H bond and the stretching modes of the Si-O bond in the silicate groups, respectively. Due to the broad band in the range 3200-3600 cm^{-1} is attributed to the stretching modes of hydroxyl groups and molecular water. The stretching vibrations of alkanes can be observed at 2960-2850 and the bending vibrations of alkanes can be observed at 1470 and 1350. According to spectra, the band at 2877 which is attributed to C-H stretching and the bands at 1455 and 1351 which is attributed to the bending modes of C-H was observed. The peak at 1644 is due to C=C stretching. The other important infrared vibrations of silica that are the band at 1250-1020 cm^{-1} is attributed to asymmetric stretching of Si-O-Si and at 3400-3500 cm^{-1} which belongs to stretching of Si-OH.

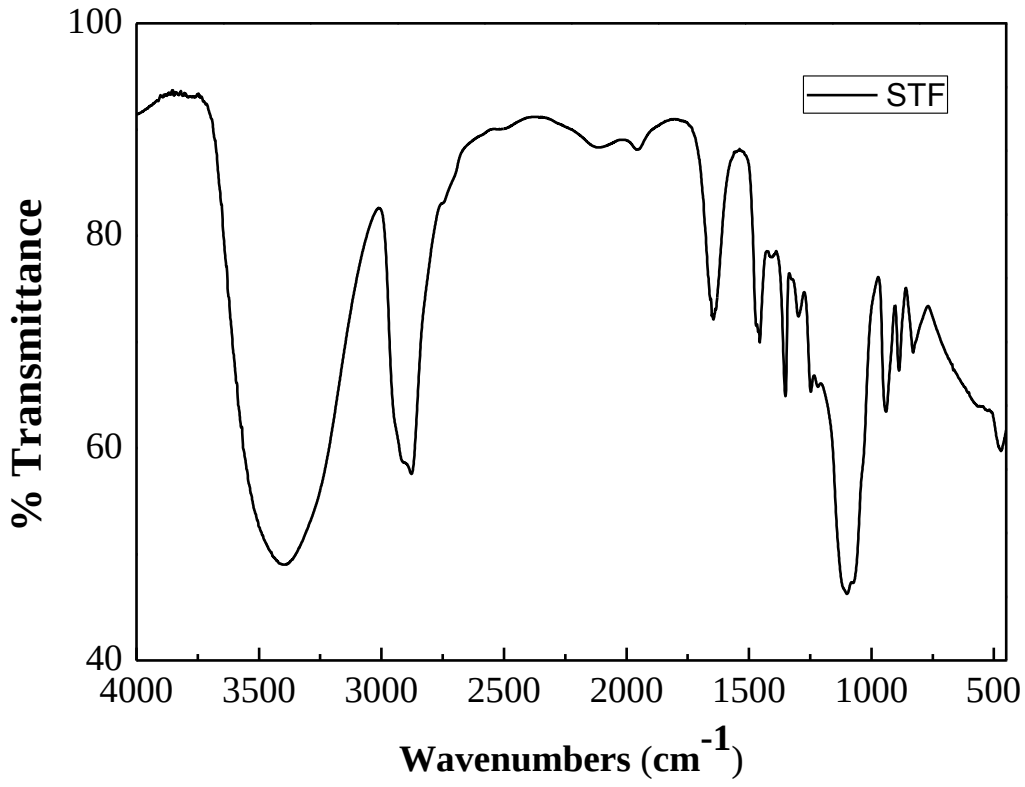

Figure 4.8. FTIR spectrum of shear thickening fluid (STF)

4.2.3. Thermogravimetric Analysis (TGA) of STFs and PEG

Figure 4.9 shows typical thermogravimetric analysis (TGA) weight loss curves of neat PEG and STFs that contains 5, 7.5, 10, 15, 20 and 25 wt% of the silica. The actual weight percentages of silica and PEG in STF samples were estimated using TGA experiments. TGA test results show that there are two weight loss stages. The first weight loss was observed to start at around 160 °C due to the evaporation of the PEG. The PEG decomposes at around 260 °C where a major weight loss stage is noticed as seen in TGA curves. The TGA curves clearly show that the huge weight loss of the sample indicating the total decomposition of the PEG between 250-300 °C. The remaining sample residue is silica. There is a small weight loss up to 200°C indicating the thermal stability of the material up to this temperature. There are slight differences between the remaining amount of the sample containing the silica nanoparticles and the concentration measured during the STFs preparation. This difference may be associated with the loss of some minimal amount of this light feathery small size nanopowders during the mechanical mixing process. The residual weight percentage of silica is about 4, 7, 9, 14, 20 and 20 wt% for the corresponding concentrations of 5, 7.5, 10, 15, 20 and 25 wt% respectively.

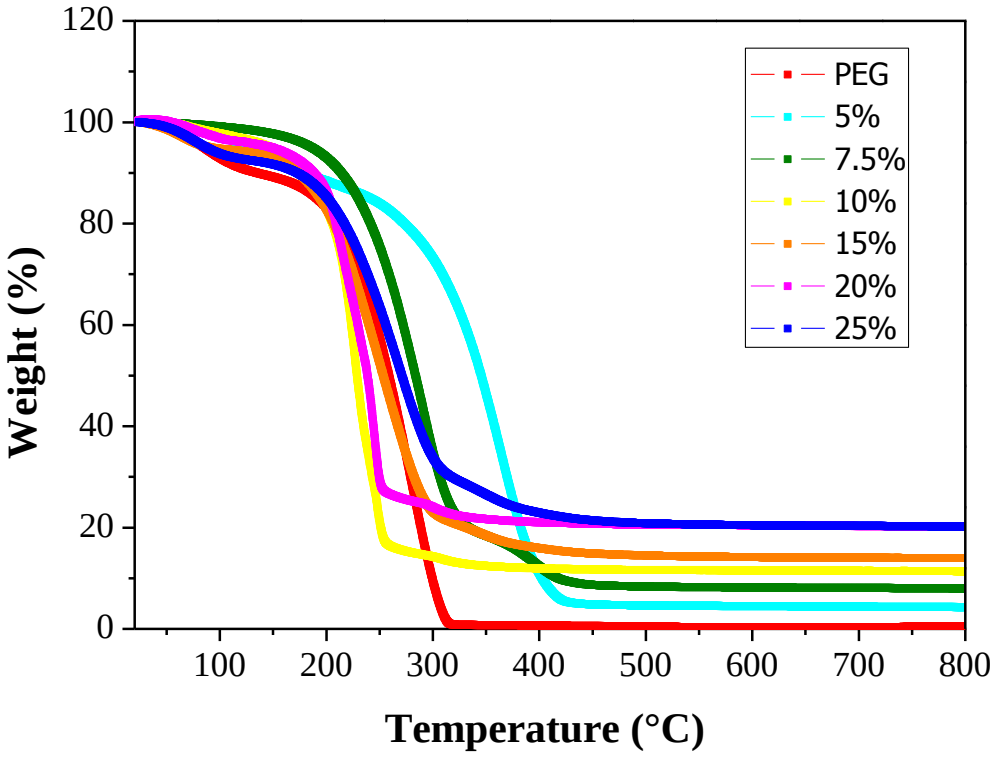

Figure 4.9. TGA curves of shear thickening fluids (STFs)

4.3. Rheological Properties of Shear Thickening Fluids

4.3.1. Steady Shear Rheology

Rheological measurements for the STF were performed with a TA AR2000ex rheometer in stress-controlled mode, with a cone-plate geometry having a cone angle of 2° and diameter of 40 mm. At higher silica concentrations and dynamic oscillatory shear mode, different cone-plate geometry having a cone angle of 0.1 radians and a diameter of 25 mm was used. To remove loading effects, a preshear of 1 s^{-1} was applied for 60 s prior to further measurement. All measurements were performed at 25 °C. In this study, steady state flow mode, dynamic strain sweeps and dynamic frequency sweeps were conducted to investigate the rheological properties of the STF samples. The rheological properties of STF samples were studied to understand shear thickening or shear thinning behavior at room temperature. Figure 4.10 shows the steady state shear viscosity as a function of shear rate of the silica/PEG dispersion systems with various silica particle weight fractions. The viscosity value of PEG as a function of shear rate is also given within the same figure. Typical shear stress versus shear rate curves is illustrated in Figure 4.11 for the same concentrations.

Based on the rheological results, it was observed that the PEG sample exhibits Newtonian fluid behavior. As the shear rate increases, the viscosity remains constant. The additions of silica nanoparticles into the PEG results with the increase of the viscosity over the entire range of shear rates. So, STF exhibit non-Newtonian behavior. It can be seen from figure 4.12 that the colloidal suspensions do not have notable shear thickening effect up to 1 s^{-1} shear rate. At lower shear rates shear thinning behavior was observed. Conversely, the rheograms of the suspensions exhibit sharp increase in viscosity at a critical shear rates and stress. At a particle concentration of 5 wt% silica suspension, significant shear thinning was observed at shear rates within the range of 0.01-1000 s^{-1}. Furthermore, it was found that the viscosity of the STF samples increases with increasing silica weight fraction. Also, the shear thickening behavior and critical shear rate depends on the weight fraction of silica nanoparticles. Reversible shear thickening behavior was observed in most of the silica/PEG systems.

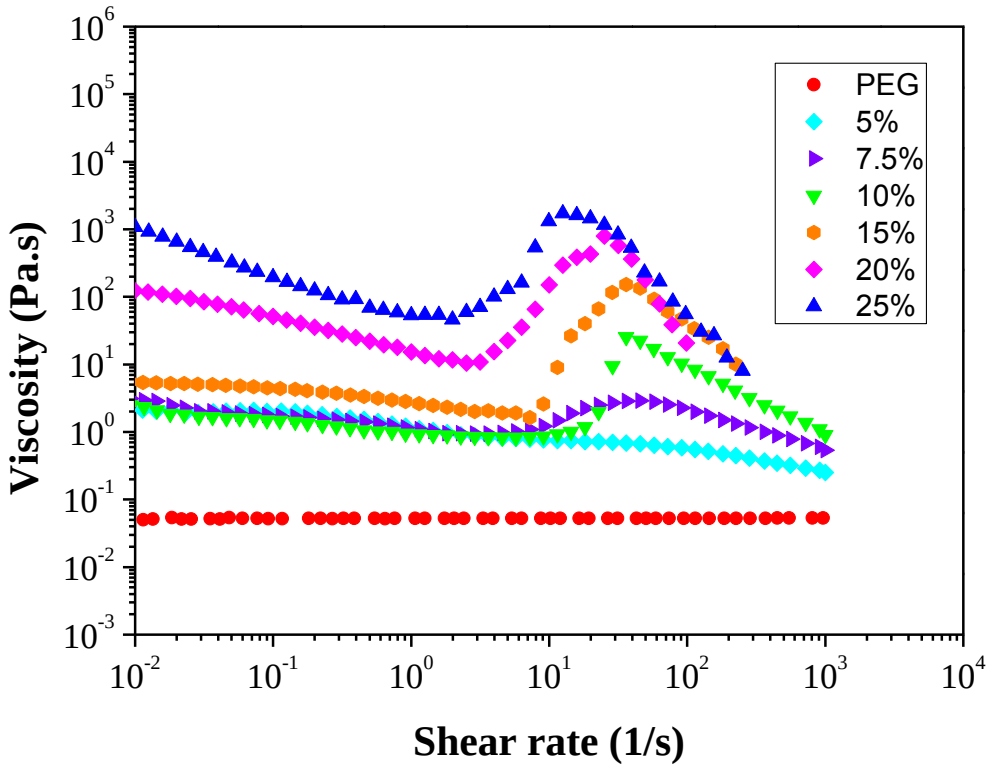

Figure 4.10. Steady shear viscosity as a function of shear rate for colloidal dispersions at varying weight fractions

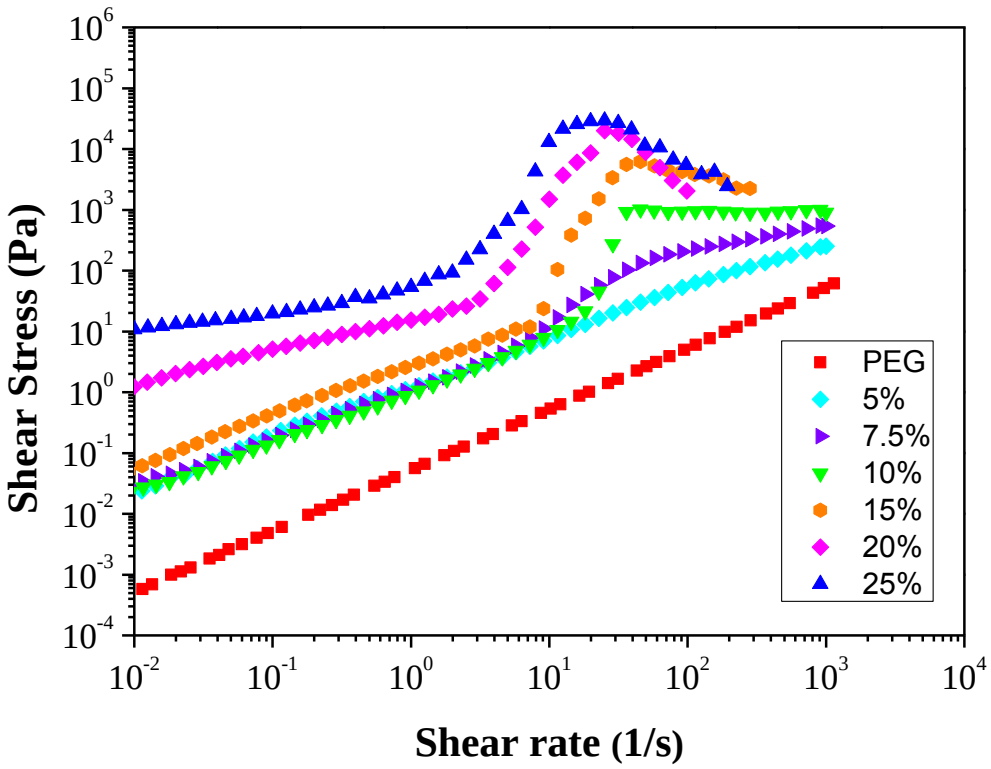

Figure 4.11. Shear stress versus shear rate for colloidal dispersions at varying weight fractions

Comparing the results of the samples with 7.5, 10, 15, 20 and 25 wt%, it was found that as the weight fraction increases the viscosity increases. The shear rate at which shear thickening behavior is first observed decreases as particle loading increases. Also, note that the strength of the shear thickening response increases as particle loading increases with continuous shear thickening at the lower and highest particle loadings. It was also observed that there is a significant difference between shear rates of the STF samples. For the sample containing 7.5 wt% of silica, slight reversible shear thickening effect in the range of 4-45 s^{-1} shear rate was visible and the sample viscosity increases from about 0,95 to 2.9 Pa·s. On the other hand, for the suspension containing 10 wt% of silica a shear thickening effect in the range of 7-36 s^{-1} shear rate was visible and the viscosity increases from about 0.85 to 26 Pa·s before reversible trend is seen. When the shear thickening effect ends the viscosity begins to decrease until shear rate of 1000 s^{-1}. The rheological property of STF sample with a higher concentration (15 wt% of silica nanoparticles) indicate that a significant shear thickening behavior with an increase in the viscosity from about 2.6 to 153 Pa·s between 9 and 36 s^{-1} shear rates was observed. Also, STF sample with 20 wt% silica shows a shear thickening transition in the range of 3-25 s^{-1} shear rates and the sample viscosity increases from about 11 to 797 Pa·s. For the sample containing 25 wt% of silica, the viscosity changes from 60 Pa·s at 2.5 s^{-1} shear rate to 1720 Pa·s at 13 s^{-1} shear rate before a reversal trend is seen. The increasing value of viscosity indicates an incredibly high shear thickening effect. Shear rate values for shear thickening transition are lower than the other samples. It was found that higher viscosity values and better shear thickening effect can be obtained from this concentration. Continuous increase in sample's viscosity at low and very narrow shear rates range was observed. All STF samples demonstrate shear thinning behavior before they start to exhibit a shear thickening behaviour. The sudden increase in the viscosity of silica dispersions and the shear thickening transitions are due to microstructural changes in the fluid along with the hydrocluster mechanism. The formation of particle clusters increases the hydrodynamic stress in the shear thickening fluid that leads to the dramatic increase in the viscosity. In addition, it was observed that after shear thickening transition, the second shear thinning regime is visible at higher shear rates. This behavior shows that our samples have a reversible shear thickening effect. The most important difference between the all suspensions is the value of the critical shear rates for the onset of shear thickening. One of the important parameters characterizing the phenomena is the critical

shear rate corresponding to the onset of steady shear thickening. This parameter is observed to decrease with increasing silica concentration. Critical shear rates for steady shear thickening are illustrated in Table 4.1.

Table 4.1. Critical shear rates for steady shear thickening

Silica concentration (wt %) in STF	Critical shear rate (s^{-1})	Viscosity at critical shear rate (Pa·s)
7.5	4	0.95
10	7	0.85
15	9	2.6
20	3	11
25	2.5	60

Among all STF samples, sample with 25 wt% of silica shows the best rheological properties. These results suggest that the optimal silica nanoparticles loading mechanical mixing method is 25 wt%. Above, this concentration mixing of the solid particles within the liquid polymer is not practically feasible. Also these results prove that mechanical mixing method is an effective synthesis technique for preparation of shear thickening fluids for liquid body armor applications.

4.3.2. Dynamic Shear Rheology

The viscoelastic behavior of the 5% silica suspension in PEG is illustrated in Figures 4.12 and 4.13. As seen in the figures, the experiment was conducted from low to high frequency at constant strain amplitudes of 250, 500, 750 and 1000%. The viscous G'' modulus is observed to be greater than the elastic G' modulus at the same frequency values. Furthermore, the elastic G' and the viscous G'' modulus increase when the strain amplitude of the deformation is kept constant and the frequency is increased. Additionally, the elastic G' and the viscous G'' modulus were found to be strongly dependent on frequency and the loss modulus dominates the storage modulus. It can be seen that there is no significant change in the elastic G' and the viscous G'' modulus values when the strain amplitudes are changed. It was observed that the viscous G'' modulus begin to increase more steeply as compared to the elastic G' modulus at the same frequency.

The elastic G' and the viscous G'' modulus as a function of frequency of 7.5% silica suspension in PEG at different strain amplitudes are illustrated in Figures 4.14 and 4.15. The viscous G'' modulus is found to be greater than the elastic G' modulus at the same frequency values. The same behavior is observed when the strain amplitude of the deformation is kept constant and the frequency is increased similar like those for the 5% silica suspension. Furthermore, there is a slight difference between the elastic G' and the viscous G'' modulus values when the strain amplitudes are changed. As seen in the in the figures, the elastic G' and the viscous G'' modulus increase with increasing the strain amplitudes at the same frequency. On the other hand, the elastic G' modulus starts to increase at lower values for the higher strain amplitudes. It can be concluded that the elastic G' and the viscous G'' modulus strongly depend on frequency.

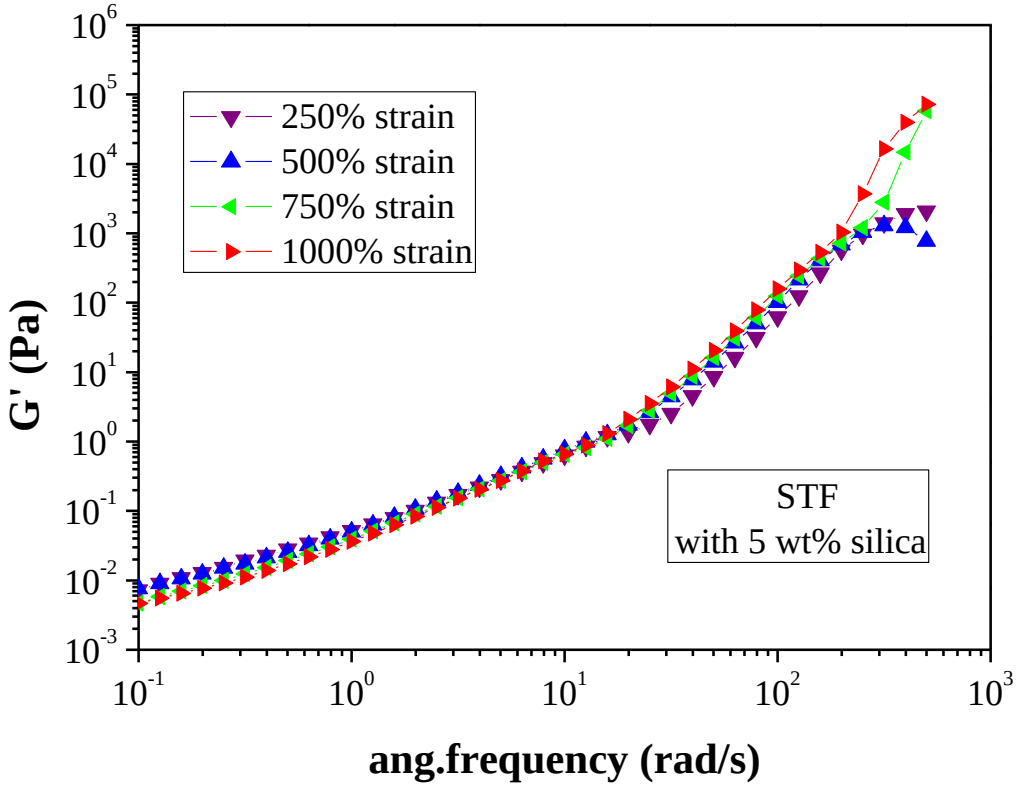

Figure 4.12. Elastic G' modulus as a function of frequency for STF containing 5 wt% silica in PEG

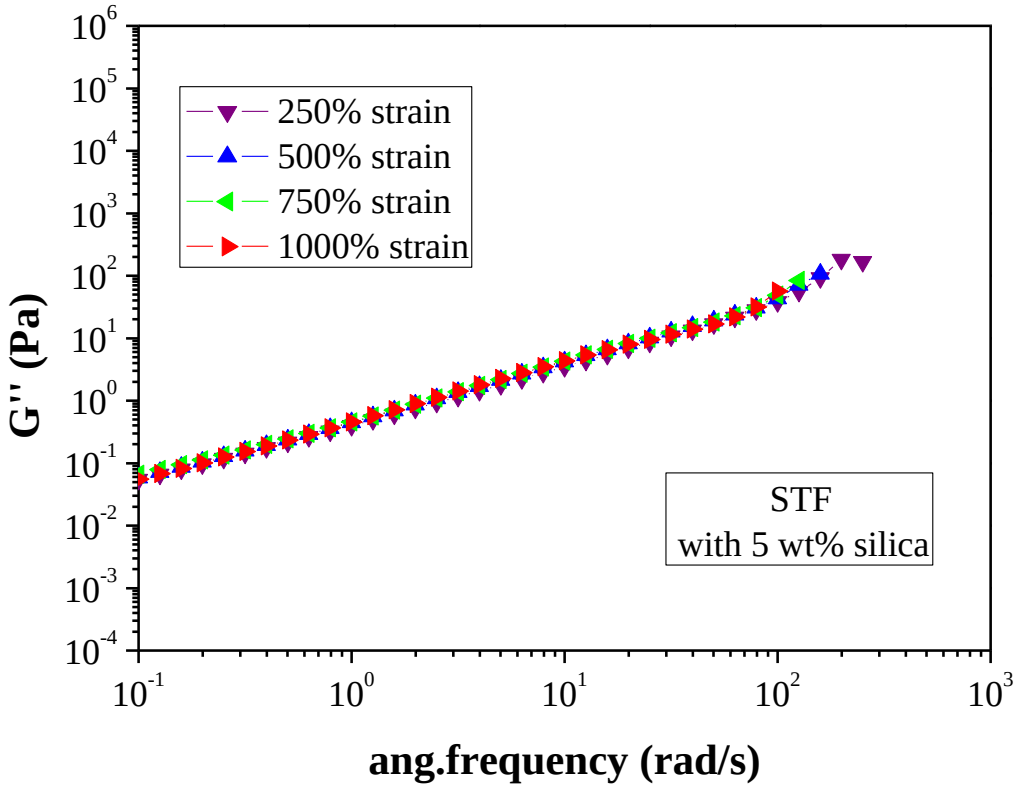

Figure 4.13. Viscous G'' modulus as a function of frequency for STF containing 5 wt% silica in PEG

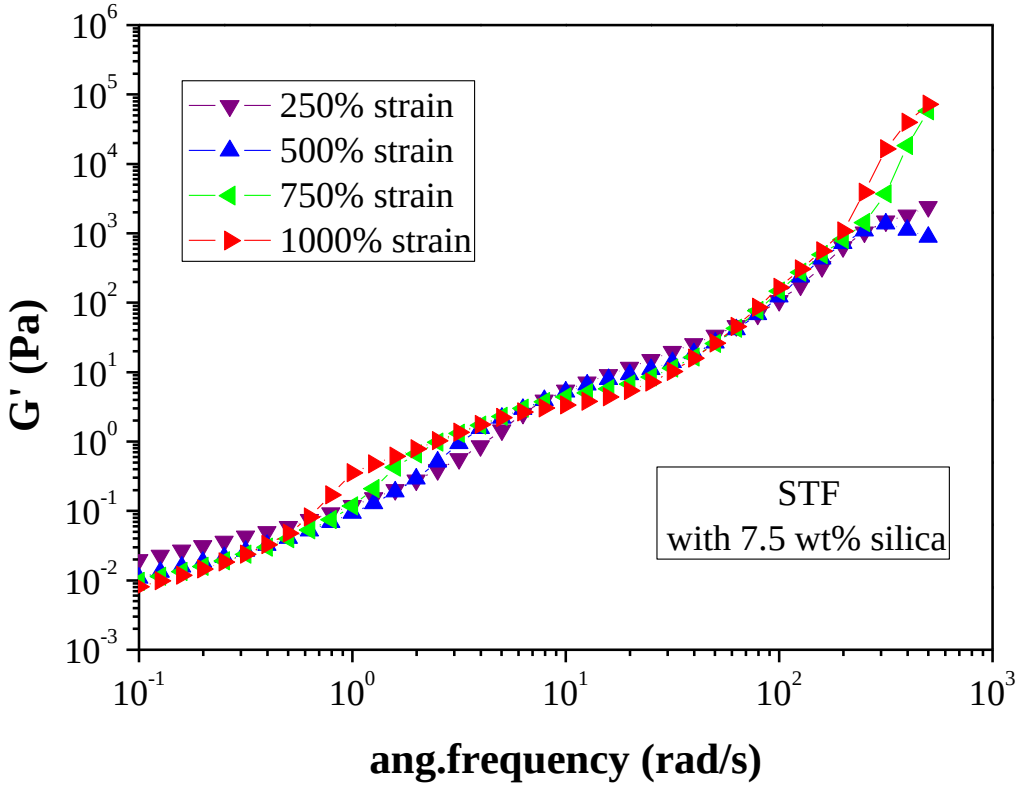

Figure 4.14. Elastic G' modulus as a function of frequency for STF containing 7.5 wt% silica in PEG

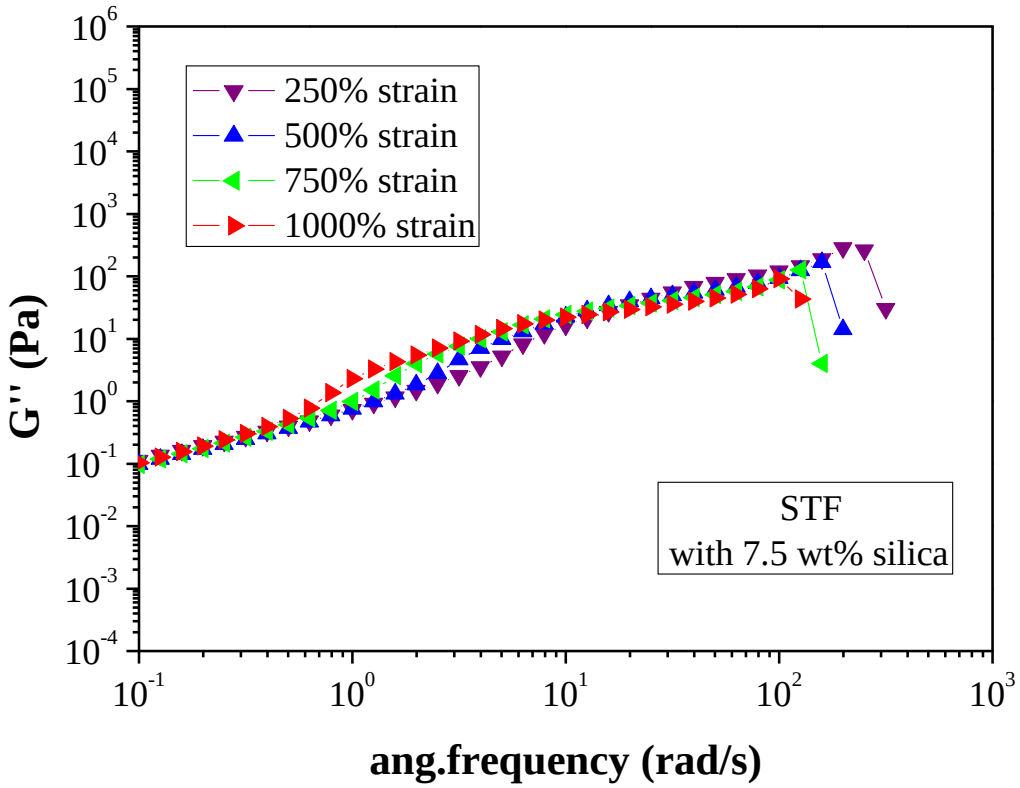

Figure 4.15. Viscous G'' modulus as a function of frequency for STF containing 7.5 wt% silica in PEG

The viscoelastic response of a suspension of 10% silica in PEG is shown in Figures 4.16 and 4.17. As seen in the figures, the elastic G' and the viscous G'' modulus were found to be strongly dependent on frequency and the loss modulus dominates the storage modulus. It was observed that the elastic G' and the viscous G'' modulus values change when the strain amplitudes are increased. Furthermore, the elastic G' and the viscous G'' modulus increase when the strain amplitude of the deformation is kept constant and the frequency is increased. The viscous G'' modulus was observed to be greater than the elastic G' modulus at the same frequency values. It can be seen that the elastic G' and the viscous G'' modulus steeply increase until a critical value then the modulus values make an abrupt transition to higher levels when the frequency reached to a critical point. This critical frequency was found to decrease with increasing the strain amplitudes. This behavior was related with the shear thickening state. The increase of the elastic G' and the viscous G'' modulus values is seen for the strain amplitudes of 250, 500, 750 and 1000%. On the other hand, this dramatic increase was found to be reversible. At lower frequencies the elastic G' and the viscous G'' modulus increase until a critical value then begin to decrease at the higher frequencies.

The elastic G' and the viscous G'' modulus as a function of frequency of 15% silica suspension in PEG at different strain amplitudes are illustrated in Figures 4.18 and 4.19. As seen in the figures, the elastic G' and the viscous G'' modulus increase when the strain amplitude of the deformation is kept constant and the frequency is increased. It can be seen that there is a sharp increase until a critical frequency. It was observed that the elastic G' and the viscous G'' modulus steeply increase until a critical value then the modulus makes a sudden transition to higher levels when the frequency reached at a critical point. This critical frequency was found to decrease with increasing the strain amplitudes. On the other hand, at lower frequencies the elastic G' and the viscous G'' modulus increase until a critical value then begin to decrease at higher frequencies. This increase in modulus occurs due to shear thickening, which is most appreciable at the higher concentrations. It can be concluded that this dramatic increase is reversible.

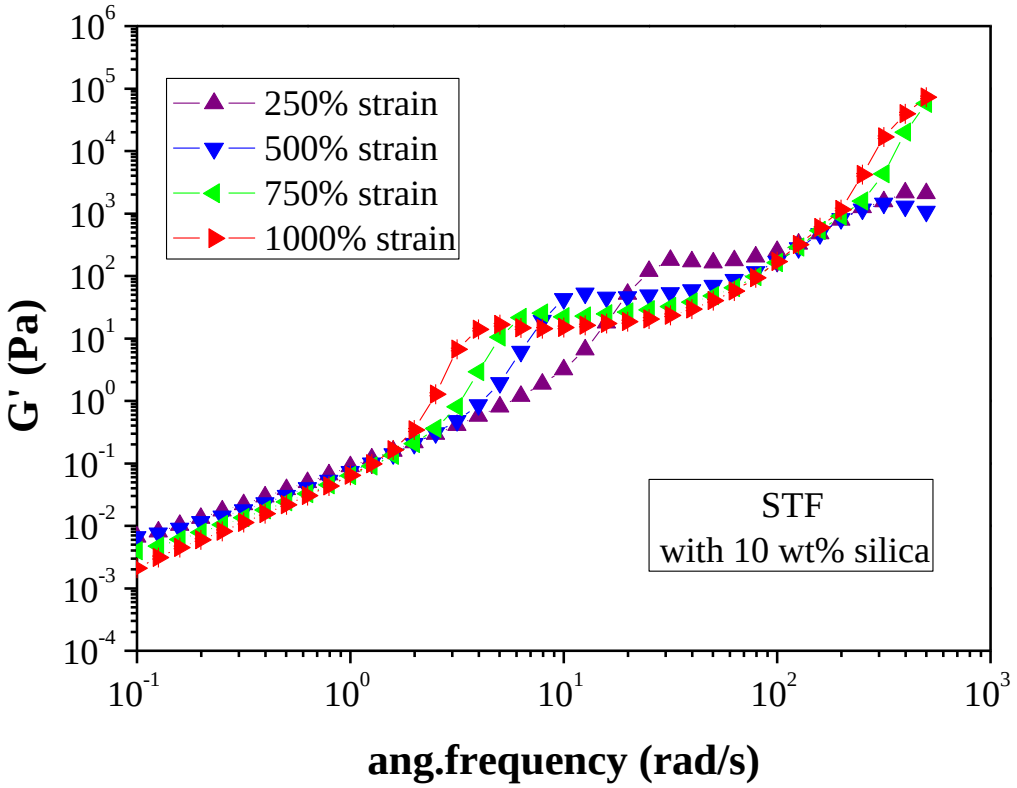

Figure 4.16. Elastic G' modulus as a function of frequency for STF containing 10 wt% silica in PEG

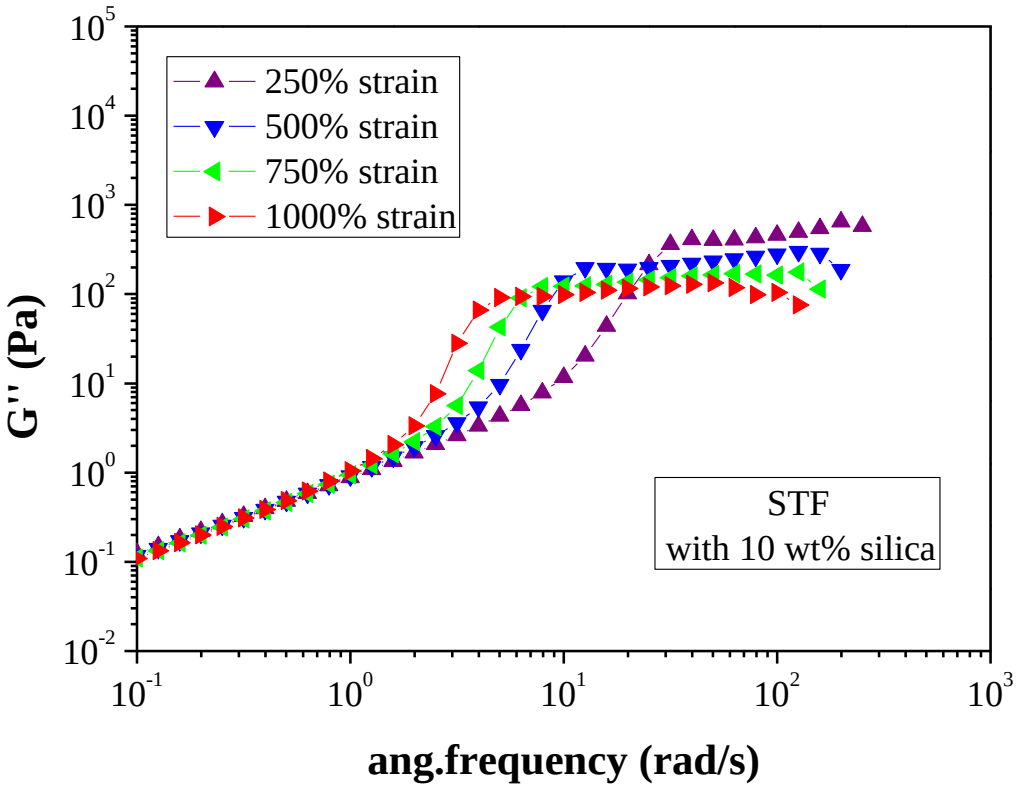

Figure 4.17. Viscous G'' modulus as a function of frequency for STF containing 10 wt% silica in PEG

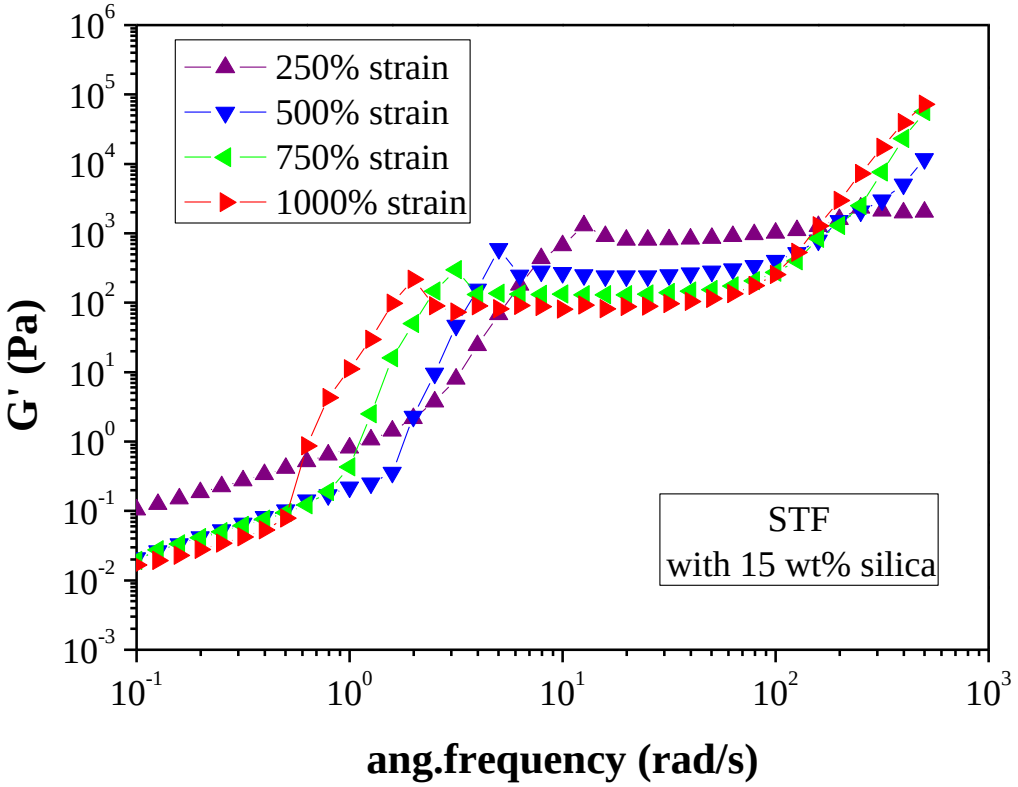

Figure 4.18. Elastic G' modulus as a function of frequency for STF containing 15 wt% silica in PEG

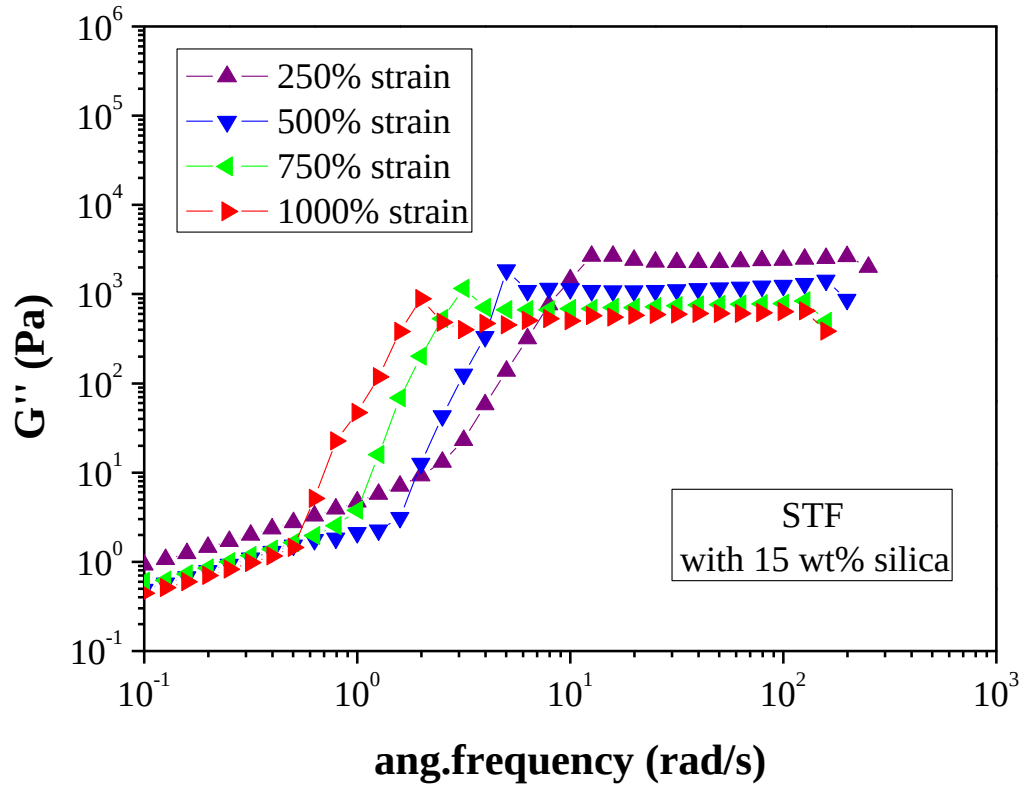

Figure 4.19. Viscous G'' modulus as a function of frequency for STF containing 15 wt% silica in PEG

The dynamic rheological response of the 20% silica suspension in PEG is illustrated in Figures 4.20 and 4.21. A similar behavior was observed as compared to the other suspensions. The elastic G' and the viscous G'' modulus increase when the strain amplitude of the deformation is kept constant and the frequency is increased. As seen in the figures, the elastic G' and the viscous G'' modulus depend on frequency. The viscous G'' modulus was found to be greater than the elastic G' modulus at the same frequency values. It was found that the elastic G' and the viscous G'' modulus values change when the strain amplitudes are increased. Also, the elastic G' and the viscous G'' modulus begin to increase at lower values for the higher strain amplitudes and reach the maximum value then decrease as the frequency is increased. On the other hand, the elastic G' and the viscous G'' modulus decrease with increasing the strain amplitudes. It can be seen that the elastic G' and the viscous G'' modulus steeply increase until a critical value then the modulus values make an abrupt jump to higher levels when the frequency reached at a critical point. This critical frequency was found to decrease with increasing the strain amplitudes. Additionally, this behavior is related with the shear thickening state. The increase in the elastic G' and the viscous G'' modulus values is seen for strain amplitudes of 250, 500, 750 and 1000%. On the other hand, this dramatic increase is observed to be reversible. At lower frequencies the elastic G' and the viscous G'' modulus increase until a critical value then begin to decrease at higher frequencies. The elastic and viscous modulus begin to increase at lower modulus values for the strain amplitudes of 750 and 1000% than the strain amplitudes of 250%, 500%.

The elastic G' modulus and the viscous G'' modulus as a function of frequency of 25% silica suspension in PEG at different strain amplitudes are illustrated in Figures 4.22 and 4. 23. As seen in the figures, the elastic G' and the viscous G'' modulus increase for strain amplitudes of 250, 500, 750 and 1000% when the frequency is increased. On the other hand, the elastic G' and the viscous G'' modulus decrease with increasing the strain amplitudes at the same frequency values. There is an important difference between the elastic G' and the viscous G'' modulus at constant strain amplitudes of 250, 500, 750 and 1000%. At lower frequencies, the critical strain amplitude decreases with increasing weight fraction of the silica in PEG. At these lower frequencies the critical strain amplitude is more sensitive to the frequency with the less concentrated suspensions.

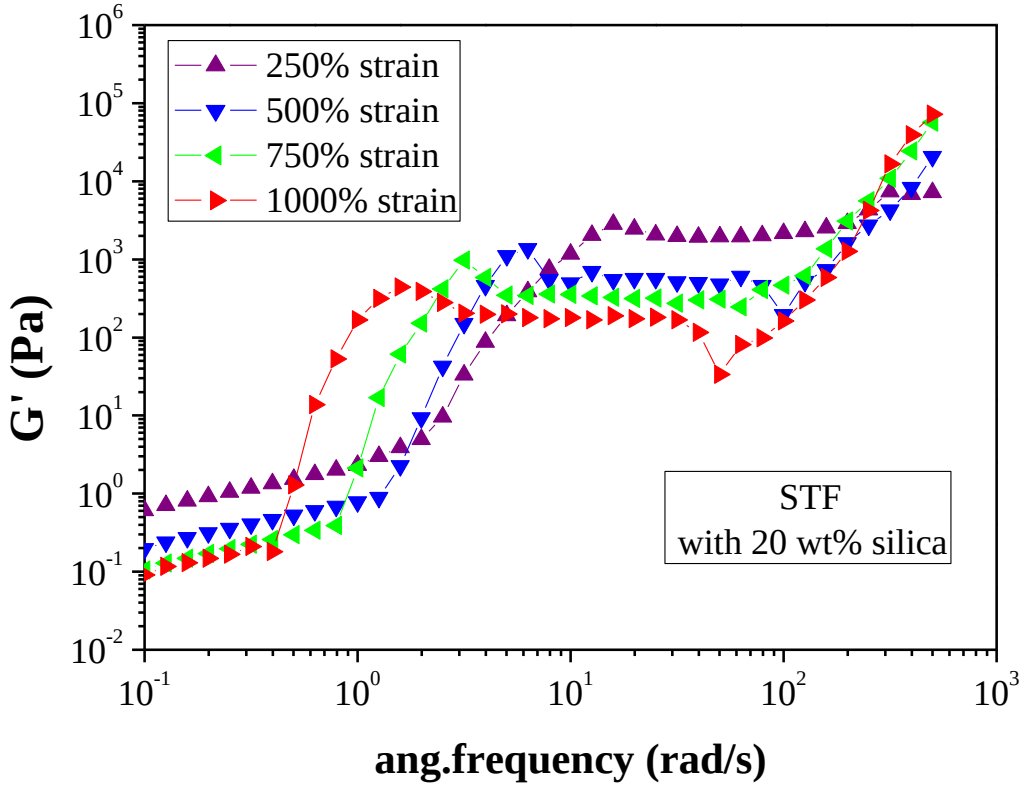

Figure 4.20. Elastic G' modulus as a function of frequency for STF containing 20 wt% silica in PEG

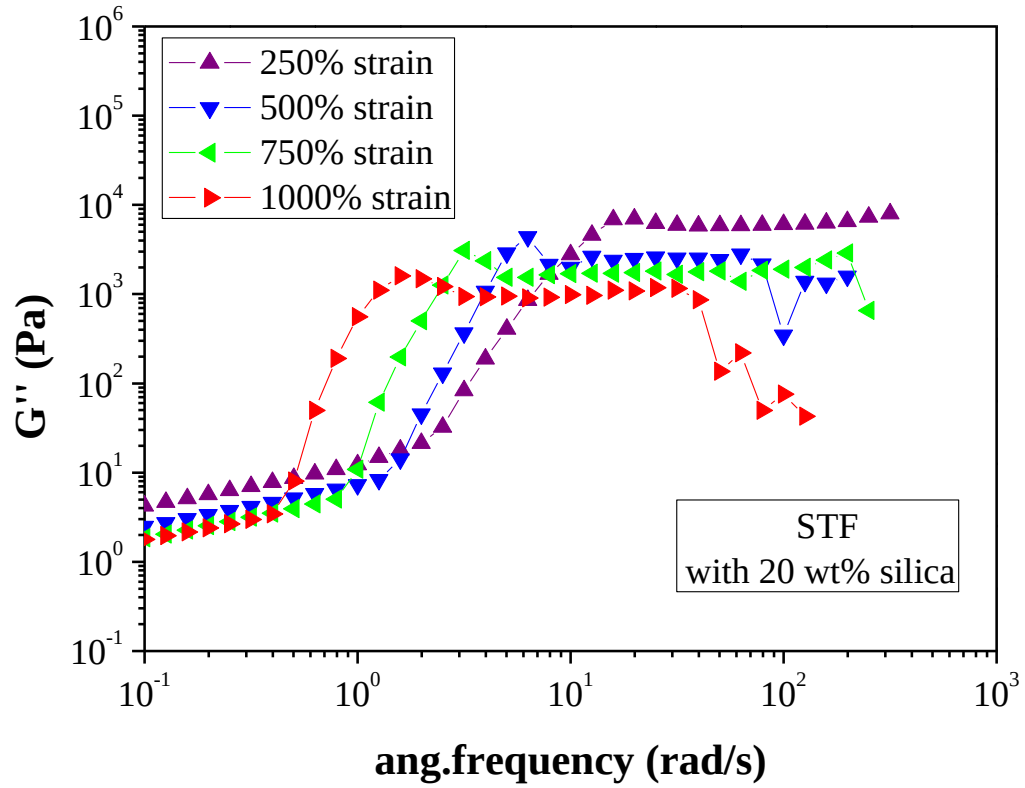

Figure 4.21. Viscous G'' modulus as a function of frequency for STF containing 20 wt% silica in PEG

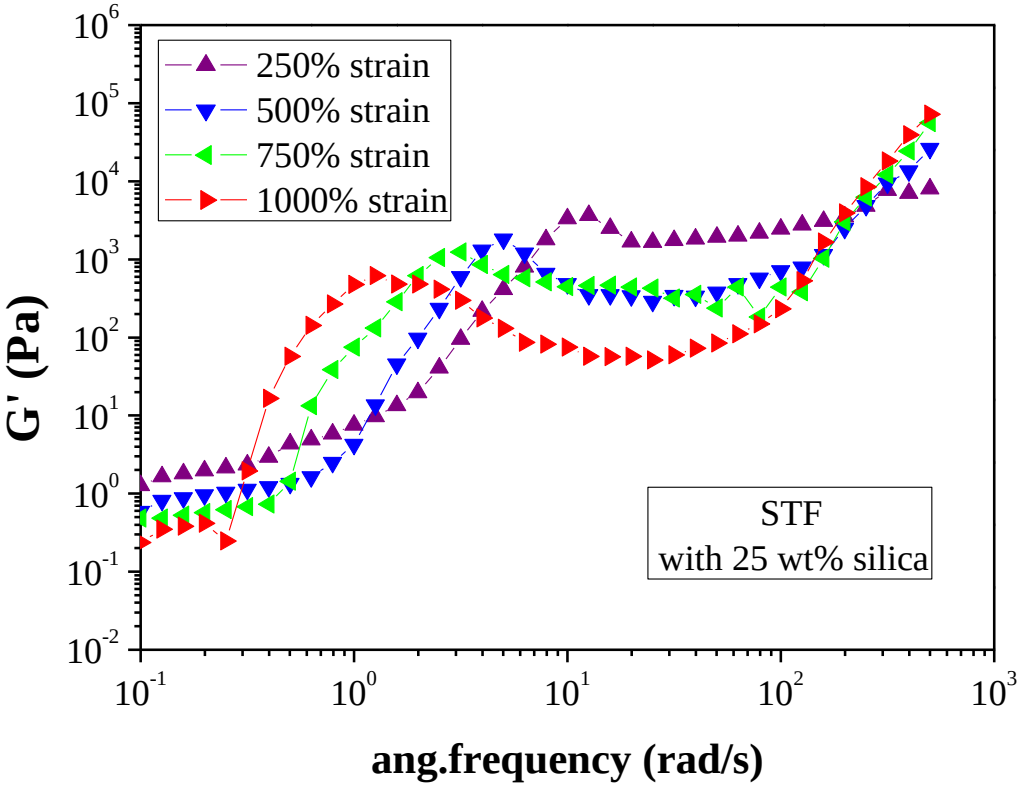

Figure 4.22. Elastic G' modulus as a function of frequency for STF containing 25 wt% silica in PEG

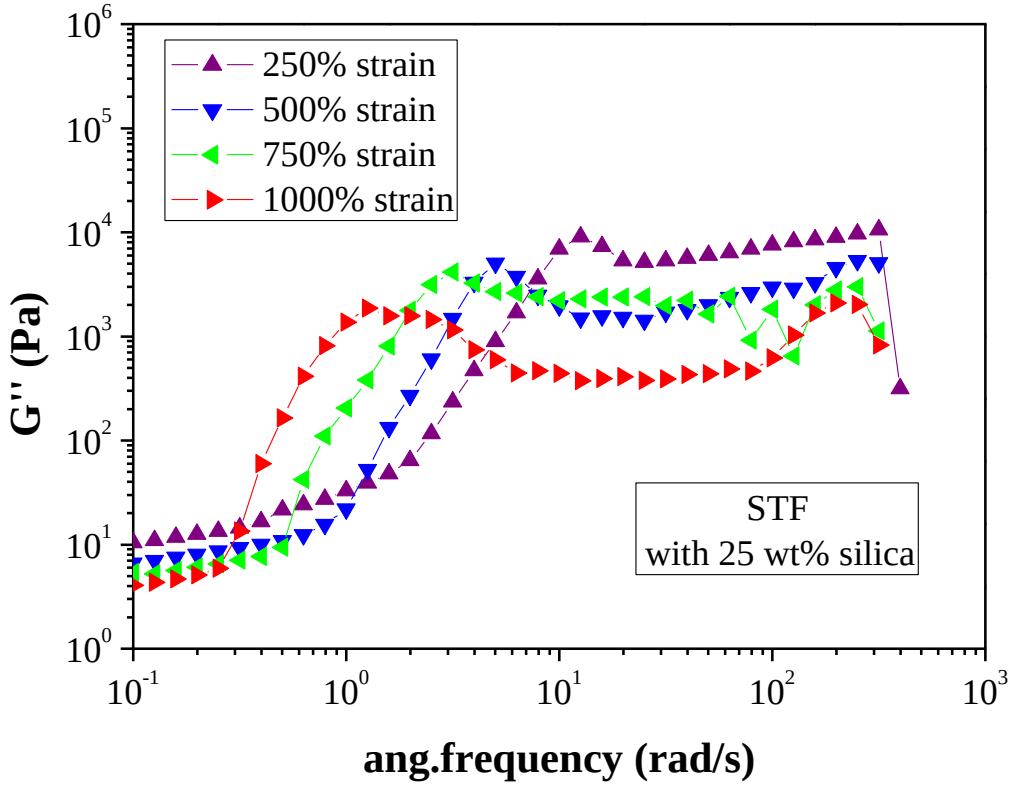

Figure 4.23. Viscous G'' modulus as a function of frequency for STF containing 25 wt% silica in PEG

The elastic G' and the viscous G'' modulus as a function of frequency for different weight fraction of silica suspension in PEG are illustrated in Figures 4.24 to 4.31 at strain amplitudes of 250, 500, 750 and 1000%, respectively. It was observed that the viscous G'' modulus is greater than the elastic G' modulus for several weight fraction of silica in PEG at the same frequency values. Also, the elastic G' and the viscous G'' modulus increase when the strain amplitude of the deformation is kept constant and the frequency is increased. This behavior is observed for all suspensions at several strain amplitudes. The elastic G' and the viscous G'' modulus depend on the frequency. It can be seen that the elastic G' and the viscous G'' modulus increase when the weight fraction is increased. The elastic G' and the viscous G'' modulus steeply increase until a critical frequency then make a sudden transition to higher levels when the frequency reached at a critical point. On the other hand, the critical frequency is found to be dependent on the weight fraction and the critical frequency decreases with increasing the concentration. Also, this critical frequency is found to decrease with increasing the strain amplitude. There are important parameters, which are the critical shear rate and the critical frequency to occur shear and strain thickening. Both of these parameters were found to decrease with increasing the concentration. Furthermore, at low frequencies, high strain amplitudes are required to occur strain thickening, that is, the critical strain amplitude was observed to be inversely proportional to the critical frequency for all the suspensions. As the frequency is increased at constant strain amplitude, the elastic G' and the viscous G'' modulus increase until at a critical frequency then begin to increase. It can be concluded that strain thickening occurs at critical combination of strain amplitude and frequency. Also, the strain thickening is found to be reversible. Silica dispersions, which show shear thickening behavior at a lower shear rate in steady state flow the same behavior was observed at lower frequency indicating strain thickening behavior. The frequency at which strain thickening transition occurs at the higher strain amplitude is different for different weight fractions. It is clear that at a certain frequency, the elastic G' and the viscous G'' modulus suddenly increase. This occurs at different frequency for all suspensions. The critical condition for strain thickening is a combination of strain amplitude and frequency. At lower frequencies, the critical strain amplitude for strain thickening decreases with increasing the concentration. At higher strain amplitudes, the strain thickening occurs at a smaller frequency.

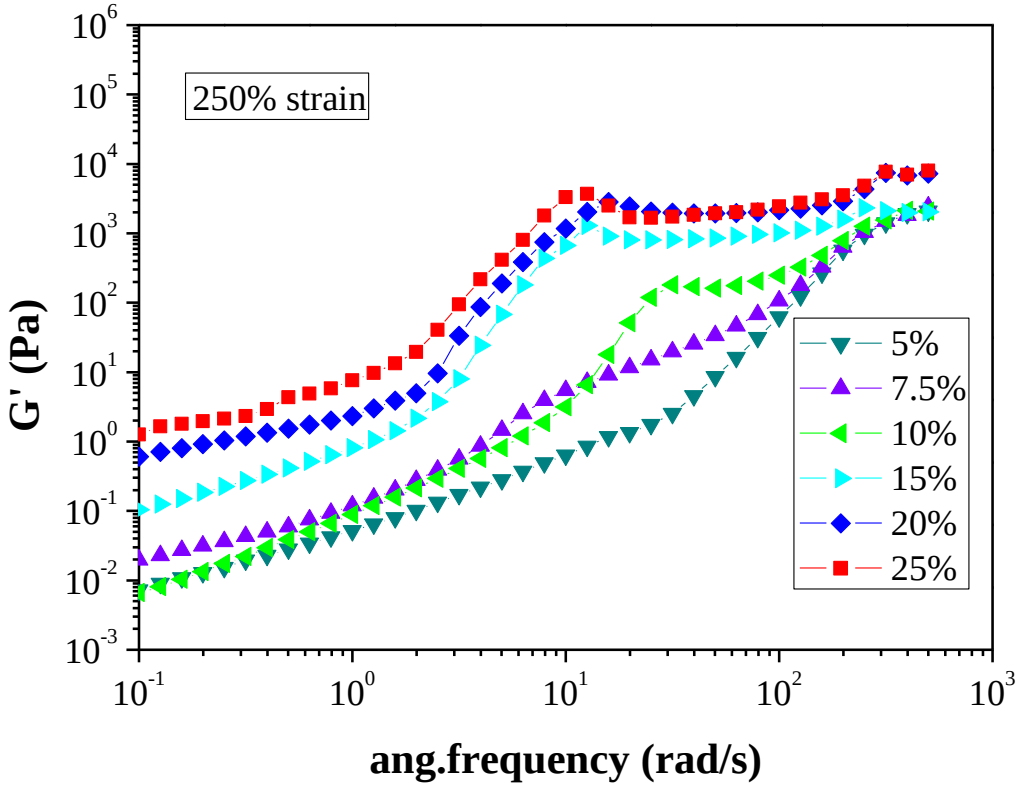

Figure 4.24. Elastic G' modulus as a function of frequency at a strain of 250% for several concentrations of the STF suspensions

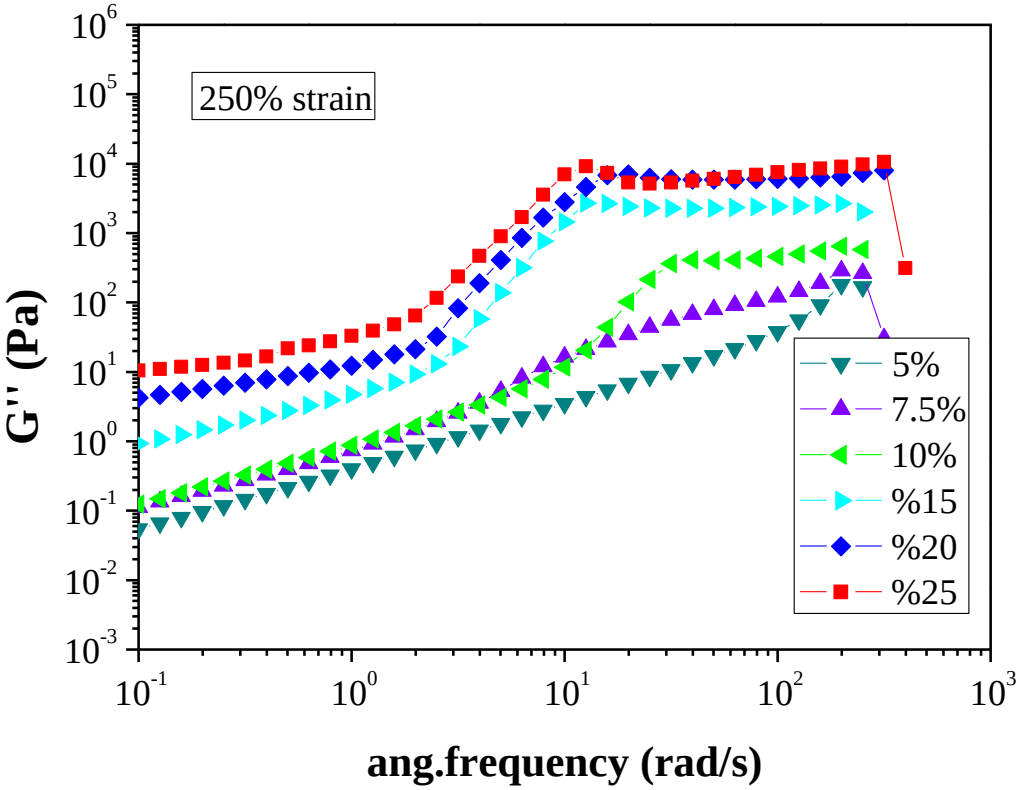

Figure 4.25. Viscous G'' modulus as a function of frequency at a strain of 250% for several concentrations of the STF suspensions

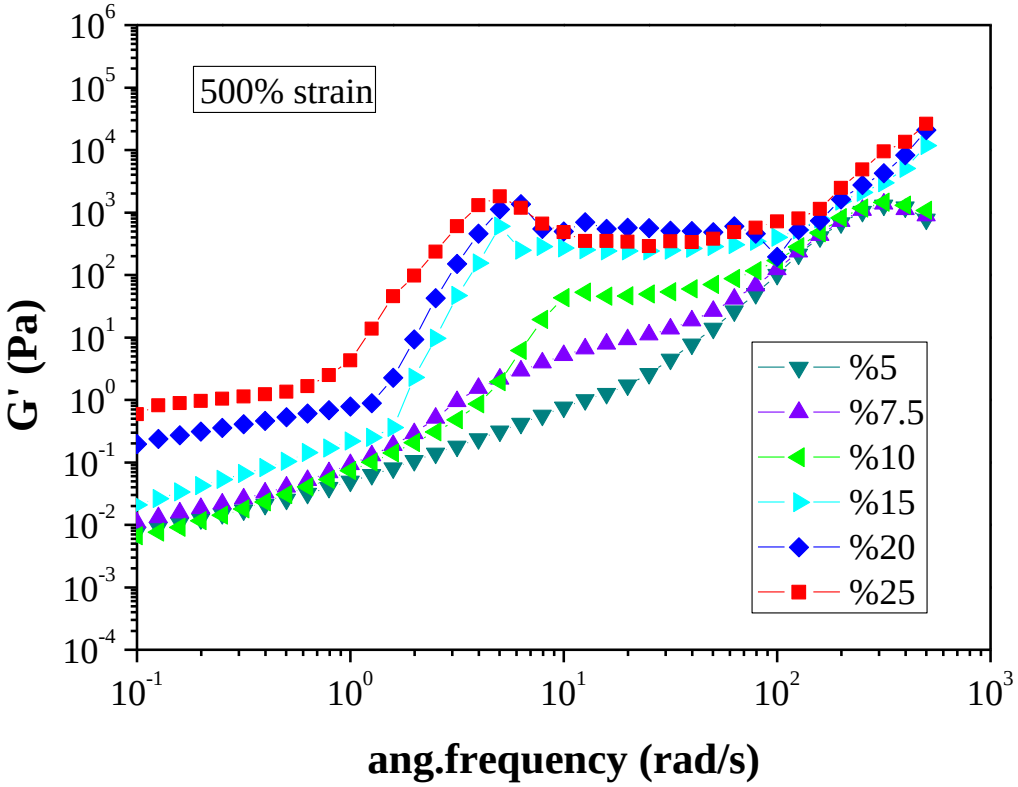

Figure 4.26. Elastic G' modulus as a function of frequency at a strain of 500% for several concentrations of the STF suspensions

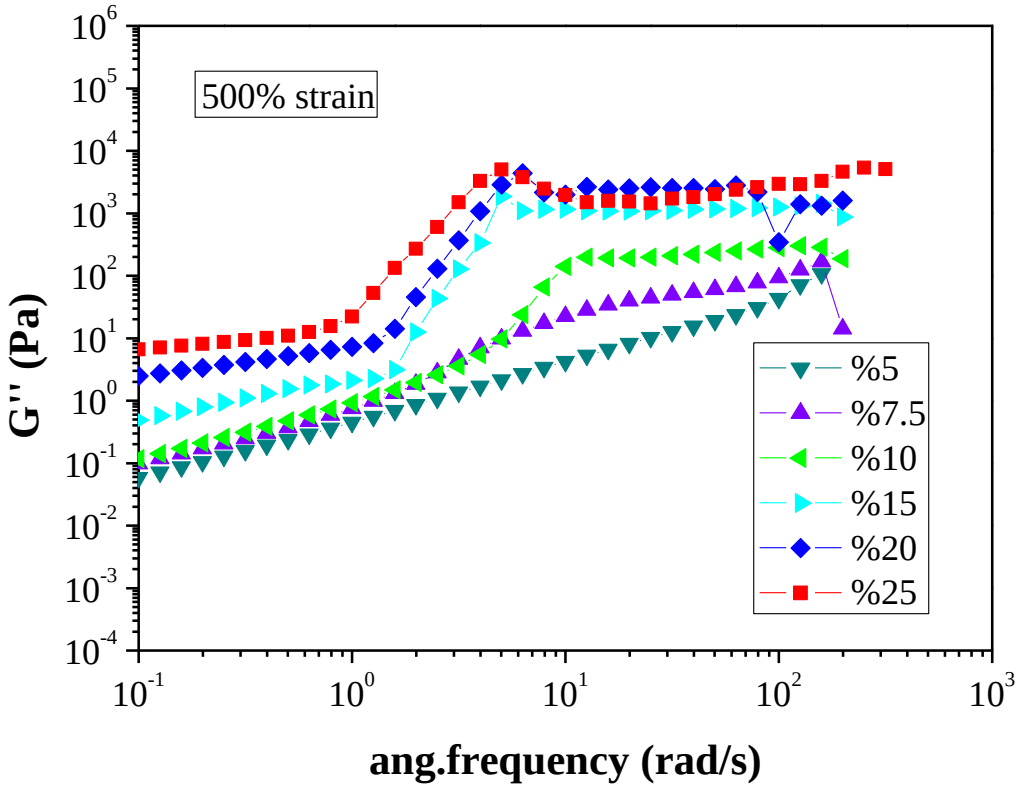

Figure 4.27. Viscous G'' modulus as a function of frequency at a strain of 500% for several concentrations of the STF suspensions

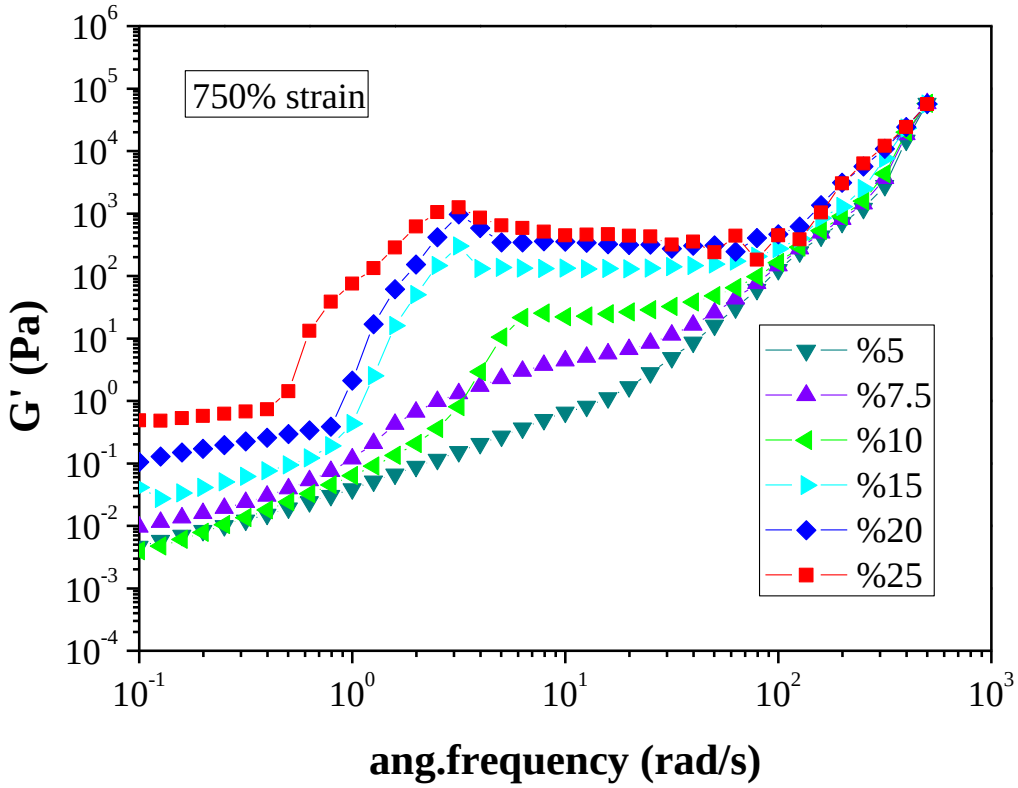

Figure 4.28. Elastic G' modulus as a function of frequency at a strain of 750% for several concentrations of the STF suspensions

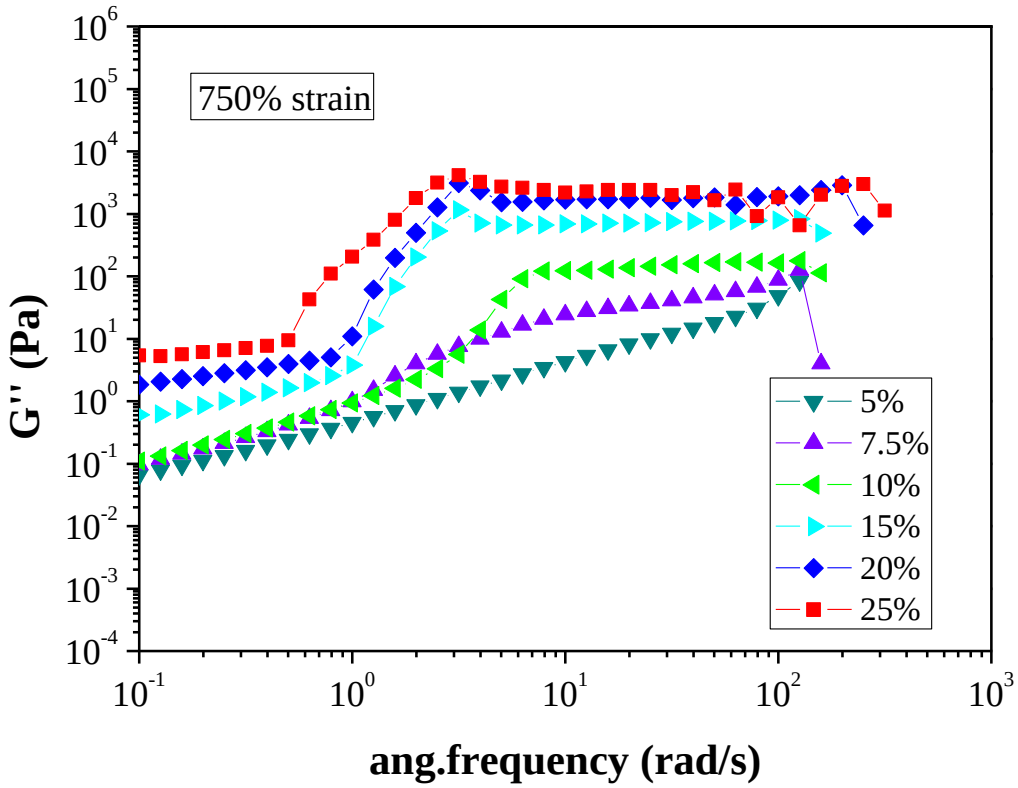

Figure 4.29. Viscous G'' modulus as a function of frequency at a strain of 750% for several concentrations of the STF suspensions

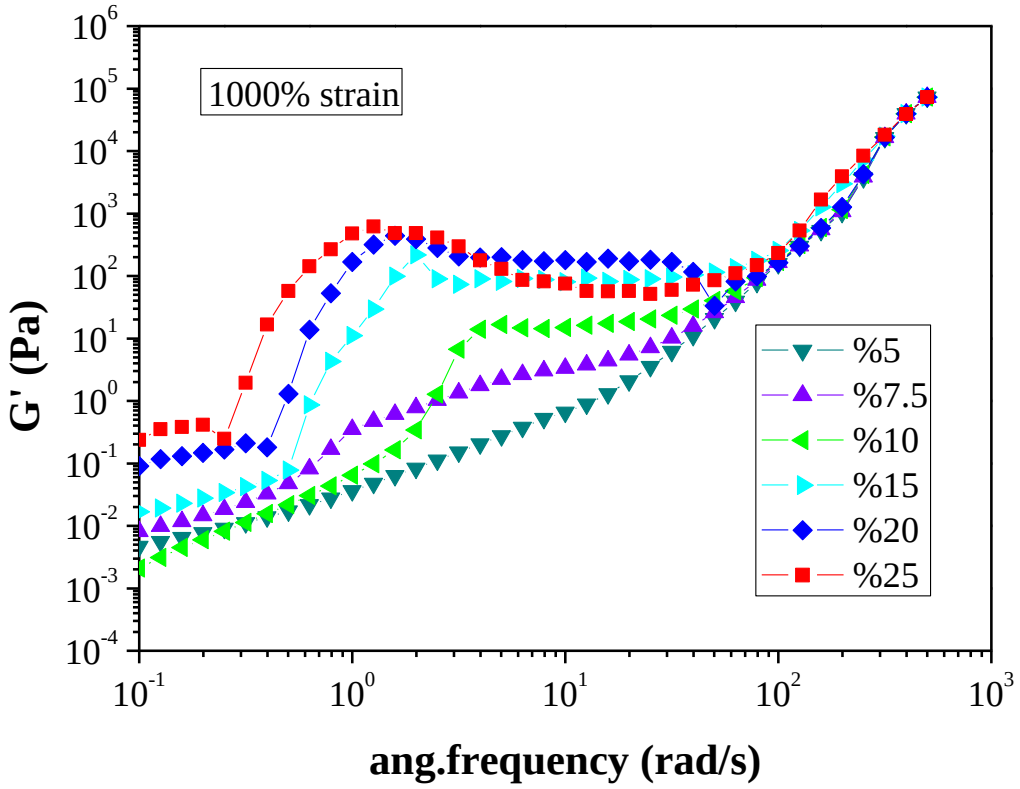

Figure 4.30. Elastic G' modulus as a function of frequency at a strain of 1000% for several concentrations of the STF suspensions

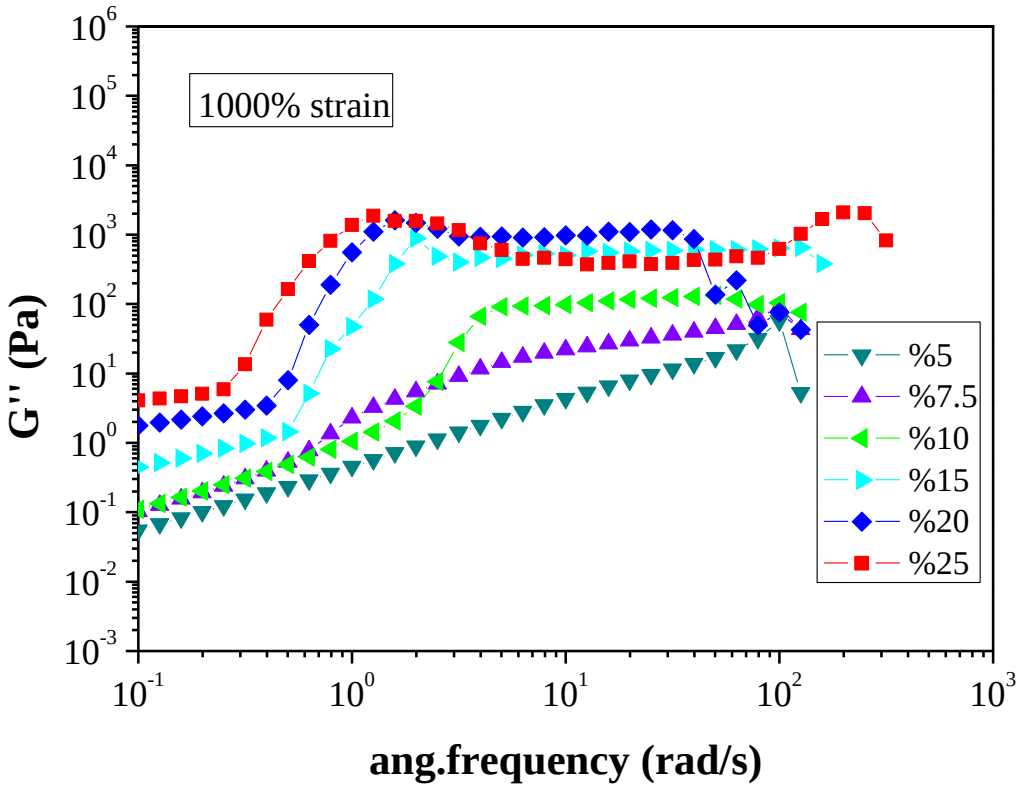

Figure 4.31. Viscous G'' modulus as a function of frequency at a strain of 1000% for several concentrations of the STF suspensions

The viscoelastic behavior of the 5% silica suspension in PEG is illustrated in Figures 4.32 and 4.33 in terms of strain sweep. The experiment was performed from low to high strain amplitude at different frequencies. As seen in the figures, the viscous G'' modulus was observed to be greater than the elastic G' modulus at the same strain amplitudes. The elastic G' and the viscous G'' modulus are found to be constant when the frequency is kept constant and the strain amplitude is increased. Additionally, the elastic G' and the viscous G'' modulus increase with increasing the frequency at the same strain amplitudes. It can be seen that there is no significant change in the elastic G' and the viscous G'' modulus values when the strain amplitudes are changed. On the other hand, at a frequency of 50 and 100 rad/s, the elastic G' modulus makes a slight transition to higher level at a particular strain amplitude. Also, the elastic G' modulus slightly decreases until a critical point then begin to increase when the strain amplitude is increased. It can be concluded that the elastic G' and the viscous G'' modulus are found to depend strongly on frequency. The elastic G' and the viscous G'' modulus as a function of strain amplitude of 7.5% silica suspension in PEG at different frequencies as shown in Figures 4.34 and 4.35. As seen in the figures, the elastic G' and the viscous G'' modulus increase with increasing the frequency. Furthermore, the viscous G'' modulus was found to be greater than the elastic G' modulus at the same strain amplitudes. At a frequency of 1 rad/s, the elastic G' and the viscous G'' modulus was observed to be constant when the strain amplitude is increased. Conversely, at the higher frequencies the elastic G' and the viscous G'' modulus are found to be constant until critical strain amplitude then make an important transition to higher values. This transition is related with strain thickening. The suspension shows strain-thickening at high strain amplitudes, with both modulus G' and G'' indicating a sudden transition to higher levels. It was observed that the transition to strain thickening behavior occurs at smaller strain amplitudes at the frequency is increased. Furthermore, this transition was found to be reversible. It should be also noted that at low frequencies, high strain amplitudes are required for strain thickening. This critical strain was found to decrease with increasing frequency. Also, at lower frequencies the critical strain amplitude was found to be more sensitive.

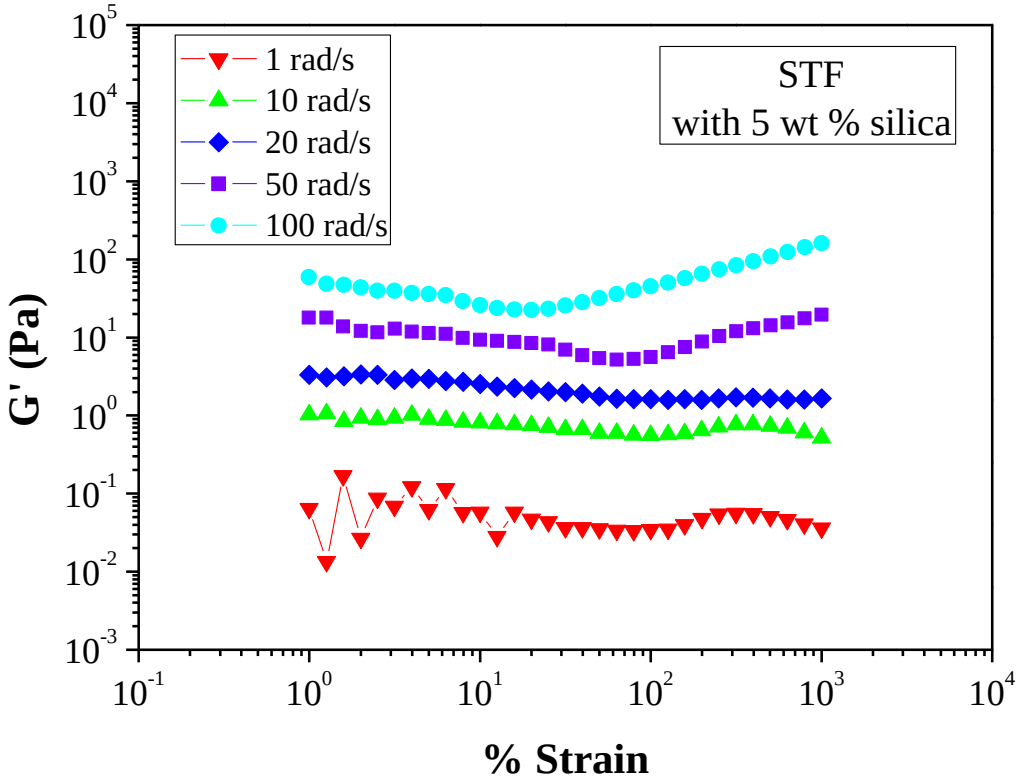

Figure 4.32. Elastic G' modulus as a function of strain amplitude for STF containing 5 wt% silica in PEG

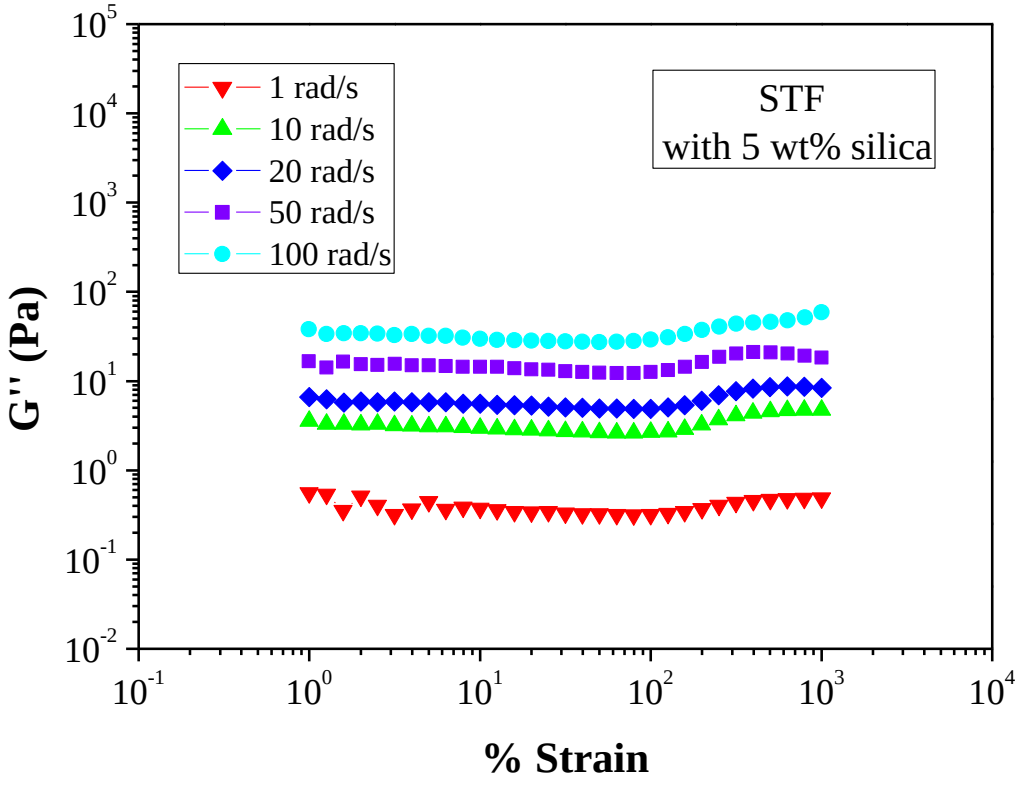

Figure 4.33. Viscous G'' modulus as a function of strain amplitude for STF containing 5 wt% silica in PEG

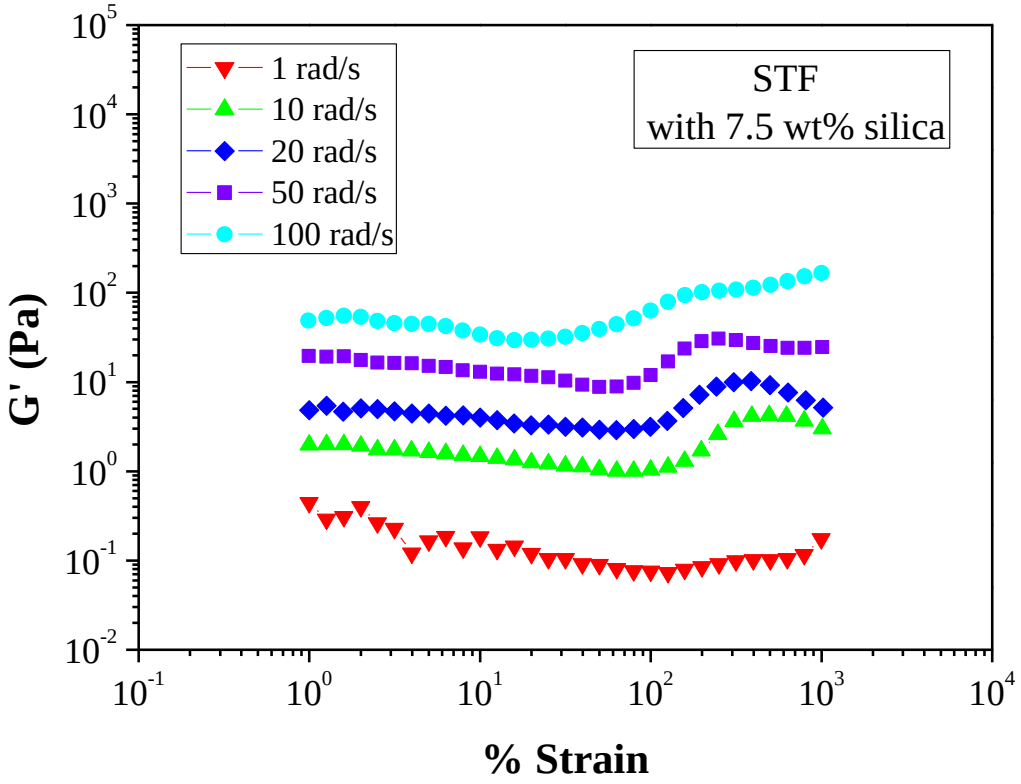

Figure 4.34. Elastic G' modulus as a function of strain amplitude for STF containing 7.5 wt% silica in PEG

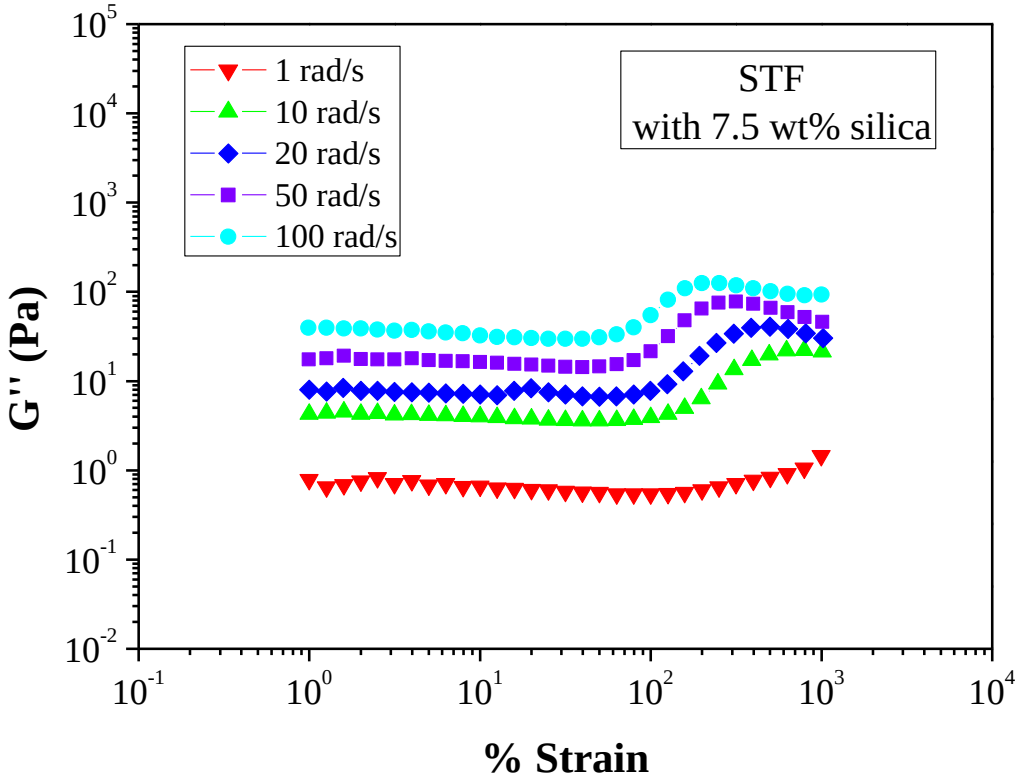

Figure 4.35. Viscous G'' modulus as a function of strain amplitude for STF containing 7.5 wt% silica in PEG

The viscoelastic behavior of the 10% silica suspension in PEG is shown in Figures 4.36 and 4.37. The viscous G'' modulus was found to be nearly higher than the elastic G' modulus. Furthermore, the elastic G' and the viscous G'' modulus were observed to be constant until critical strain amplitude when the frequency is kept constant and the strain amplitude is increased. At a frequency of 1 rad/s, the elastic G' modulus slightly increases until critical strain amplitude then make an abrupt transition to higher levels at high strain amplitude. It was observed that the elastic G' and the viscous G'' modulus increase with increasing the frequency at the same strain amplitudes. Additionally, at the higher frequencies the elastic G' and the viscous G'' modulus are found to be constant until critical strain amplitude then make sudden jump to higher levels at a particular strain. The increase in the elastic G' and the viscous G'' modulus are related with the shear thickening phenomenon, which is observed in the steady shear measurements. It can be seen that there is a sudden jump at critical strain amplitude until reversible transition occur. Also, the transition to strain thickening occurs at smaller strains as the frequency is increased, such that the required strain amplitude decrease with the increasing frequency.

The elastic G' and the viscous G'' modulus as a function of strain amplitude for the suspension of 15% silica in PEG are illustrated in Figures 4.38 and 4.39. The suspension shows strain thickening behavior at high strain amplitude, with both modulus elastic G' and viscous G'' indicating a sudden jump to higher levels at critical strain. On the other hand, the elastic G' and the viscous G'' modulus were observed to increase when the frequency is increased. Furthermore, the viscous G'' modulus is found to be nearly greater than the elastic G' modulus. It was observed that there is a significant difference between the strain amplitude values at different frequencies to occur strain thickening when the frequency is increased. The strain amplitude decreases with increasing the frequency to occur transition. Also, this transition is observed to be reversible. The elastic G' and the viscous G'' modulus increase until reversible transition then decrease at high strain amplitudes. It can be concluded that the strain thickening occurs at smaller strains when the frequency is increased. The elastic G' and the viscous G'' modulus were found to be strongly depending on frequency. At high strain amplitude low frequency and at high frequency low strain amplitude values were observed, which indicates the strain thickening behavior.

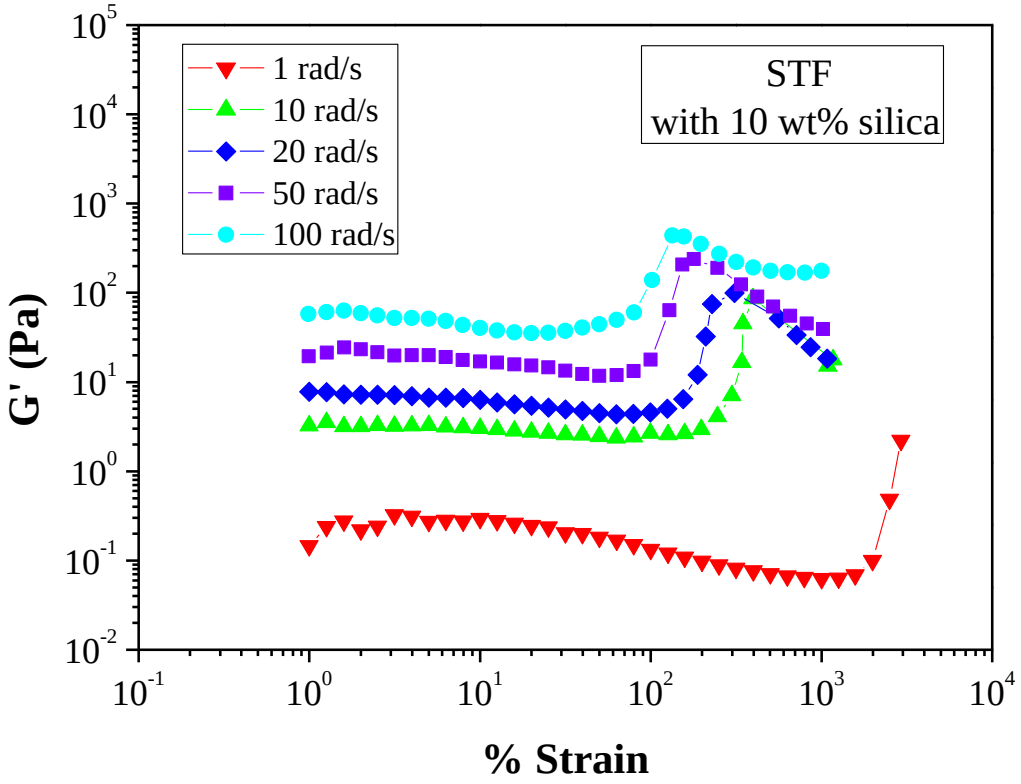

Figure 4.36. Elastic G' modulus as a function of strain amplitude for STF containing 10 wt% silica in PEG

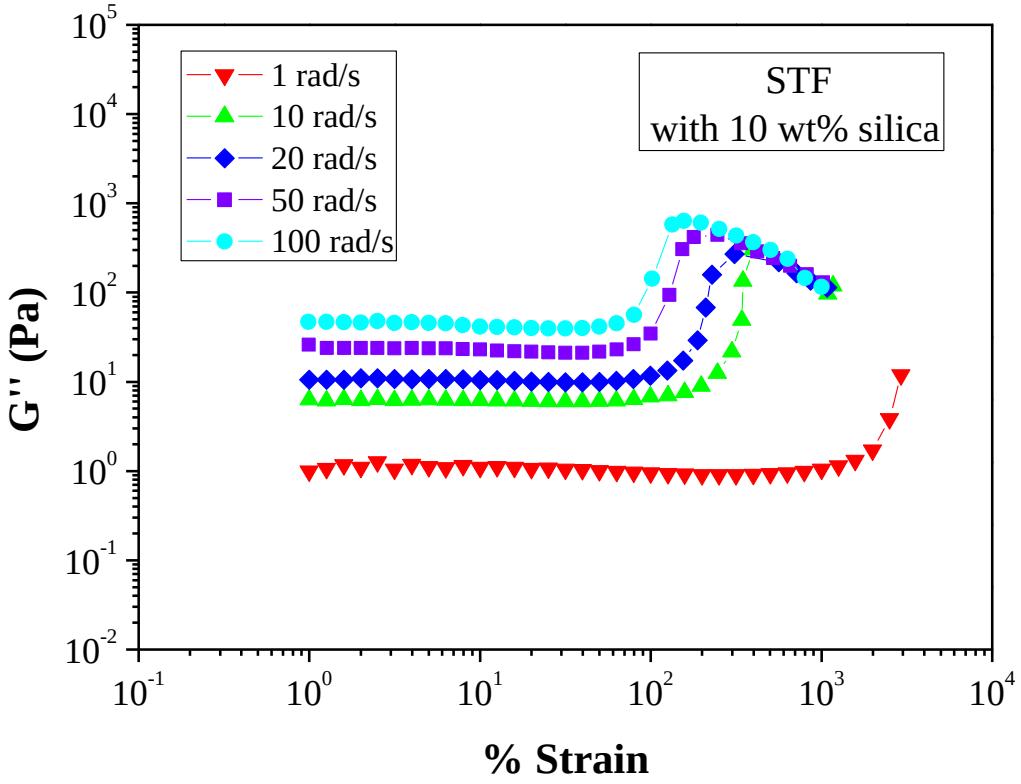

Figure 4.37. Viscous G'' modulus as a function of strain amplitude for STF containing 10 wt% silica in PEG

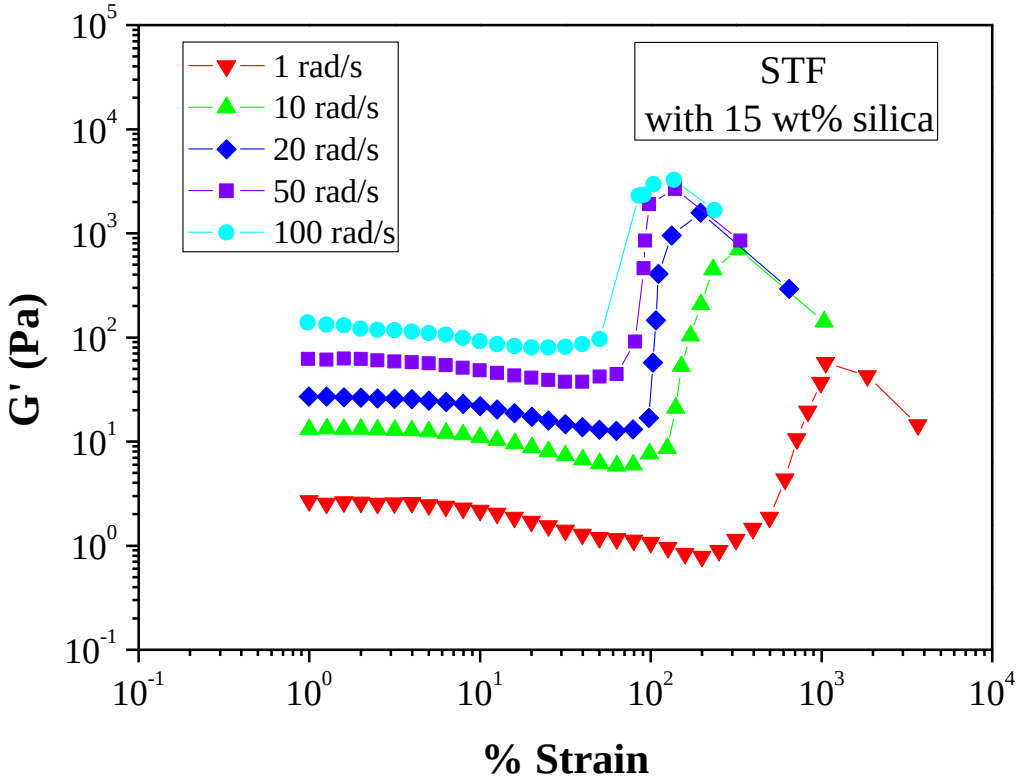

Figure 4.38. Elastic G' modulus as a function of strain amplitude for STF containing 15 wt% silica in PEG

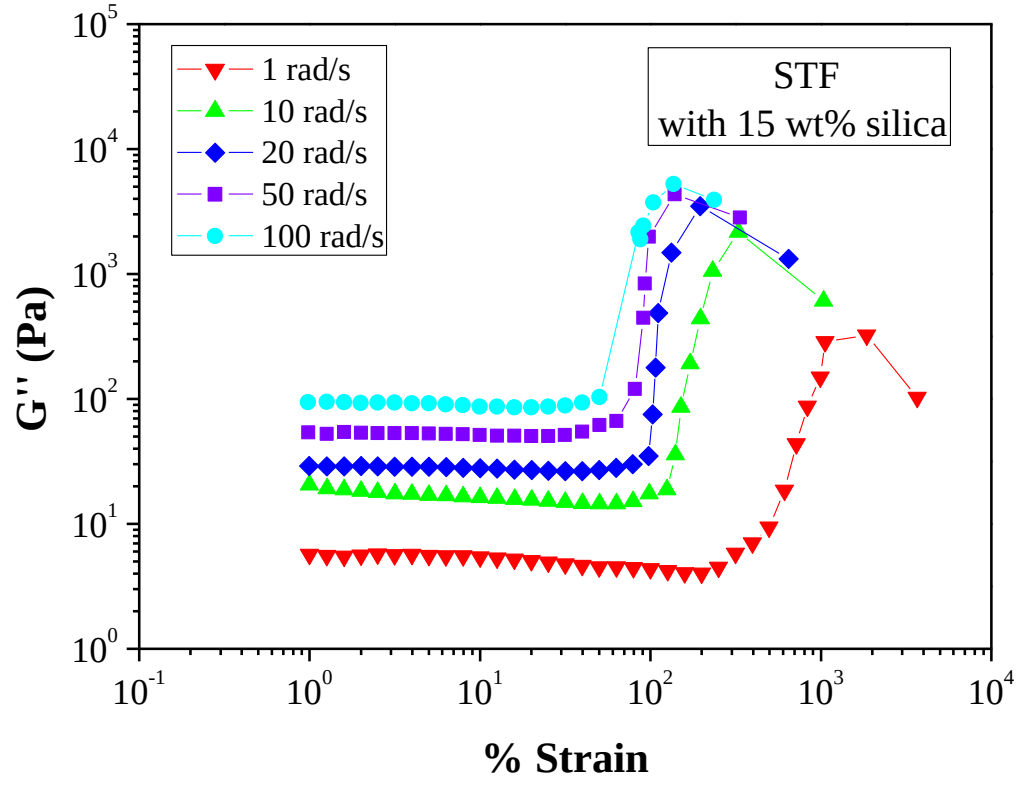

Figure 4.39. Viscous G'' modulus as a function of strain amplitude for STF containing 15 wt% silica in PEG

The dynamic rheological behavior of the 20% silica suspension in PEG is illustrated in Figure 4.40 and 4.41 in terms of strain sweep. The experiment was performed from low to high amplitude strains at several frequencies. The elastic G' and the viscous G'' modulus increase with increasing the frequency at the same strain amplitudes. The dramatic increase in elastic G' and the viscous G'' modulus is observed as a consequence of critical strain amplitude and frequency. However, the elastic G' modulus and the viscous G'' modulus were observed to be constant until critical strain amplitude reached. The transition is observed at the critical strain amplitude for different frequencies. Additionally, the same strain thickening phenomenon was found for the suspension of 20% silica in PEG. The suspension shows strain thickening when the frequency is kept constant and the strain amplitude is increased. Furthermore, the transition to strain thickening behavior occurs at smaller strains as the frequency is increased. It is possible to claim that the elastic G' and the viscous G'' modulus values are dependent on the frequency. Also, the strain thickening behavior was observed to be reversible. The critical condition for strain thickening is a combination of strain amplitude and frequency. At higher frequencies the strain thickening occurs at a smaller strain amplitude. It can be concluded that the viscoelastic properties of shear thickening suspensions are strongly dependent on the critical combination of frequency and strain amplitude.

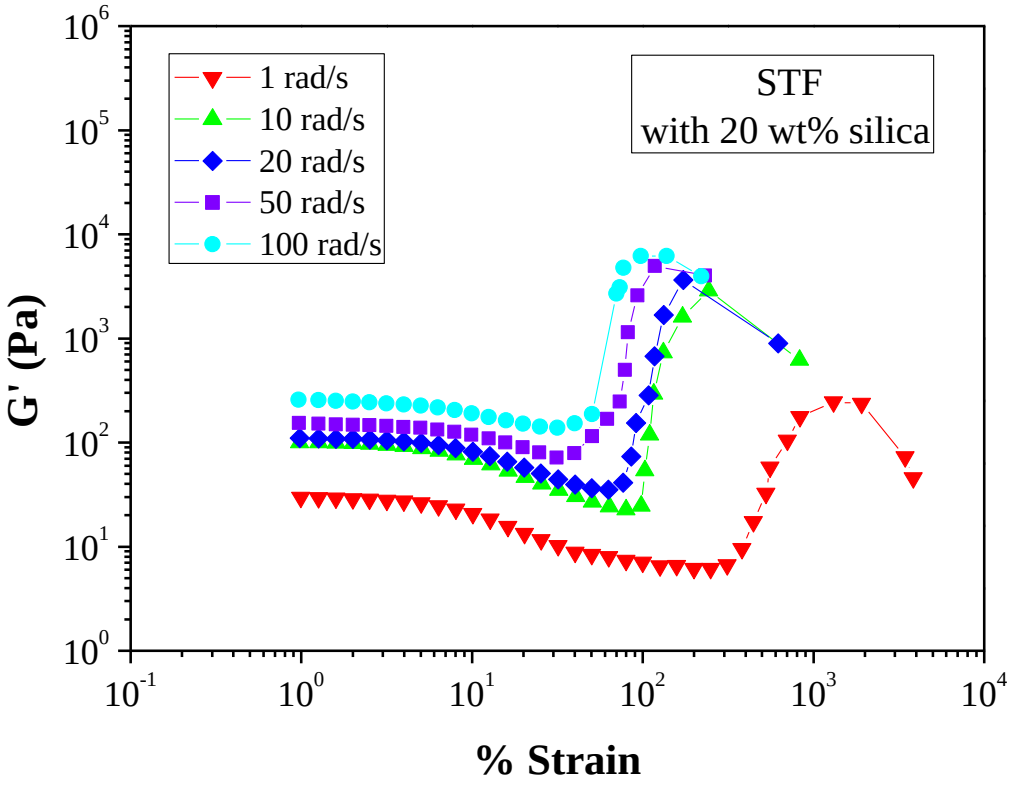

Figure 4.40. Elastic G' modulus as a function of strain amplitude for STF containing 20 wt% silica in PEG

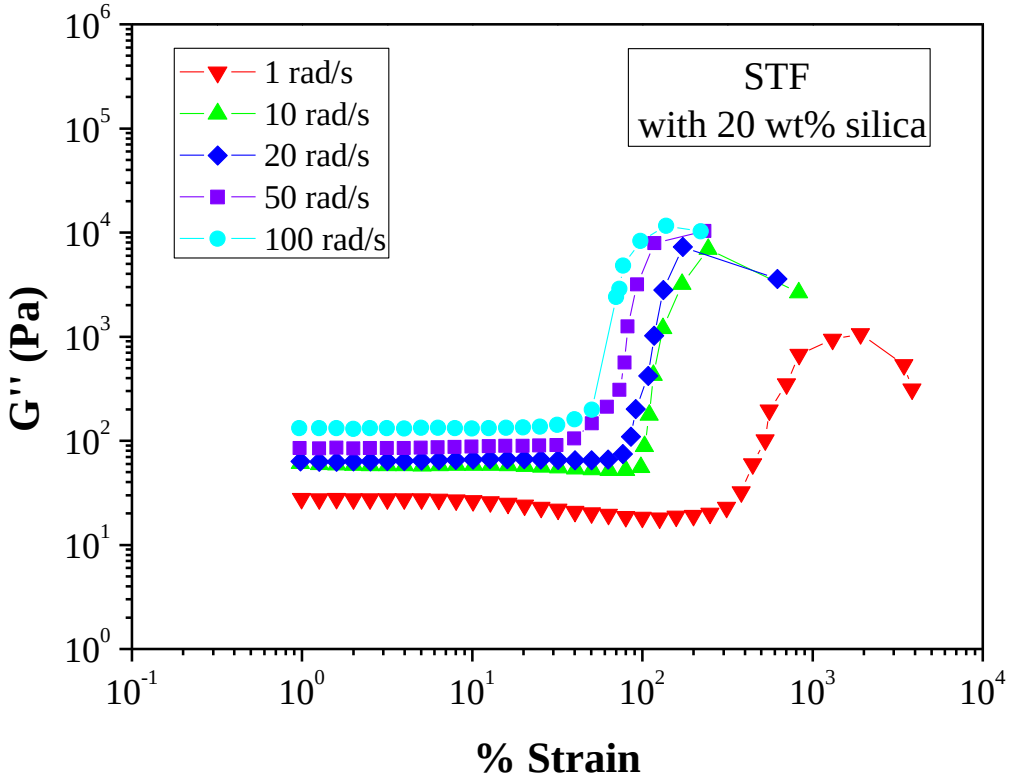

Figure 4.41. Viscous G'' modulus as a function of strain amplitude for STF containing 20 wt% silica in PEG

The elastic G' and the viscous G'' modulus as a function of strain amplitude for different weight fraction of silica suspension in PEG are shown in Figures 4.42 to 4.51 at constant frequencies of 1, 10, 20, 50 and 100 rad/s. Strain sweeps were performed at several frequencies in order to understand the effect of the concentration on dynamic rheological properties. It was observed that the elastic G' and the viscous G'' modulus increase with increasing the weight fraction. The suspensions exhibited strain thickening behavior at high strain amplitudes. On the other hand, the strain thickening behavior occurs at smaller strain amplitudes as the frequency is increased. At low frequencies, high strain amplitudes are required for strain thickening behavior. It can be seen that when the weight fraction increases the strain amplitude decreases to occur strain thickening behavior. It was observed that the elastic G' and the viscous G'' modulus increase with increasing the frequency at the same strain amplitudes then make sudden transition to higher levels at critical strain amplitude. Also, the increase in the elastic G' and the viscous G'' modulus owing to strain thickening was observed most appreciable at the higher concentrations. Furthermore, the critical strain amplitude was found to be responsible at the onset of the strain thickening. The strain thickening behavior is observed to be reversible, that is, the elastic G' and the viscous G'' modulus increase until reversible transition then begin to decrease at the higher strain amplitude. Additionally, strain thickening showed that the sudden increase in the elastic G' and the viscous G'' modulus and occurs at critical combinations of strain amplitude and frequency. Also, it was found that there are two regions for strain thickening behavior. The first occurs at high critical strain amplitudes and low frequencies, whereas the second occurs at high critical frequencies and constant lower strain amplitude. It was observed that the occurrence of the strain thickening transition depends on the weight fraction of silica, angular frequency and strain amplitude. For all suspensions with the increase in strain amplitude at a fixed frequency similar results were obtained. It can be seen that the modulus of the most concentrated suspension suddenly increase strongly. For the less concentrated suspensions slight increase are observed. The strain amplitude at which the strain thickening transition occurs at the higher frequencies is different for different weight fractions. It can be concluded that the viscoelastic properties of shear thickening suspensions are strongly dependent on the critical combination of frequency and strain amplitude. Also, this transition is observed to be reversible.

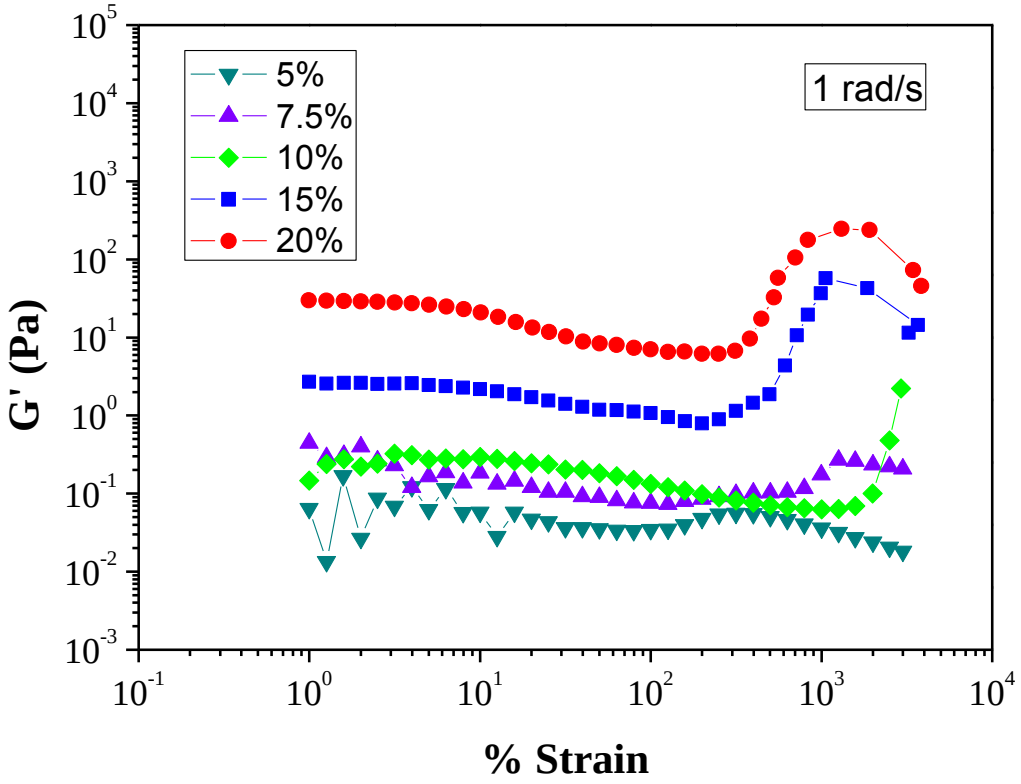

Figure 4.42. Elastic G' modulus as a function of strain amplitude at a frequency of 1 rad/s for several concentrations of the STF suspensions

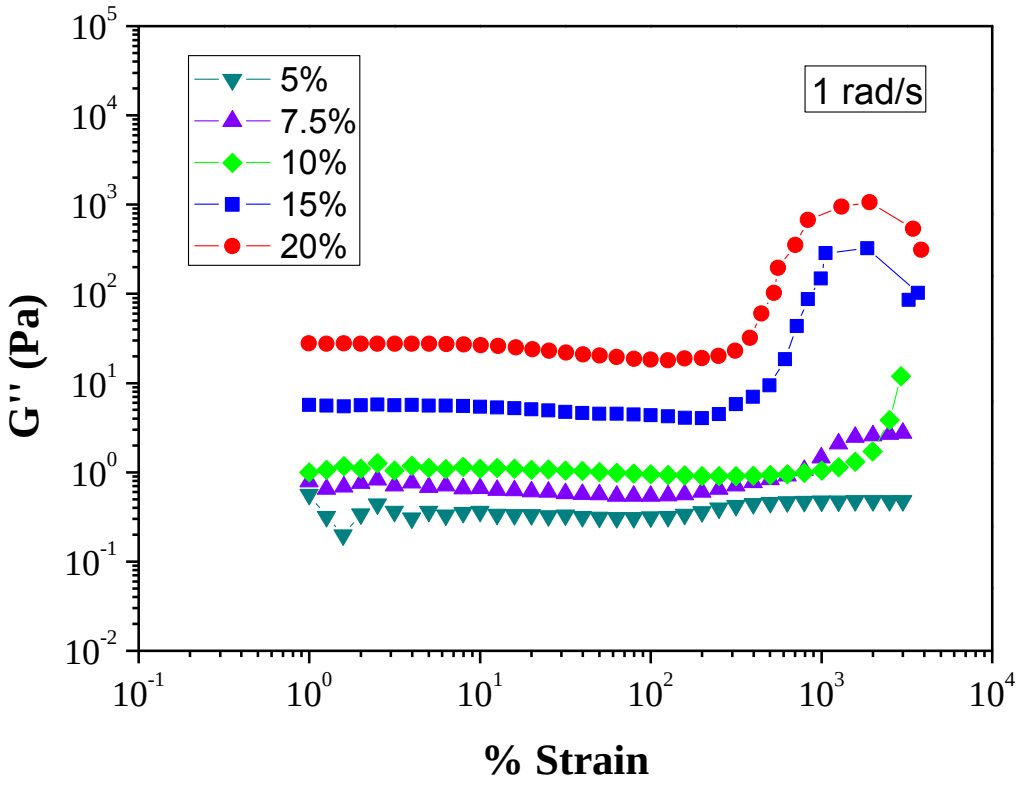

Figure 4.43. Viscous G'' modulus as a function of strain amplitude at a frequency of 1 rad/s for several concentrations of the STF suspensions

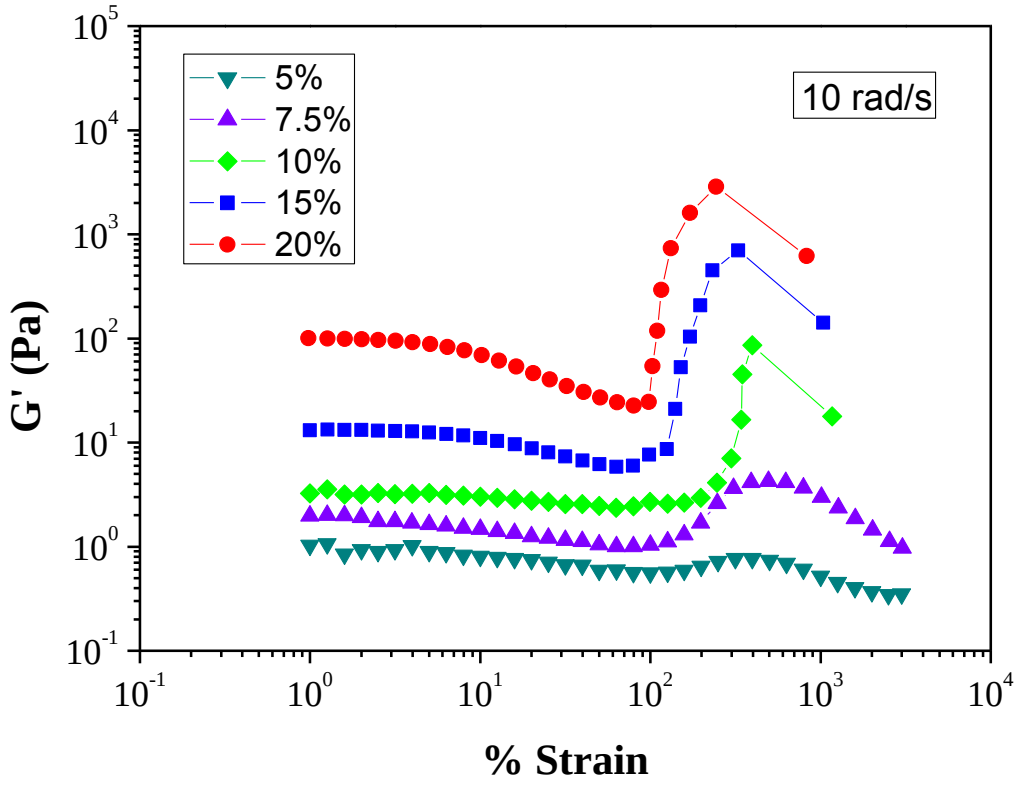

Figure 4.44. Elastic G' modulus as a function of strain amplitude at a frequency of 10 rad/s for several concentrations of the STF suspensions

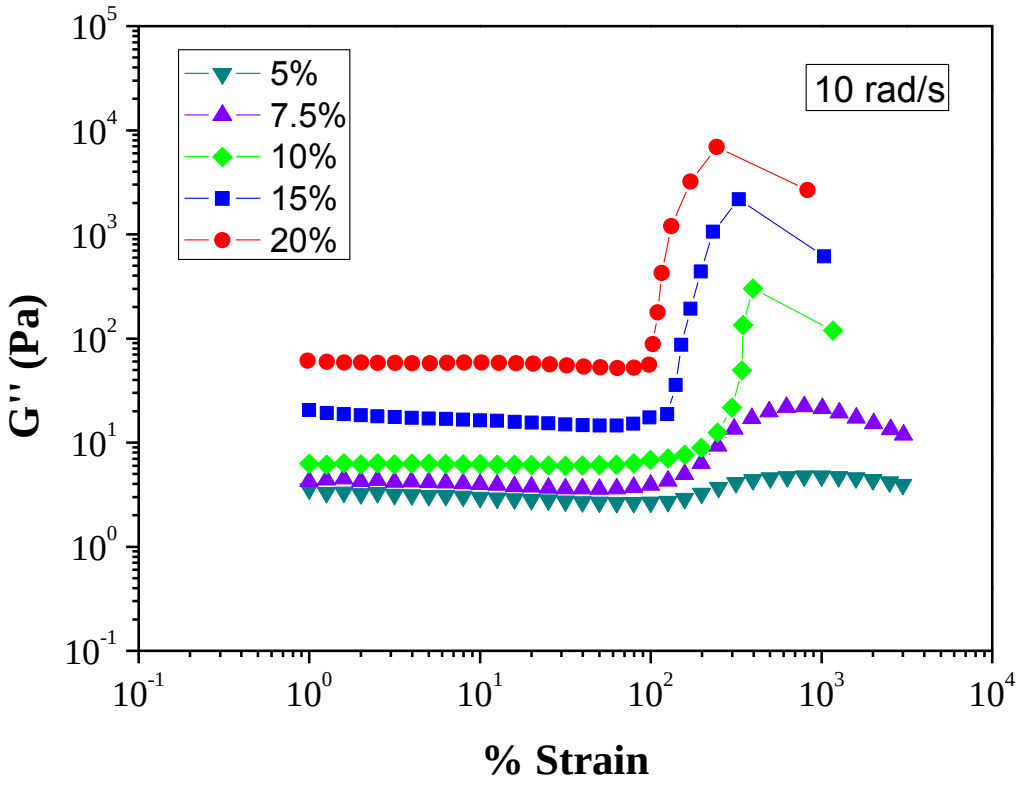

Figure 4.45. Viscous G'' modulus as a function of strain amplitude at a frequency of 10 rad/s for several concentrations of STF suspensions

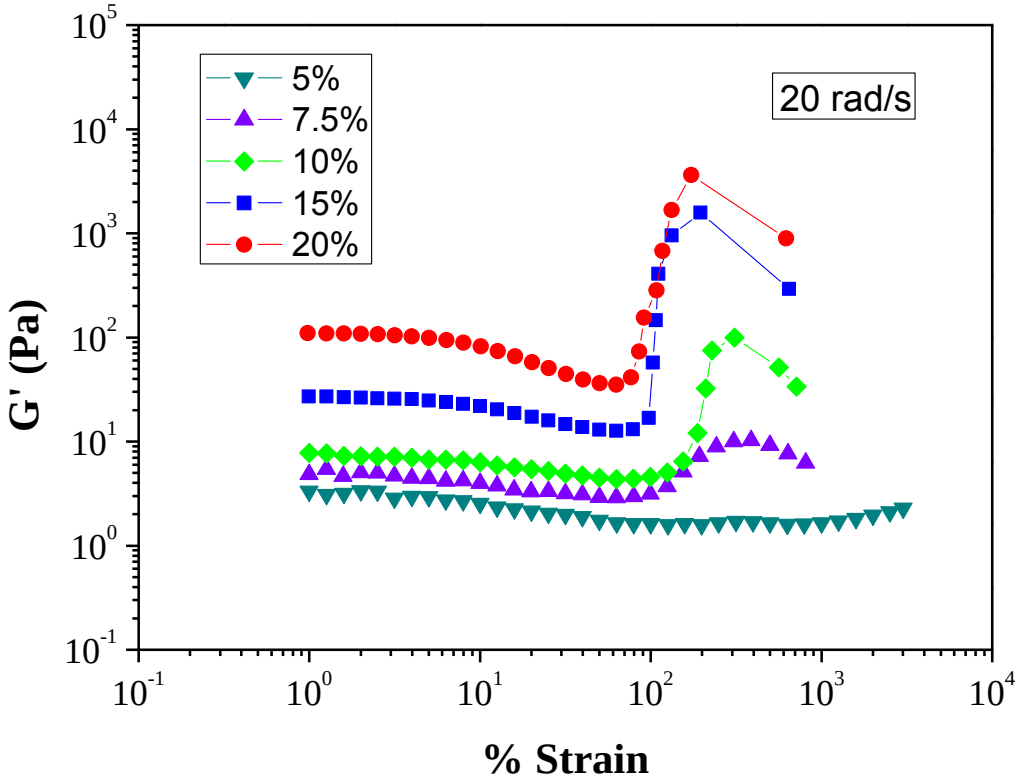

Figure 4.46. Elastic G' modulus as a function of strain amplitude at a frequency of 20 rad/s for several concentrations of the STF suspensions

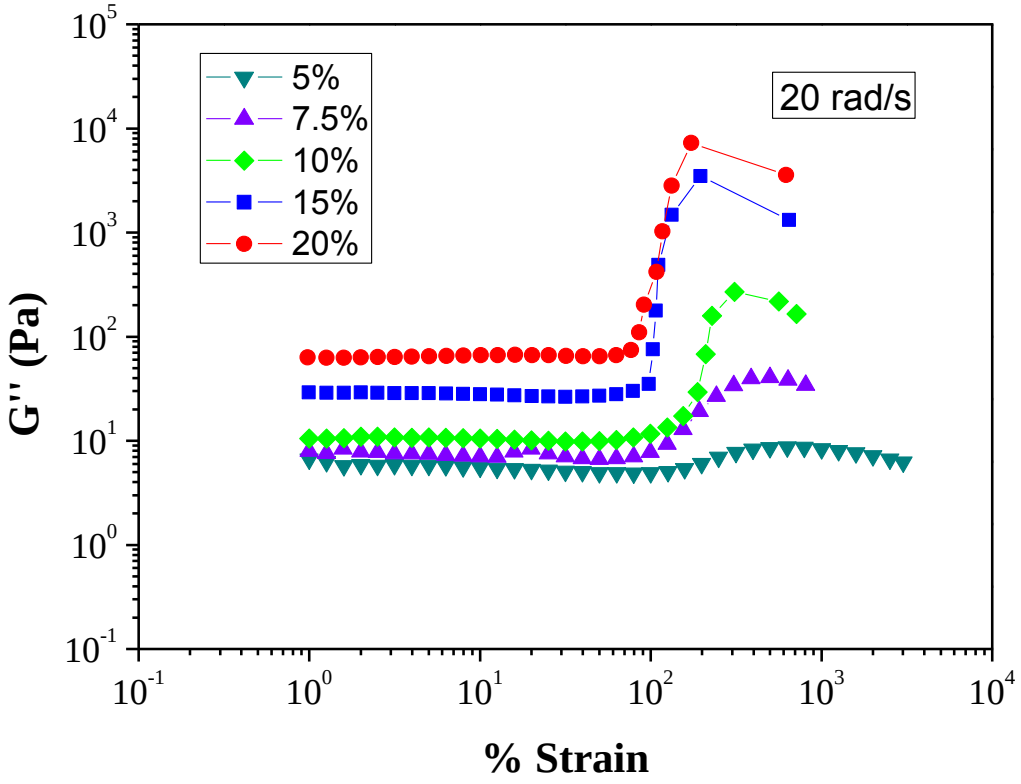

Figure 4.47. Viscous G'' modulus as a function of strain amplitude at a frequency of 20 rad/s for several concentrations of STF suspensions

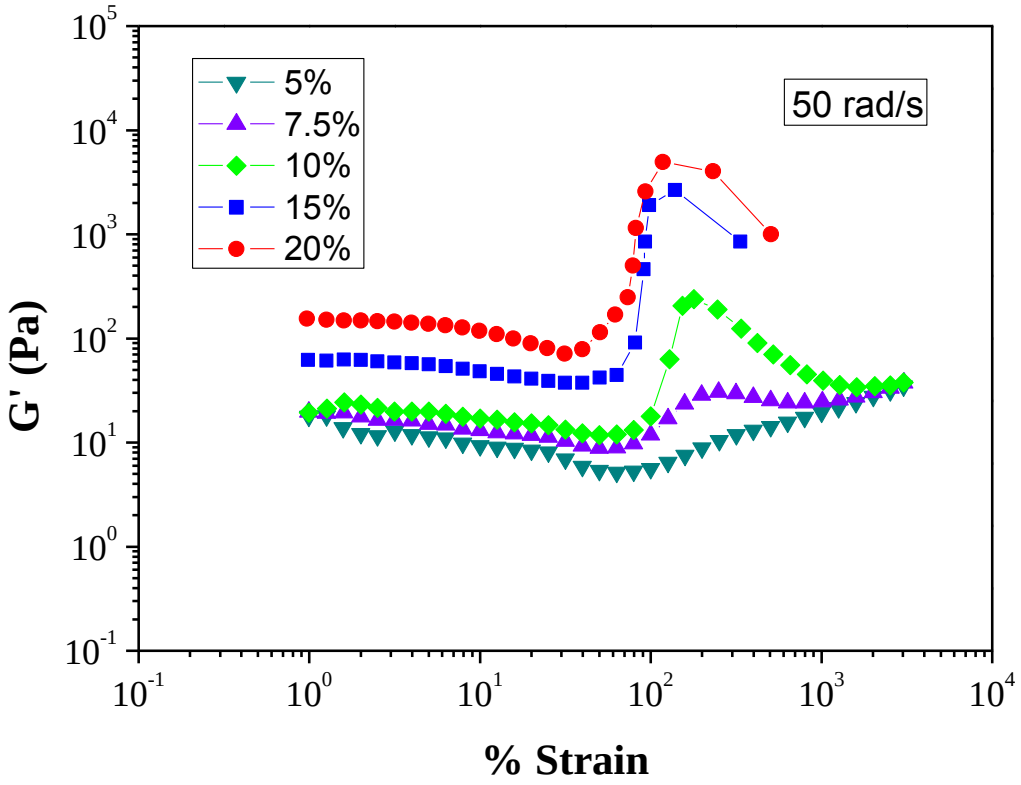

Figure 4.48. Elastic G' modulus as a function of strain amplitude at a frequency of 50 rad/s for several concentrations of the STF suspensions

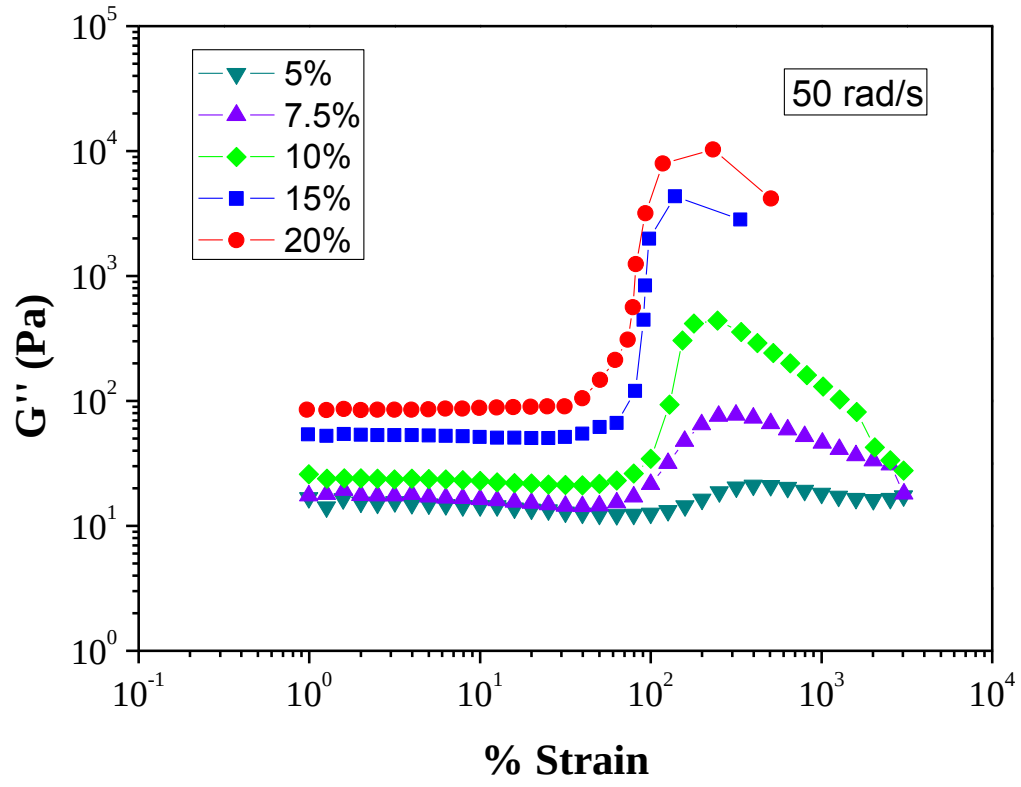

Figure 4.49. Viscous G'' modulus as a function of strain amplitude at a frequency of 50 rad/s for several concentrations of STF suspensions

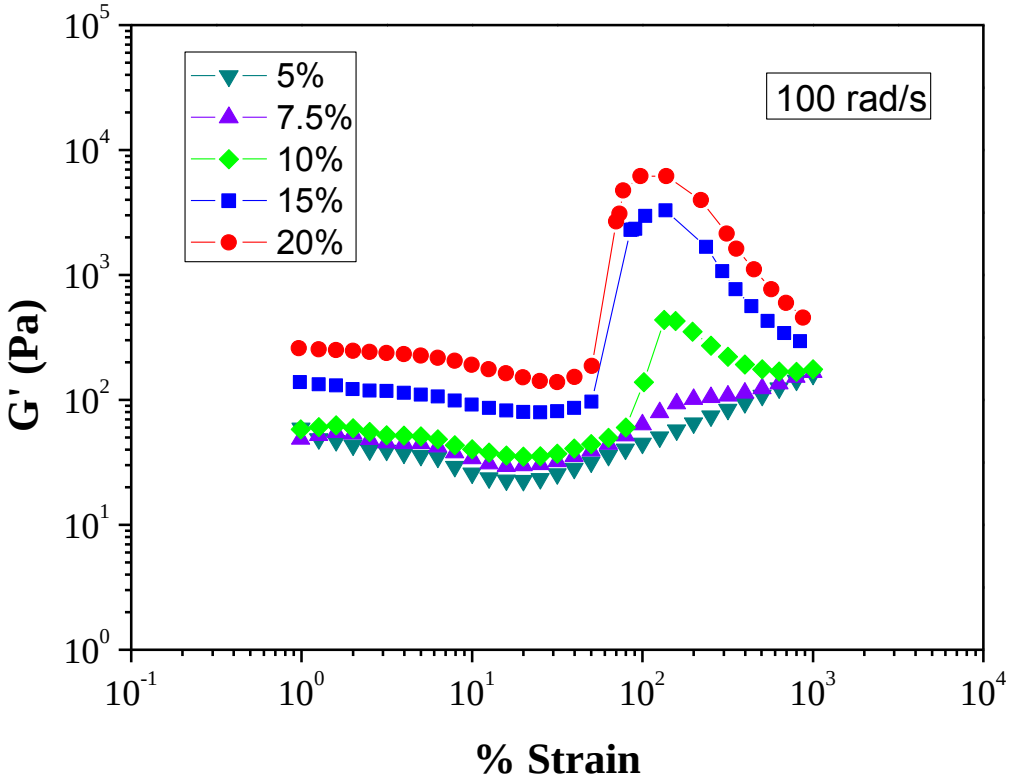

Figure 4.50. Elastic G' modulus as a function of strain amplitude at a frequency of 100 rad/s for several concentrations of the STF suspensions

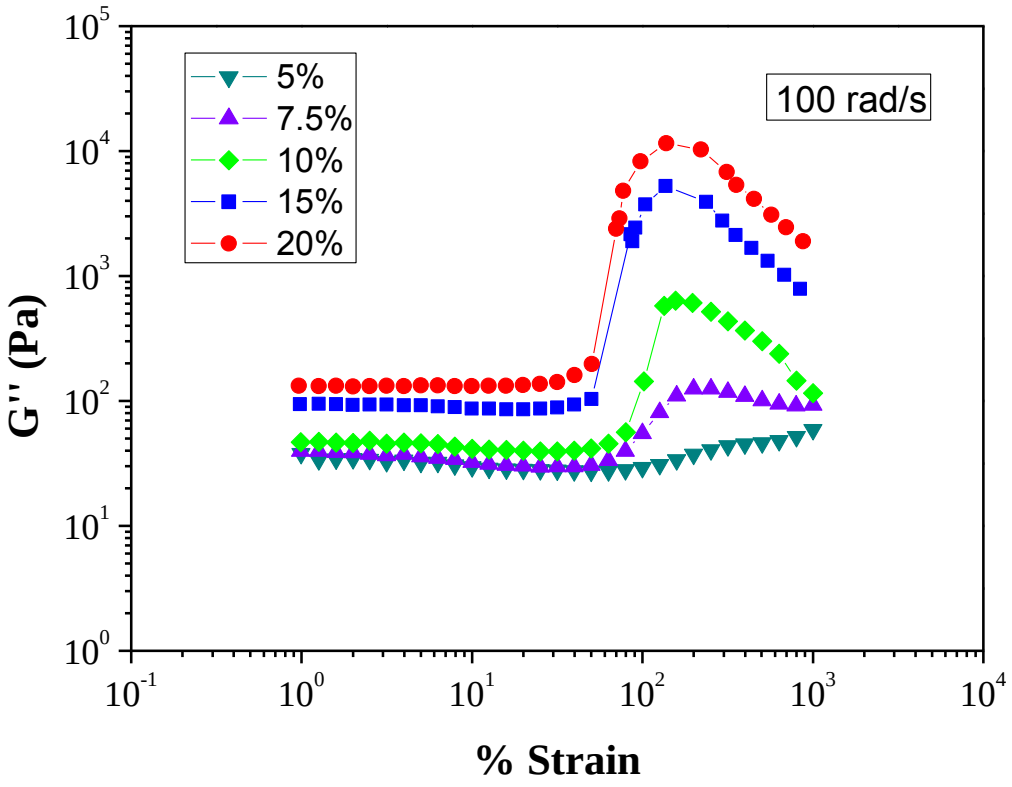

Figure 4.51. Viscous G'' modulus as a function of strain amplitude at a frequency of 100 rad/s for several concentrations of STF suspension

4.4. Mechanical Properties of STF/Kevlar Composites

4.4.1. Quasistatic Stab Resistance Test

The quasistatic stab resistance test results for the neat Kevlar and STF-Kevlar composite targets are illustrated in Figure 4.52. The front and back surface of the both samples are shown in Figures 4.53 and 4.54. As seen in the graph, STF-Kevlar composite targets exhibited significantly higher penetration load as compared to those for the neat Kevlar targets. It was observed that STF-Kevlar-3 composite target exhibited the highest load of 574 N at about 30 mm penetration, whereas the neat Kevlar target gived 286 N at the same penetration depth. Furthermore, STF-Kevlar composite targets revealed less damage as compared with the neat Kevlar. This behavior correlated with the appearance of the damage area on the targets after testing as seen in Figures 4.53 and 4.54. It can be concluded that the improvement of the stab resistance was due to the addition of STF to the fabric, which associates with the hydroclustering and resistance of the nanoparticles within the fluid coated on the fabric surface.

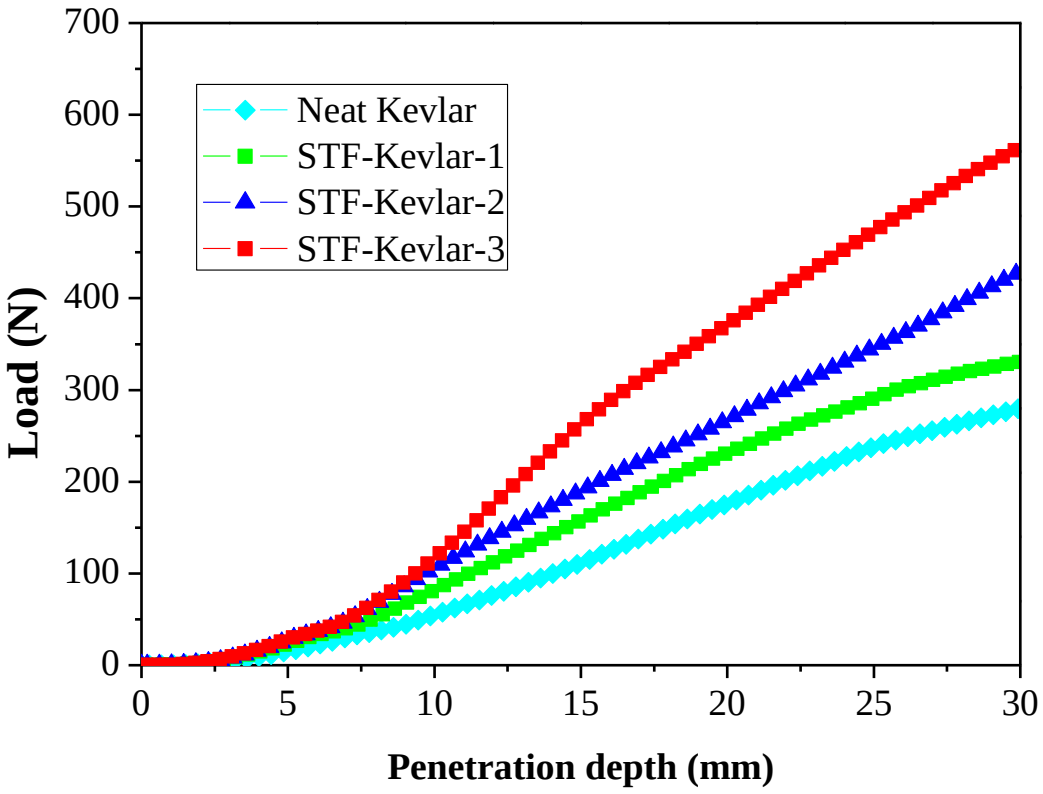

Figure 4.52. Quasistatic results for neat and STF-Kevlar composite targets

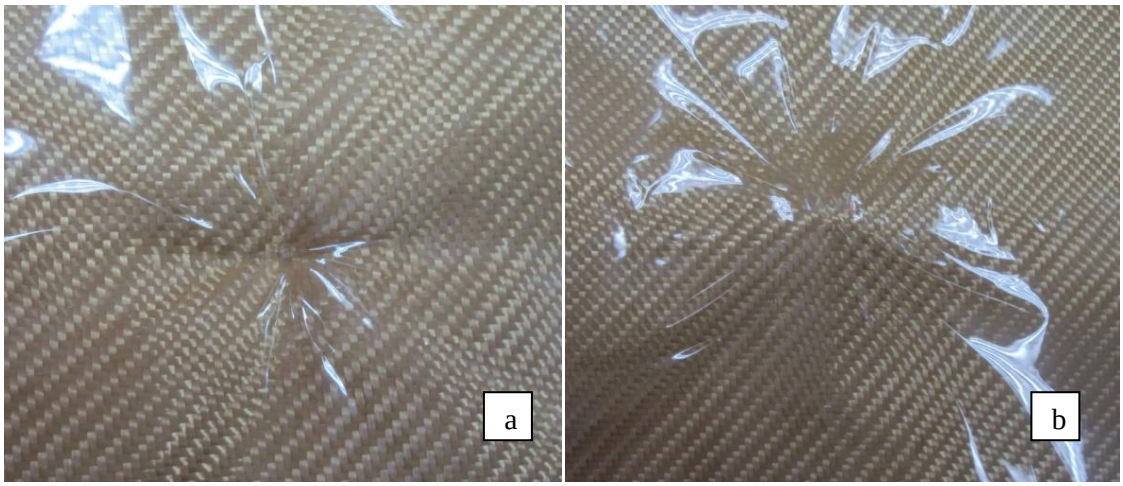

Figure 4.53. Photos of the a) front and b) back surface of Kevlar fabric after stab resistance testing

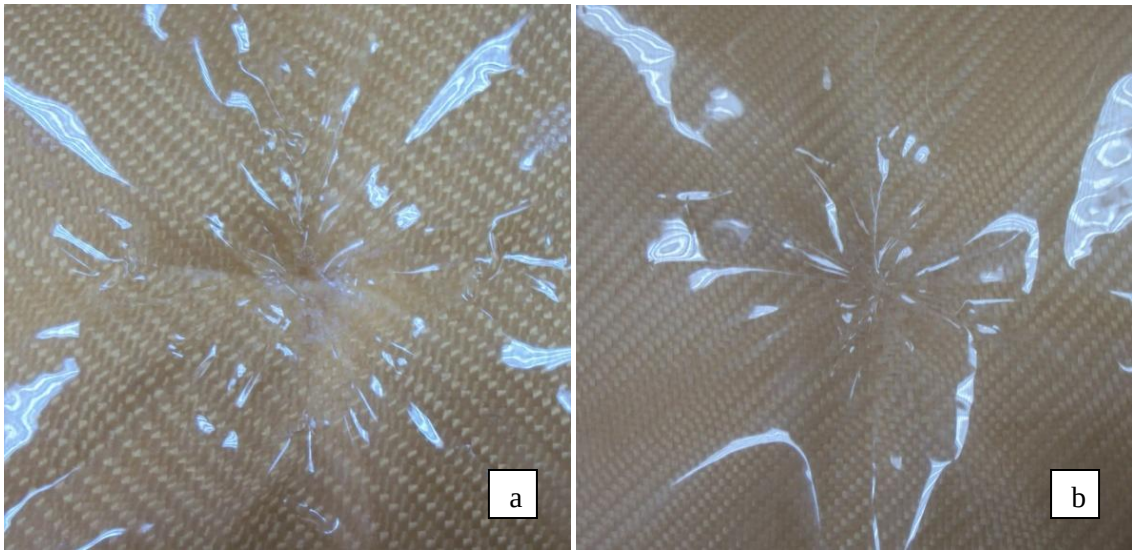

Figure 4.54. Photos of the a) front and b) back surface of STF-Kevlar fabric after stab resistance testing

4.4.2. Ballistic Test

The STF/Kevlar fabric composites were tested based on NIJ standard 0101.03 (Ballistic Resistance of Police Body Armor). The ballistic test materials produced (Unimpregnated Kevlar fabrics and STF impregnated Kevlar fabric composites) are also shown in Figures 4.55 and 4.56. The ballistic test results with different configurations are also listed in Table 4.2.

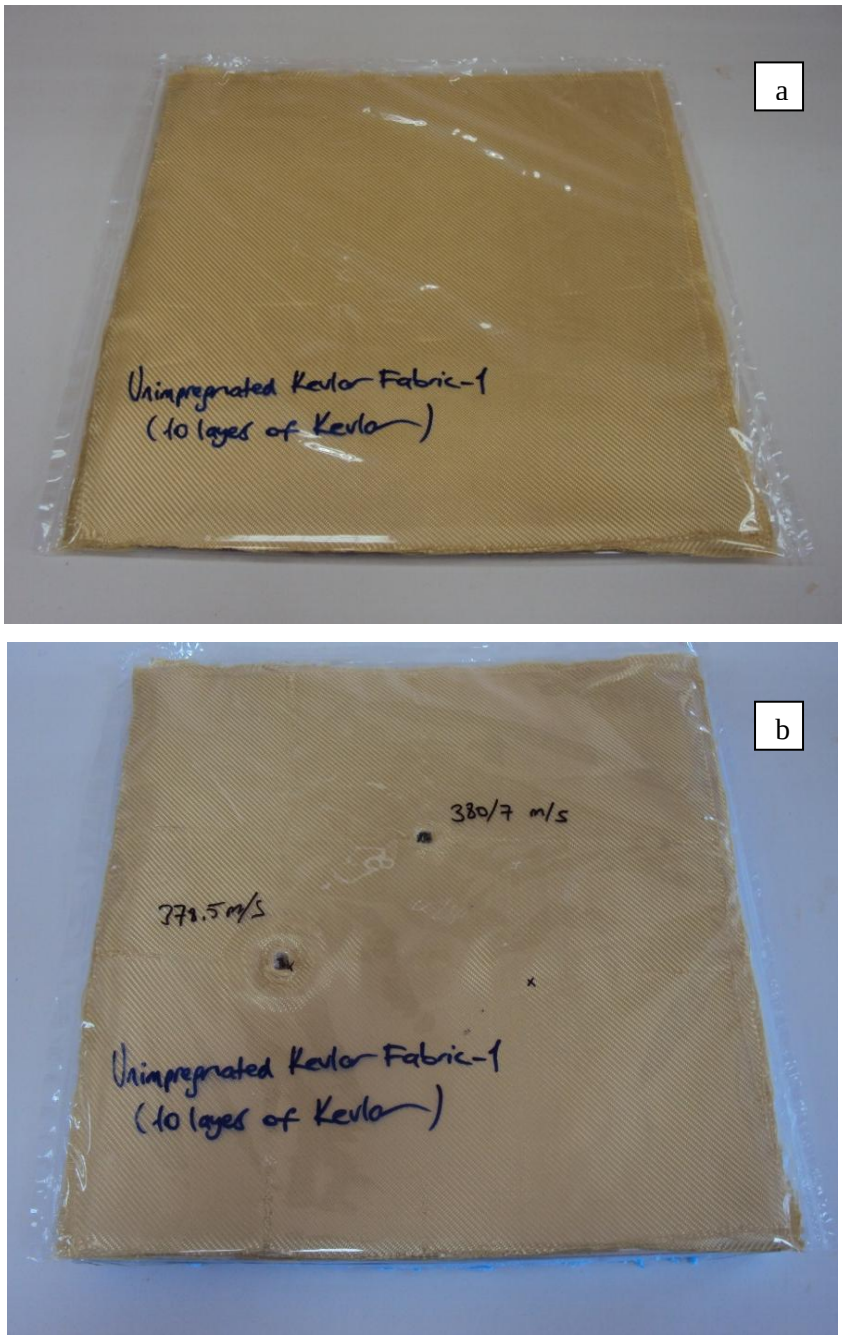

Figure 4.55. Photos of the unimpregnated Kevlar fabrics a) before and b) after ballistic test

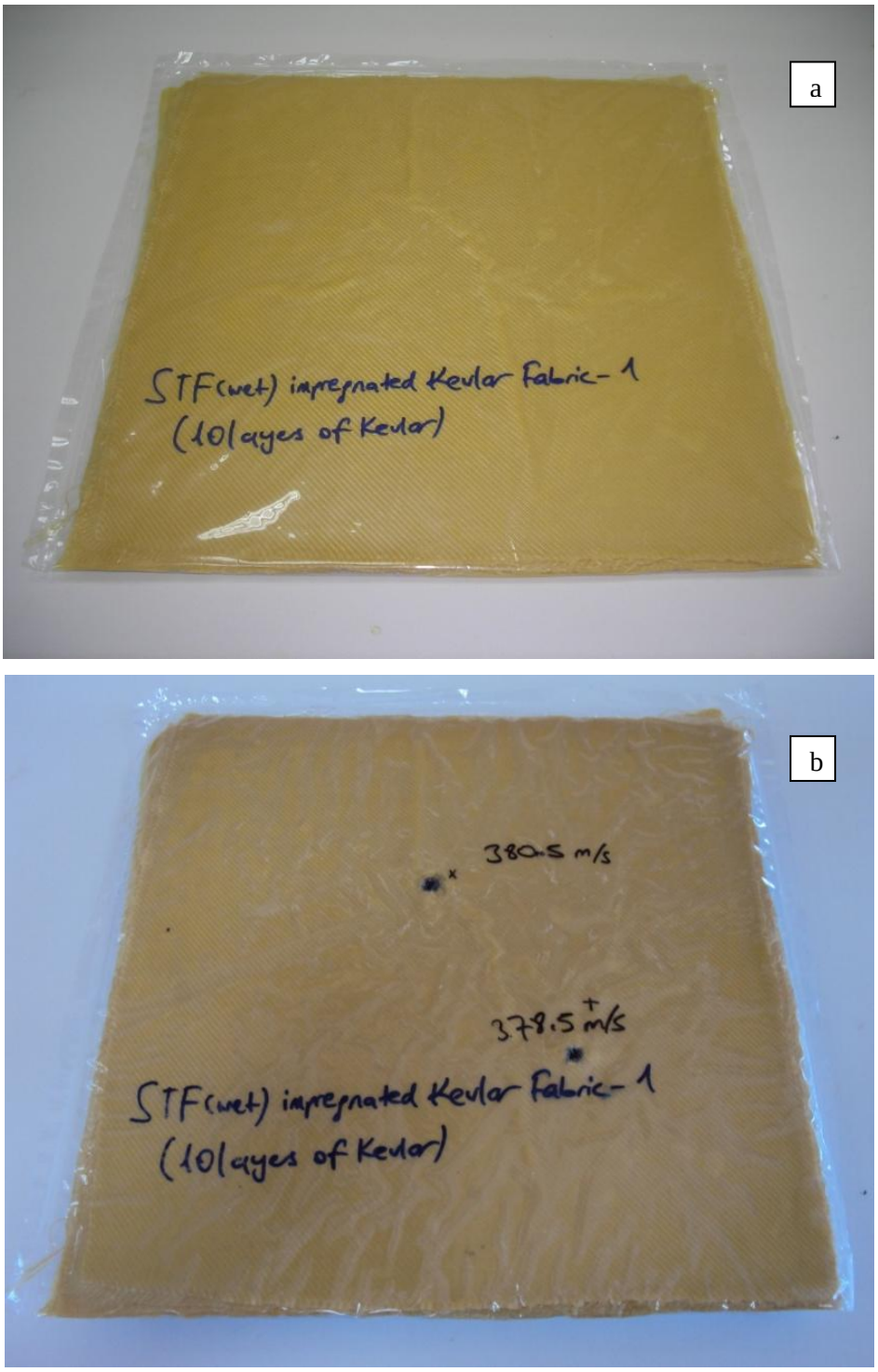

Figure 4.56. Photos of the STF-impregnated Kevlar fabrics a) before and b) after ballistic test

Table 4.2. The test results of Kevlar and STF/Kevlar fabric composites with different configurations

Sample ID	**Number of layers in target**	**Distance (m)**	**Impact Velocity (m/s)**
Unimpregnated Kevlar-1	10	5	380.7 (5 m) 378.5 (5 m)
Unimpregnated Kevlar-2	20	5 15	379.7 (5 m) 382 (15 m) 384 (15 m)
STF impregnated Kevlar-1	20	15	371 (15 m)
STF impregnated Kevlar-2	30	5 15	376.2 (5 m) 373.3 (15 m)
Diluted STF impregnated Kevlar-1	10	5	380.5 (5 m) 378.5(5 m)
Diluted STF impregnated Kevlar-2	20	5 15	380.1 (5 m) 376 (15 m)
Softened STF impregnated Kevlar-1	10	5	381.6 (5 m)
Softened STF impregnated Kevlar-2	10	5	379.2 (5 m) 374.7 (5 m)

For selected projectile type and velocity, all of the samples exhibited full penetration of the projectiles. Therefore, an adequate comparison was not able to made to evaluate the effect of STF impregnation on the Kevlar fabrics. However, based on the visiual observations on the impacted panels, it is concluded that STF has some positive effect on the Kevlar fabrics.

4.4.3. Microstructure Characterization

The SEM micrographs presented in Figures 4.57 and 4.58 show images of neat Kevlar fabric without any addition of STF and STF-Kevlar composites, respectively. These images clearly demonstrate that STF is well impregnated over the entire surface on the Kevlar fabric. It can be seen in Figure 4.58 (c and d) that STF is well penetrated within the fiber bundles. The high magnification SEM images presented in Figure 4.58 (e and f) show that the Kevlar fabrics are completely coated with STF.

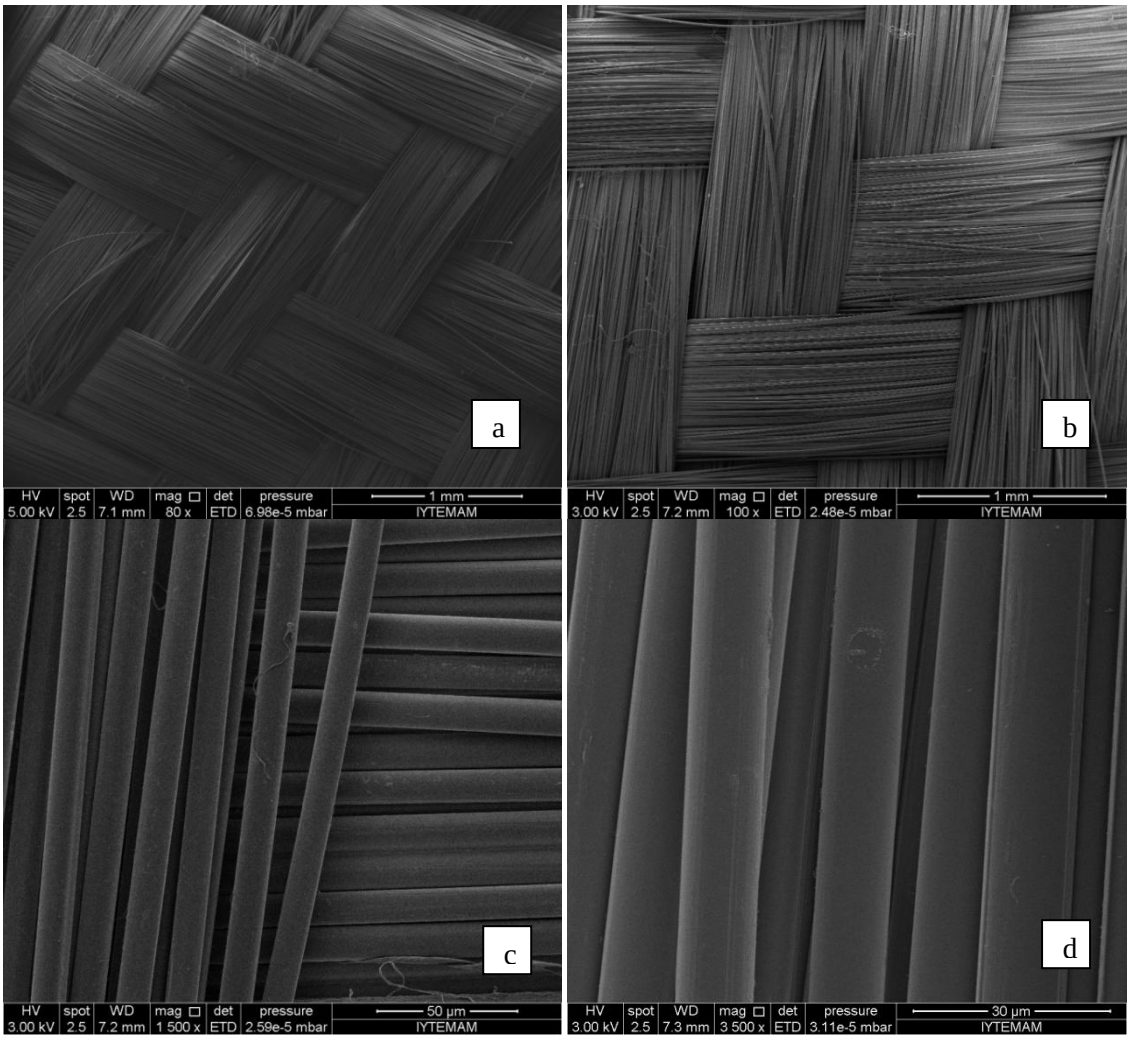

Figure 4.57. SEM images of neat Kevlar fabrics at various magnifications
a) 80x, b) 100x, c) 1500x, d) 3500x

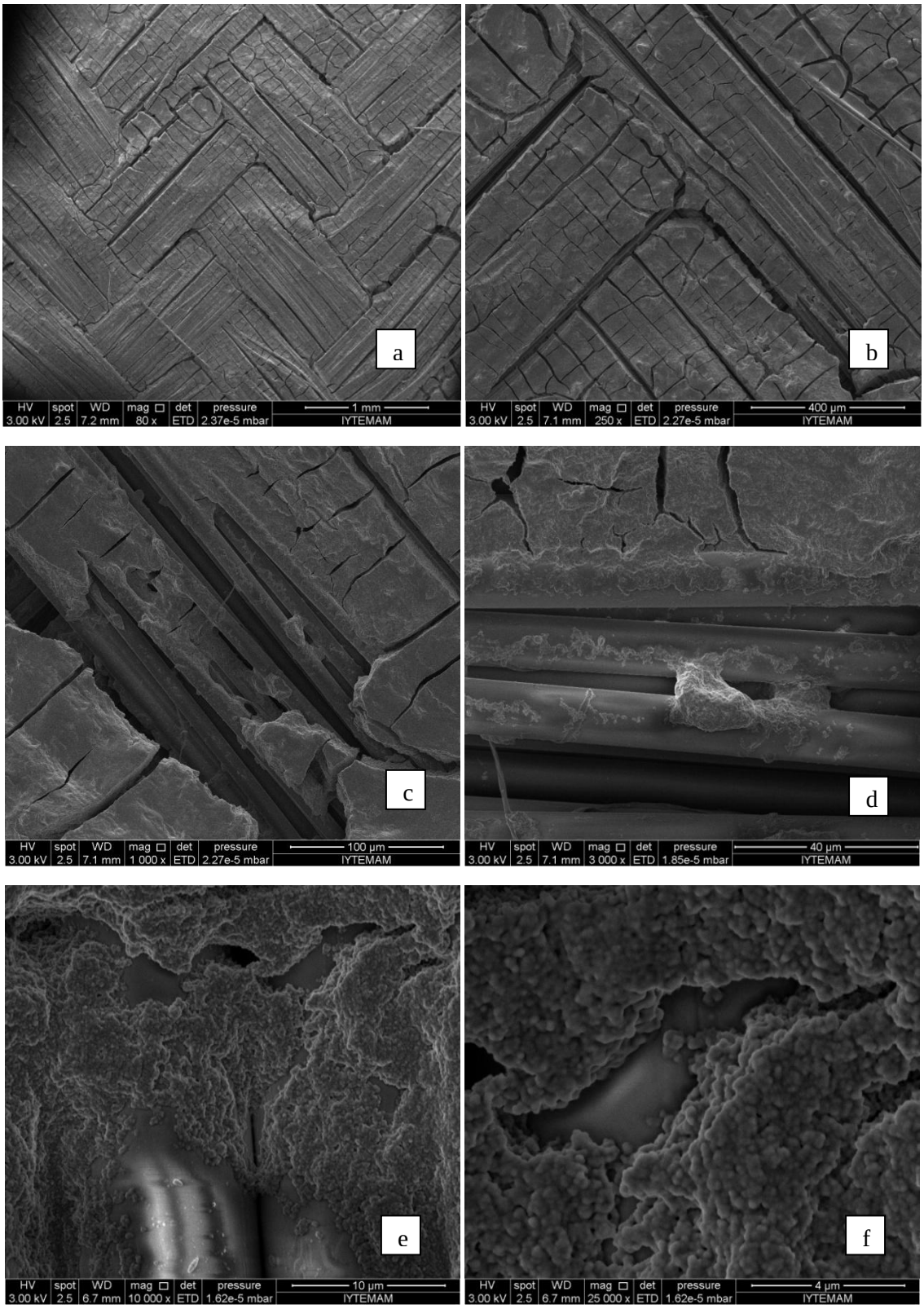

Figure 4.58. SEM images of STF/Kevlar fabric composite at various magnifications a) 80x, b) 100x, c) 1000x, d) 3000x, e) 10000x, f) 25000x

CHAPTER 5

CONCLUSIONS

In the present study, the rheological and thermal properties of shear thickening fluids (STFs) were presented. The effects of the various impregnation techniques on the Kevlar woven fabrics were investigated. The stab performance of shear thickening fluid (STF) impregnated Kevlar woven fabrics was also investigated in order to reveal the effects of the shear thickening fluid (STF) on the Kevlar fabrics.

Fumed silica suspensions in low molecular weight polyethylene glycol exhibited shear thickening under steady flow and strain thickening under oscillatory shear. The sample containing 7.5 wt% of silica showed shear thickening behavior in the range of 4-45 s^{-1} shear rate and the viscosity was found from about 0.95 to 2.9 Pa·s. For the suspension containing 10 wt% of silica shear thickening behavior was found with an increase in the viscosity from about 0.85 to 26 Pa·s between 7 and 36 s^{-1} shear rates. The sample containing 15 wt% of silica indicated a shear thickening effect in the range of 9-36 s^{-1} shear rate and with increase in the viscosity from about 2.6 to 153 Pa·s before a reversible trend is seen. For the suspension containing 20 wt% of silica shear thickening transition was found with an increase in the viscosity from about 11 to 797 Pa·s between 3-25 s^{-1} shear rates. The rheological property of STF sample with the highest concentration 25 wt% of silica showed a significant shear thickening behavior from about 60 to 1720 Pa·s between 2.5 and 13 s^{-1} shear rates. The increasing value of viscosity indicated an incredibly high shear thickening effect. As compared to the others, continuous increase in sample's viscosity was found at low and very narrow shear rates range. In all STF samples shear thinning behavior was found before they started to exhibit shear thickening behavior. It was concluded that the shear thickening behavior was found to be reversible for all the suspensions.

The strain thickening behavior was found at critical combination of strain amplitude and frequency. The elastic G' and the viscous G'' modulus values were found to increase when the strain amplitude was kept constant and frequency was increased. The same strain thickening behavior was also found when the frequency was kept constant and the strain amplitude was increased. The viscous G'' modulus values

were found to be greater than the elastic G' modulus. The suspensions indicated strain thickening at high strain amplitudes and the elastic G' and the viscous G'' modulus values were found to make an abrupt transition to higher levels at the critical strain amplitudes. Besides, the transition to strain thickening behavior was obtained at smaller strain amplitudes as the frequency was increased. It was concluded that the strain thickening transition was found to be reversible. Based on the rheological results, important parameters controlling the thickening behavior are the critical shear rate corresponding to the onset of the steady shear thickening and the critical frequency and strain amplitude at the onset of the strain thickening. Both these parameters were found to decrease with increasing concentration. The increase in viscosity and both G' and G'' owing to shear and strain thickening was found most noticeably at higher concentrations.

The quasistatic spike tests showed addition of the STF significantly improved the puncture resistance of Kevlar fabrics. The STF-Kevlar composites were found to show significantly higher load than the neat Kevlar target. The neat Kevlar target exhibited small load 286 N, whereas the STF-Kevlar composite targets showed higher loads 574, 433 and 333. The STF-Kevlar composite targets exhibited better stab resistance as compared to the neat Kevlar target. This improvement showed that the impregnation of the fabric with a colloidal shear thickening fluid has enhanced the performance of the fabric for body armor applications.

Based on SEM images, it was concluded that STF is well impregnated over the entire surface on the Kevlar fabric. STF penetrated within the fiber bundles and the Kevlar fabrics completely coated with STF. Also, the ballistic test results replied that the incorporation of STF into Kevlar fabrics has some potential to produce liquid armor materials.

REFERENCES

Barnes H. A.,“Shear-Thickening ("Dilatancy") in Suspensions of Nonaggregating Solid Particles Dispersed in Newtonian Liquids”, *Journal of Rheology*, **1989**, 33, 329-366.

Barnes H. A., Hutton J. F., Walters F.R.S. K. An introduction to Rheology *New York: Elsevier*, **1989**.

Bender J. and Wagner N. J. “Reversible shear thickening in monodisperse and bidisperse colloidal dispersions”, *Journal of Rheology*, **1996**, 40(5), 899-916.

Boersma W. H., Laven J., Stein H. N.,“Shear Thickening (Dilatancy) in Concentrated Dispersions”, *AIChE Journal*, **1990**, 36(3). 321-332

Boersma W. H., Laven J., Stein H. N.,“Viscoelastic Properties of Concentrated Shear-Thickening Dispersions”, *Journal of Colloid and Interface Science*, **1992**, 149(1), 10-22.

Bossis G. and Brady J. F.“The rheology of Brownian suspensions”, *Journal of Chemical Physics*, **1989**, 91(3), 1866-1874.

Brady J. F. and Bossis G. “Stokesian Dynamics”, *Annu. Rev. Fluid. Mech*, **1988**, 20, 111-157.

Chellamuthu M., Arndt E. M., Rothstein J. P.,“Extensional rheology of shear-thickening nanoparticle suspensions”, *Soft Matter*, **2009**, 5, 2117-2124.

Chhabbra R. P. and Richardson J. F. Non-Newtonian Flow and Applied Rheology: Engineering Applications, **2008**.

Chow M. K. and Zukoski C. F.“Nonequilibrium behavior of dense suspensions of uniform particles: Volume fraction and size dependence of rheology and microstructure”, *Journal of Rheology*, **1995**, 39(1), 33-59.

Decker M. J., Halbach C. J., Nam C. H., Wagner N. J., Wetzel E. D., “Stab resistance of shear thickening fluid (STF)-treated fabrics”, *Composites Science and Technology*, **2007**, 67, 565-578.

Egres R. G. and Wagner N. J. “The rheology and microstructure of acicular precipitated calcium carbonate colloidal suspensions through the shear thickening transition”, *Journal of rheology*, **2005**, 49(3), 719-746.

Fischer C., Braun S. A., Bourban P-E., Michaud V., Plummer C. J. G., Månson J-A. E., “Dynamic properties of sandwich structures with integrated shear-thickening fluids”, *Smart Materials and Structures*, **2006**, 15, 1467-1475.

Frith W. J., d'Haene P., Buscall R., Mewis J.,“Shear thickening in model suspensions of sterically stabilized particles”, *Journal of Rheology*, **1996**, 40(4), 531-548.

Galindo-Rosales F. J. and Rubio-Hernández F. J.“Static and dynamic yield stresses of Aerosil® 200 suspensions in polypropylene glycol”, *Applied Rheology*, **2010**, 20(2), 22787-22797.

Galinda-Rosales F. J. and Rubio-Hernández F. J. Cap.18. “Numerical Simulation in Steady flow of Non-Newtonian Fluids in Pipes with Circular Cross-Section”, *Examples and Applications in Computational Fluids Dynamics*. Intech Open Publications, **2010**. ISBN: 978-953-307-153-4.1.

Hassan T. A., Rangari V. K., Jeelani S.,“Sonochemical synthesis and rheological properties of shear thickening silica dispersions”, *Ultrasonics Sonochemistry*, **2010**, 17, 947-952.

Hassan T. A., Rangari V. K., Jeelani S.,“Synthesis, processing and characterization of shear thickening fluid (STF) impregnated fabric composites”, *Materials Science and Engineering A*, **2010**, 527, 2892-2899.

Hoffman R. L.,“Discontinuous and Dilatant Viscosity Behavior in Concentrated Suspensions. I. Observation of a Flow Instability”, *Transactions of the Society of Rheology*, **1972**, 16(1), 155-173.

Hoffman R. L.,“Discontinous and Dilatant Viscosity Behavior in Concentrated Suspensions II. Theory and Experimental Tests”, *Journal of Colloid and Interface Science*, **1974**, 46(3), 491-506.

Kalman D. P. and Wagner N. J.“Microstructure of shear-thickening concentrated suspensions determined by flow-USANS”, *Rheol Acta*, **2009**, 48, 897-908.

Kalman D. P., Merill R. L., Wagner N. J., Wetzel E. D., “Effect of Particle Hardness on the Penetration Behavior of Fabrics Intercalated with Dry Particles and Concentrated Particle-Fluid Suspensions”, *Applied Materials and Interfaces*, **2009**, 1(11), 2602-2612.

Kamibayashi M., Ogura H., Otsubo Y.,“Shear-Thickening flow of nanoparticle suspensions flocculated by polymer bridging”, *Journal of Colloid and Interface Science*, **2008**, 321, 294-301.

Krishnamurthy L. N., Wagner N. J., Mewis J.,“Shear thickening in polymer stabilized colloidal dsipersions”, *Journal of Rheology*, **2005**, 49(6), 1347-1360.

Kissa E. Dispersions Characterization, Testing and Measurement *New York: Marcel Dekker, Inc.* **1999**.

Laun H. M., Bung R., Hess S., Loose W., Hess O., Hahn K., Hädicke E., Hingmann R., Schmidt F., Lindner P.,“Rheological and small angle neutron scattering investigation of shear-induced particle structures of concentrated polymer dispersions submitted to plane Poiseuille and Couette flow”, *Journal of Rheology*, **1992**, 36(4), 743-787.

Laun H. M., Bung R., Schmidt F.,"Rheology of Extremely Shear Thickening Polymer Dispersions (Passively Viscosity Switching Fluids)", *Journal of Rheology*, **1991**, 35, 999-1034.

Lee Y. S. and Wagner N. J."Dynamic properties of shear thickening colloidal suspensions", *Rheol Acta*, **2003**, 42, 199-208.

Lee Y. S., Wetzel E. D., Wagner N. J.,"The ballistic impact characteristics of Kevlar woven fabrics impregnated with a colloidal shear thickening fluid", *Journal of Materials Science*, **2003**, 38, 2825-2833.

Lee Y. S. and Wagner N. J."Rheological Properties and Small-Angle Neutron Scattering of a Shear Thickening, Nanoparticle Dispersion at High Shear Rates", *Ind. Eng. Chem. Res*, **2006**, 45, 7015-7024.

Lim A. S., Lopatnikov S. L., Wagner N. J., Gillespie Jr. J. W.,"Investigating the transient response of a shear thickening fluid using the split Hopkinson pressure bar technique", *Rheol Acta*, **2010**, 49, 879-890.

Macosko C. W. Rheology: Principles, Measurements and Applications *Wiley-VCH*, **1994**.

Maranzano B. J. and Wagner N. J."The effects of particle size on reversible shear thickening of concentrated colloidal dispersions", *Journal of Chemical Pyhsics*, **2001b**, 114(23), 10514-10527.

Maranzano B. J. and Wagner N. J."Flow-small angle neutron scattering measurements of colloidal dispersion microstructure evolution through the shear thickening transition", *Journal of Chemical Physics*, **2002**, 117(22), 10291-10302.

Melrose J. R., van Vliet J. H., Ball R. C.,"Continous Shear Thickening and Colloid Surfaces", *Pyhsical Review Letters*, **1996**, 77(22), 4660-4663.

Mewis J. and Biebaut G.,"Shear thickening in steady and superposition flows effect of particle interaction forces", *Journal of Rheology*, **2001**, 45(3), 799-813.

Muñoz M. E., Santamaría A., Guzmán J., Riande E.,"Enhancement of the first normal stress coefficient and dynamic moduli during shear thickening of a polymer solution", *Journal of Rheology*, **2003**, 47(4), 1041-1050.

Raghavan S. R. and Khan S. A."Shear-Thickening Response of Fumed Silica Suspensions under Steady and Oscillatory Shear", *Journal of Colloid and Interface Science*, **1997**, 185, 57-67.

Zhang X. Z., Li W.H., Gong X. L.,"The rheology of shear thickening fluid (STF) and the dynamic performance of an STF-filled damper", *Smart Materials and Structures*, **2008**, 17, 1-7.